



Vietnamese-German University

## **COPYRIGHT WARNING**

This paper is protected by copyright. You are advised to print or download **ONE COPY** of this paper for your own private reference, study and research purposes. You are prohibited having acts infringing upon copyright as stipulated in Laws and Regulations of Intellectual Property, including, but not limited to, appropriating, impersonating, publishing, distributing, modifying, altering, mutilating, distorting, reproducing, duplicating, displaying, communicating, disseminating, making derivative work, commercializing and converting to other forms the paper and/or any part of the paper. The acts could be done in actual life and/or via communication networks and by digital means without permission of copyright holders.

The users shall acknowledge and strictly respect to the copyright. The recitation must be reasonable and properly. If the users do not agree to all of these terms, do not use this paper. The users shall be responsible for legal issues if they make any copyright infringements. Failure to comply with this warning may expose you to:

- Disciplinary action by the Vietnamese-German University.
- Legal action for copyright infringement.
- Heavy legal penalties and consequences shall be applied by the competent authorities.

The Vietnamese-German University and the authors reserve all their intellectual property rights.





RUHR-UNIVERSITÄT BOCHUM

**MechEng**  
Mechanical Engineering



Vietnamese-German University

# EXPERIMENTAL INVESTIGATION OF VIBRATION REDUCTION BASED ON GRANULAR MATERIALS

BACHELOR THESIS

MAGDEBURG 2021



Vietnamese-German University

**Submitted by:** Tran Le Hoang

**RUB Student ID:** 108 018 206 572

**VGU Student ID:** 14154

**Supervisor:** Prof. Dr.-Ing. Daniel Juhre

**Co-supervisor:** M.Sc. Braj Bhushan Prasad

# Abstract

Vibration control is an important field to study on many mechanical components, aiming to increase safety, lifetime, or comfort for the user. Thus, the vibration must be controlled, and in many cases, reduced. In this thesis, the vibration of a scaled component of a wind turbine would be damped by Particle damping with granulated rubber, and the effectiveness will be evaluated with a Laser Doppler Vibrometer.

During such experiments, the parameters are critical to obtaining a correct, efficient, and reproducible measurement procedure. For this reason, the Parameter study will be considered as the main part of this thesis, followed by the actual experiments to study the effectiveness to reduce the vibration of Particle damping. The parameters being investigated are broadly divided into four groups: general, experimental, software and hardware parameters. The thesis concludes that Particle damping has a noticeable effect in reducing the vibration of the test specimen, and thus, other mechanical components.



Vietnamese-German University

# List of abbreviations

BPT .....	Blade Passing Frequency
DFT .....	Discrete Fourier Transform
FFT .....	Fast Fourier Transform
FIR .....	Finite Impulse Response
FR.....	Frequency Resolution
OvGU .....	Otto-von-Guericke University
PD .....	Particle Damping



# List of figures

Figure 1-1: Different possible solutions for sound reduction methods .....	2
Figure 2-1: Contribution to the total sound power level of a wind turbine .....	5
Figure 2-2: Classification of particle dampers .....	7
Figure 2-3: Experiment of mutli-unit particle damper on a bracket-wheel structure .....	8
Figure 2-4: Particle filling .....	9
Figure 2-5: The original oil pan bottom and the structure partially filled with sand.....	10
Figure 2-6: Brake drum with cavities on the wall for application of particle damping.....	10
Figure 2-7: An oscillatory saw with prototype particle dampers attached.....	11
Figure 2-8: Power spectrum of the oscillatory saw, with and without particle damper .....	11
Figure 2-9: Pounding tuned mass damper.....	12
Figure 2-10: Displacement of the jumper in the free vibration test.....	12
Figure 2-11: Shaking table setup, in scheme and actual view.....	13
Figure 2-12: Displacement frequency response of the model without and with damper .....	14
Figure 2-13: Experimental set up to study the seismic protection of PD .....	15
Figure 2-14: Displacement of the column under earthquake excitation .....	16
Figure 2-15: Experimental scheme of attaching the particle damper on turbine blade .....	16
Figure 2-16: Combined results of undamped and damped cases .....	17
Figure 3-1: Doppler effect.....	18
Figure 3-2: Overall structure of the Laser Doppler Vibrometer.....	19
Figure 3-3: 3D visualization of the test specimen .....	21
Figure 3-4: Assembled test specimen .....	21
Figure 3-5: Overview of the hardware and equipment used .....	22
Figure 3-6: Signal conditioner for force sensor and shaker controller .....	23

Figure 3-7: Measuring in linear scale and logarithmic scale .....	24
Figure 3-8: Using Fourier series to represent different signal waveforms .....	25
Figure 3-9: The frequency spectrum of a square wave .....	28
Figure 3-10: An apparently perfect sine wave in the time and frequency domain.....	28
Figure 3-11: Conversion between time and frequency domains .....	28
Figure 3-12: Input force signals with different hammers .....	31
Figure 3-13: Transfer functions for different hammers .....	32
Figure 3-14: Transfer functions for measurements at different distances .....	33
Figure 3-15: Complex and magnitude averaging of signals $S_1$ and $S_2$ .....	34
Figure 3-16: First study on signal averaging.....	35
Figure 3-17: Second study on signal averaging .....	36
Figure 3-18: Third study on signal averaging .....	37
Figure 3-19: Filter characteristic .....	38
Figure 3-20: Transfer functions with different filters applied.....	39
Figure 3-21: A low sample rate failed to replicate the original signal .....	41
Figure 3-22: Alias .....	41
Figure 3-23: Effect of frequency resolution on the frequency spectrum.....	43
Figure 3-24: Signal captured with $\Delta f = 3.91$ Hz .....	43
Figure 3-25: Signal captured with $\Delta f = 0.781$ Hz .....	44
Figure 3-26: Signal captured with $\Delta f = 0.0488$ Hz .....	44
Figure 3-27: Transfer function $H_\Omega$ for different bandwidth with 12800 FFT lines.....	47
Figure 3-28: Input force signals using 12800 FFT lines and different bandwidths .....	48
Figure 3-29: Time domain input force signals using different bandwidths on 12800 FFT lines.....	50
Figure 3-30: Transfer function $H_\Omega$ for different numbers of FFT lines on 20 kHz bandwidth.....	51



Vietnamese-German University

Figure 3-31: Force signals with 20 kHz bandwidth and different numbers of FFT lines.....	52
Figure 3-32: Vibration speed with 12800 FFT lines and different bandwidths .....	53
Figure 3-33: Example of a periodic signal.....	54
Figure 3-34: Converting a sine wave from the time domain to the frequency domain .....	55
Figure 3-35: Measuring a non-integer number of periods .....	55
Figure 3-36: Application of window function in the time domain.....	56
Figure 3-37: Main lobe and side lobes of a window function.....	57
Figure 3-38: Rectangular window function .....	58
Figure 3-39: Collected data in time domain for input force signal and vibration speed .....	59
Figure 3-40: Hann window function.....	60
Figure 3-41: Capture a sine wave periodically.....	60
Figure 3-42: Capture a sine wave non-periodically.....	61
Figure 3-43: Hann and Hamming window functions in the time domain .....	61
Figure 3-44: Flat Top window function.....	62
Figure 3-45: Comparing Hann and Flat Top window functions (1).....	63
Figure 3-46: Comparing Hann and Flat Top window functions (2).....	63
Figure 3-47: Usage of Exponential window function.....	64
Figure 3-48: Loss of signal information due to using window function.....	65
Figure 3-49: FFT of a sum of 3 sine waves, using Rectangular and Hann window functions .....	66
Figure 3-50: FFT of a transient signal, using Rectangular and Hann window functions .....	66
Figure 3-51: Window functions in the time domain.....	67
Figure 3-52: Transfer functions with different window functions .....	68
Figure 3-53: Input force signals with different window functions.....	69
Figure 3-54: Vibration speed signals with different window functions .....	70

Figure 3-55: Transfer functions from different measurement areas .....	74
Figure 3-56: Transfer functions from different areas without granulated materials .....	75
Figure 3-57: Transfer functions from different areas with granulated materials .....	75
Figure 3-58: Excitation points on the generator ring .....	77
Figure 3-59: Transfer functions for different excitation points .....	78
Figure 3-60: Force signal from different excitation points .....	78
Figure 3-61: Fixing the force sensor on the generator ring .....	79
Figure 3-62: Inability to reproduce the result with the Pseudo random signal .....	80
Figure 3-63: Inability to reproduce the result with the White noise signal .....	80
Figure 3-64: 1/3 Octave band helps to improve visibility .....	82
Figure 3-65: OvGU Rubber .....	83
Figure 4-1: Reproducibility of the first set of experiments .....	84
Figure 4-2: Filling the stator arm with 400 mL rubber .....	85
Figure 4-3: Transfer functions of different filling volumes of granulate materials (1) .....	86
Figure 4-4: Transfer functions of different filling volumes of granulate materials (2) .....	87
Figure 4-5: Big balloons being packed into the stator arm .....	88
Figure 4-6: Small balloons being packed into the stator arm .....	89
Figure 4-7: Transfer functions of granulated material in different packages (1) .....	90
Figure 4-8: Transfer functions of granulated material in different packages (2) .....	91



# List of tables

Table 2-1: Summary of Wind turbine noise types.....	6
Table 3-1: Dimensions of the test specimen .....	21
Table 3-2: Number of multiply and add operations, FFT versus DFT .....	27
Table 3-3: Different hammers available for the experiment .....	30
Table 3-4: Hitting forces for different hammer .....	30
Table 3-5: Spikes' heights seen by using different hammer tips.....	31
Table 3-6: Evaluation time using different numbers of averaged samples .....	35
Table 3-7: Spikes' height seen by using different bandwidths .....	49
Table 3-8: Spikes' heights seen with different numbers of FFT lines .....	53
Table 3-9: Different measurement areas being compared .....	72
Table 4-1: Reduction at peak different frequencies with various rubber volumes.....	85
Table 4-2: Reduction at peak different frequencies with different types of balloons .....	89

# Table of content

Abstract .....	i
List of abbreviations .....	ii
List of figures.....	iii
List of tables .....	vii
Table of content .....	viii
1 Introduction.....	1
1.1 Motivation.....	1
1.2 Goals of the thesis .....	3
1.3 Outline of the thesis.....	3
2 State of the art .....	4
2.1 Vibration and sounds of wind turbines.....	4
2.2 Particle damping.....	7
3 Experimental method .....	18
3.1 Laser scanning vibrometry.....	18
3.1.1 Doppler effect.....	18
3.1.2 Interference .....	19
3.1.3 Scanner head .....	19
3.2 Setting up the parameters.....	20
3.2.1 General parameters .....	20
3.2.1.1 Test specimen .....	20
3.2.1.2 Hardware used .....	22
3.2.1.3 Transfer function.....	23
3.2.1.4 Frequency domain, Fourier series, and Fourier transforms .....	24
3.2.2 Experimental set-up.....	29
3.2.2.1 Securing the test specimen and the shaker to the test bench .....	29
3.2.2.2 Choosing hammer tip .....	29
3.2.2.3 Choosing distance of measurement .....	32

3.2.3	Parameter set-up .....	34
3.2.3.1	Signal averaging .....	34
3.2.3.2	Filter .....	37
3.2.3.3	The sampling rate, FFT lines, and Bandwidth .....	40
3.2.3.4	Window function .....	54
3.2.3.5	Conclusion for parameter setups .....	72
3.2.4	Measurement parameters .....	72
3.2.4.1	Choosing measurement area.....	72
3.2.4.2	Choosing excitation point.....	76
3.2.4.3	Generator's signal .....	79
3.2.4.4	1/3 Octave band .....	81
3.2.5	Final setup for the thesis's measurements .....	82
3.3	Measurement procedure.....	83
4	Result .....	84
4.1	Reproducibility.....	84
4.2	Different filling volumes .....	84
4.3	Usage of packages .....	88
5	Conclusion and discussion .....	92
6	References.....	93



# 1 Introduction

In this section, the motivation for the thesis will be presented. Afterward, the desired goals and the outlines of this document will be explained.

## 1.1 Motivation

Vibration is generally defined as oscillation over an equilibrium position, where it has been studied in various fields. By itself, vibration is neither good nor bad, but rather, it depends on the particular cases. For example, speech, one of the primary ways for humans to communicate, is transmitted by disturbances in the air. The motion of a pendulum leads to the production of the first precision timekeeping tools in the 1660s, which can be seen as a beneficial vibration.

However, more often than not, vibrations should there are situations that it is not desirable. The oscillation of a work piece is linked toward cyclic stress, which is linked toward fatigue (Callister & Rethwisch, 2014). The more vibration is generated, the more serious the fatigue will become, leading to a decrease in its useful lifetime. Another issue is the noise generated by vibrations of structures, the field studying this effect is called **Vibro-acoustics** (Nilsson & Liu, 2015). Within the wind turbine industry, it is also known as **mechanical noise**, coming from the operation of components such as the gearbox or generator (Wagner, et al., 1996).

The wind energy industry in particular, or renewable energy in general, is being invested heavily in recent years in various countries and regions. The list includes entries such as China and EU (Ydersbonda & Korsnesb, 2016), Viet Nam (Curto, et al., 2020), and more. This importance results from a combination of different reasons, including the depletion of fossil fuels for traditional thermal power plants in a century (Shafiee & Topal, 2009), a target for a low greenhouse gas emission according to the Paris Agreement (United Nations, 2015), or even a carbon-neutral emission target for European Union in 2050 (European Commission, 2018). However, certain barriers are preventing an immediate and large-scale application of wind energy. These issues include social acceptance (centering around noise and the allowed distance to wind turbine farms), logistics and building, as well as political and economic support (McKenna, Leye, & Fichter, 2016). Among these problems, suppressing the sound can be considered as an important and critical job.

As mentioned above, a vibrating surface can generate noise, which means if the vibration is damped, the noise would also be reduced. Broadly speaking, there are two main groups of solutions: passive and active. The difference between them is that passive devices require no power source to operate.

For an active system, three components would be deployed: sensors, actuators, and a controller. The response of the system is measured by the sensors, the result of which is used to drive the actuators. Generally, an active system is associated with higher costs and failure risks due to having more complex and specialized components. Meanwhile, a passive system would be easy to produce, more cost-effective, and more durable, which leads to its widespread application within various industry fields (Prasad, et al., 2020).

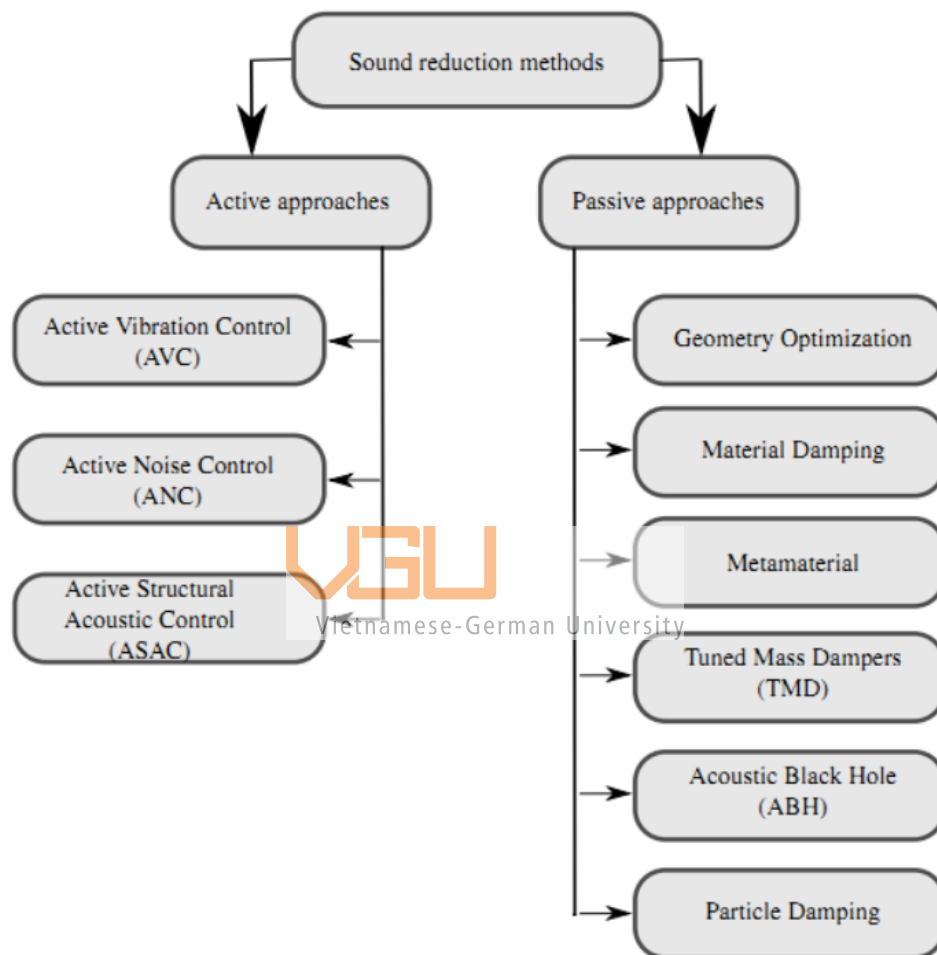


Figure 1-1: Different possible solutions for sound reduction methods (Prasad, et al., 2020)

Among the listed passive methods above, particle damping is a topic of interest. This damper’s function is based on using granulated material to absorb the kinetic energy of the excitation via friction and collisions, and there are several pieces of research applications into civil engineering (Chen & Georgakis, 2013; Zhang, et al., 2015; Papalou, et al., 2015) or automotive engineering (Xia, et al., 2011; Koch, et al., 2017).

This thesis will attempt to investigate the potential of vibration suppression using particle damping concerning a wind turbine generator component via experiments. If the vibration reduction is

effective, a study with large scale and more details can be launched, paving the way for full application into the wind turbine industry.

## 1.2 Goals of the thesis

The goal of this thesis is to experimentally evaluate the vibration reduction of particle damping on wind turbine generator components. To be more specific, the test specimen is a scale model from a section of the generator ring and stator arm, and the transferred part of the excitation will be investigated.

The material chosen for this thesis is a granulated rubber, prepared beforehand by OvGU. The damping effectiveness will be compared between different volumes of material, and between the same volume being shared among different balloon sizes.

## 1.3 Outline of the thesis

The document contains the following important parts:

Chapter 1 would introduce the background of this thesis as well as its objectives.

Chapter 2 is the State of the art, reviewing the main issue of the problem (the vibration and the mechanical sound of the wind turbine components during operation) as well as the general overview of the particle damping.

Chapter 3 is the Experimental method, how and why the tests and experiments being set up and carried out. The main method of the experiment (based on Laser Doppler Vibrometry and Signal Processing) will also be described and investigated. This chapter will also provide the arguments on why and how different parameters are applied for the experiments.

Chapter 4 will analyze the result of the main experiment, comparing the damping effectiveness of particle damping at different volumes, or the same volume but being packed differently.

Chapter 5 is the conclusion and discussion, to analyze the result and the prospects of particle damping for the wind turbine industry in particular.

## 2 State of the art

This chapter will provide a general and overall look at the current scientific knowledge on the related topic, including the noise sources on wind turbine (and brief current solutions being applied in the industry) and particle damping (the history, the definition, the advantages as well as current usage).

### 2.1 Vibration and sounds of wind turbines

Sound is defined as a mechanical and longitudinal wave traveling in a medium (usually air), which means that sound itself is a form of vibration. Under wind load and working conditions, various components of the wind turbine would be vibrating. The oscillating surface of the body would lead to the alternating compression and expansion of the air surrounding it, resulting in the vibration of air molecules. Thus, the sound is born from any sufficiently vibrated surface. This leads to the conclusion that if the mechanical vibration is damped, the movement of the surface would be smaller, and the noise would also be minimized.

As mentioned earlier, the vibration of the wind turbine is of interest in this thesis. The main reason for this is the increasingly widespread usage of wind energy. Countries and regions around the world have been investing in wind energy and other renewable energy, as a supplement and as a replacement for traditional fossil fuel power plants. In certain conditions, wind energy can supply the entire power demand for the region. The statistical report released by BP PLC in 2020 on energy production and consumption in 2019 shows that wind energy is the renewable energy with the highest growth (1.4 EJ), partially contributing to the largest increment of renewable energy as the whole. Data analysis also shows that wind energy accounts for about 2.5% of global power production.

However, there are a few concerning problems, the most common of which is the noise generated during the operational time of the wind turbines. Multiple works carried out over the years, for example, by Schmidt and Klokker in 2014, by Saavedra and Samanta in 2015, and by Michaud et al. in 2016, conclude that there is no concrete proof for any adverse health effect or major concern caused by these noises. The same studies would also note that there is a link to annoyance, lack of sleep, and possibly other psychological distress.

As mentioned above, the sound is generated from a vibrating body, and in a wind turbine, the noise can be generated from the vibration of mechanical components in the system. In late 2018, Escaler and Mebarki summarized a vibration study done on seven wind turbines of the same design from the

same on-shore wind turbine farm. In this study, components, such as the three turbine blades, the rotor, and the gearbox, influence the vibration characteristic in their unique way. The generator is shown to have the highest vibration amplitude, recorded at 84 times the frequency of the high-speed shaft of the gearbox. Furthermore, damaged wind turbines would show a much greater vibration amplitude compared to the average of the healthy ones.

An earlier work in 2017 by Mollasalehi et al. shows that when the wind turbine is not working, there will be no vibration of significant amplitude at frequencies above 2 kHz. During operation, the vibration amplitude can be increased by a factor of 10 compared to parking conditions, reaching a value of  $\pm 0.1$  g. In addition, most of the vibration is within the low-frequency range. The work also studies the sound pressure level inside the wind turbine tower on the ground level, which is indicated to be over 82 dB in operational condition, and the contribution of faulty generator bearing is stated to be nearly 68 dB. When the wind turbine is off, the pressure is just 61 dB.

On the topic of noise emitted from the wind turbine, one early work comes from Wagner et al. in 1996. In this book, two major noise mechanisms of the wind turbine are identified: mechanical and aerodynamic noises. The first is generated from machinery components, while the second from the turbine blades traveling through the air. The technical concern of this thesis is on the former.

For mechanical noise, there are two transmission paths, airborne and structure-borne. These are termed a/b and s/b in the figure below. The main component of mechanical noise comes from the gearbox, where factors such as imperfection in gear pitch, the form of meshing teeth, or gear shape would play a role in the final sound pressure level. This type of noise is considered to be tonal.

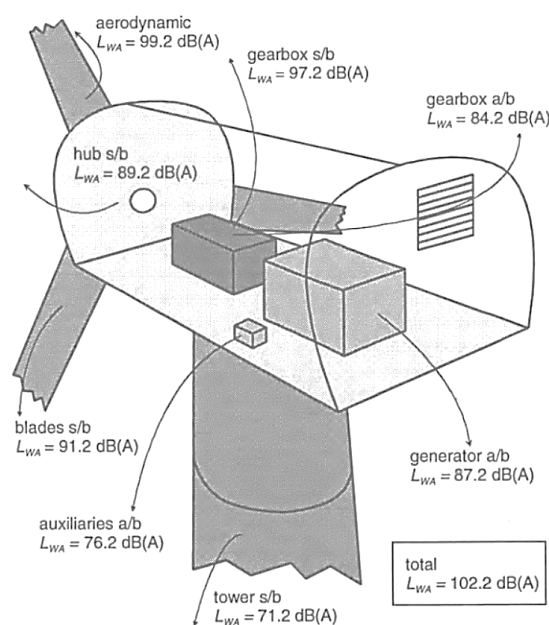


Figure 2-1: Contribution to the total sound power level of a wind turbine (Wagner, et al., 1996)



Regarding aerodynamic noises, there are different physical principles and processes involved. However, this is not within the scope of the thesis. The book also cites another noise source, which is the low-frequency noise, which is generated when the rotating blades meet the airflow field around the cylindrical tower. This encounter would lead to a rapid change in blade loading and the noise generated here can be very high for downwind turbine. This type of noise is also credited with annoyance and excitation vibration of building structures.

In a later chapter of the same book, the authors suggested a few solutions to mitigate the noise, examples include using serrated trailing edges for the turbine blades, modifications of the tip shape, and reduction of tip shape and angle of attack.

Jianu et al. revisited the topic in 2012, with an emphasis on the prevention of noise pollution. In this paper, two major noise sources are identified: mechanical and aerodynamics. The definitions of mechanical and aerodynamic noises remain the same. Regarding damping the former, the author suggests using different control laws, increasing effective mass, using sound-isolating materials, insulation, or closing the holes in the nacelles. Fault diagnostic is also credited as a potential solution. In combination, these methods would help to suppress the unwanted vibration of different components, helping to suppress the mechanical noise.

In 2015, Saavedra and Samanta also researched this matter and noted that mechanical noises can be ignored because modern gearboxes are very quiet. This means that the wind turbine sound would come mostly from the blades (or aerodynamic noise). However, the classification of different aerodynamic noises and how to minimize them, as stated before, is not a part of this thesis's target. The author also provides another way to classify wind turbine noise: by type, rather than by source.

Table 2-1: Summary of Wind turbine noise types (Saavedra & Samanta, 2015)

Type	Description
Tonal	Noise at discrete frequencies
Broadband	Continuous distribution of sound pressure
Low-frequency noise	Noise with a frequency between 20 and 100 Hz
Infrasound	Noise with frequency under 20 Hz
Impulsive	Short acoustic impulses or thumping sound with time-varying amplitude

Regarding vibration and noise reduction techniques, the paper provides some examples, such as gearbox design, upwind rotor wind design, as well as fault detection using vibration analysis.

## 2.2 Particle damping

One recent and comprehensive study on the history and working principles of Particle damping (PD) is done by Lu et al. in 2018. According to the paper, the earliest trace of PD can be found in 1937, where the damper contained a single particle, resulting in high noise levels and significant impact forces. The concept was improved in 1945, turning into an impact damper, where the moving mass would eliminate the vibration of mechanical systems. However, the applications were still limited. Starting from the 1960s, more researches were carried out, and by varying the number of units and particle per units, four distinct but still related types of dampers were made: impact damper, multi-unit damper, PD, and multi-unit PD. These are components a to d respectively in the figure below.

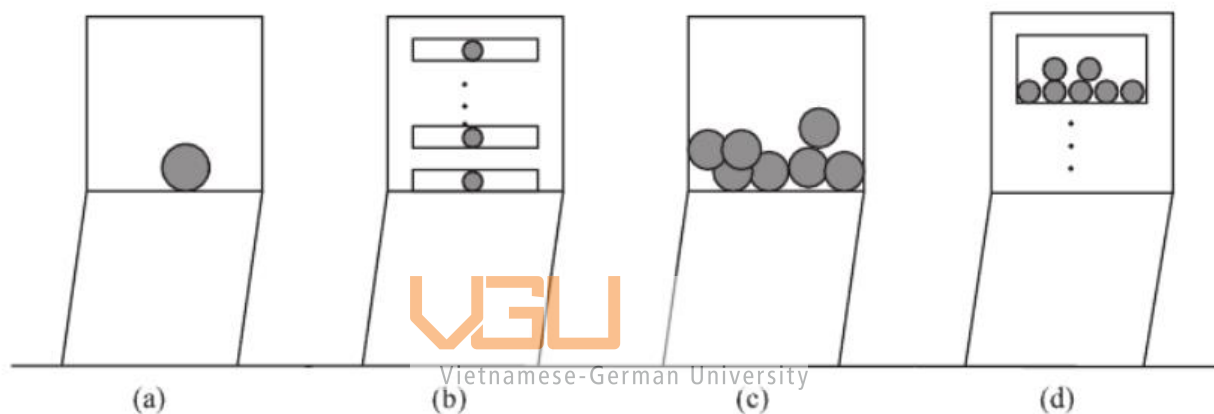


Figure 2-2: Classification of particle dampers (Lu, et al., 2018)

These four types are considered as basic traditional types of PD in the paper, and with improvements made over the year on different aspects, three other general variants are made: the configuration improved type, the material improved type, and the combination type.

Another work, done by Gagnon et al. in 2019 approaches the classification in another manner, with five sub-groups being made: single unit, multi-unit, non-obstructive particle damper, tuned particle damper, vacuum-packed particle, and fine particle impact damper. This paper also cites alternative names for particle damping, including acceleration damping, multiple impact damping, multi-particle damping, granular damping, granular-fill damping, and shot damping.

Regardless, both of these papers and others share the same definitions on the working principle of the particle damping system. Lu et al. state that the kinetic energy of the primary structure's vibrations would be absorbed remarkably thanks to a combination of particle-to-particle and particle-to-wall inelastic collisions and frictional losses. This would result in a net damping effect. Gagnon et al. cite the following mechanisms for the dissipative of vibrating energy of the system: impacts

between the particles and the wall, and among the particles themselves, as well as rolling and sliding frictions between the same. An earlier work in 2000 by Friend and Kinra attributes the damping effect to inelastic collisions between the particles and the walls, and amongst the particles themselves. These impacts would convert a part of kinetic energy into heat and thus damp the vibration.

The advantages of using particle dampers have been comprised by the cited works of Lu et al. and Gagnon et al. above. The former lists advantages such as conceptual simplicity, moderate cost, fine durability, insensitive toward temperature, and capable of working over a broad range of frequency even in harsh environmental conditions. PD is also considered as a low-maintenance option and requires few modifications for installment. Gagnon et al. add a few other benefits to that, including having negligible sensitivity to oil contamination, low weight impact can function without any power, can be designed to be sensitive in the principle direction only, and being efficient at different forms of excitation.

These advantages lead to an increasingly widespread application of particle damping. One of the latest studies is application into the spacecraft industry carried out by Ye et al. in 2019. The test specimen in question is a component of a spacecraft, consisting of three sub-parts (wheel, base, and bracket), made of aluminum with a net weight of 11.07 kg, and roughly 30 cm in all directions. The particle damper is mounted on the top of the bracket.

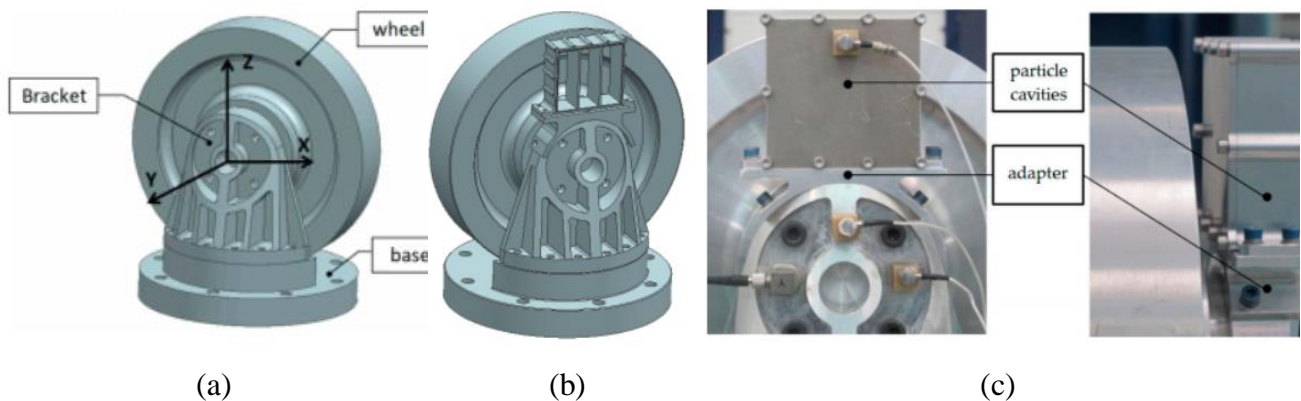


Figure 2-3: Original test specimen (a), Connection scheme of particle cavities (b), Bracket structure of test model (c) (Ye, et al., 2019)

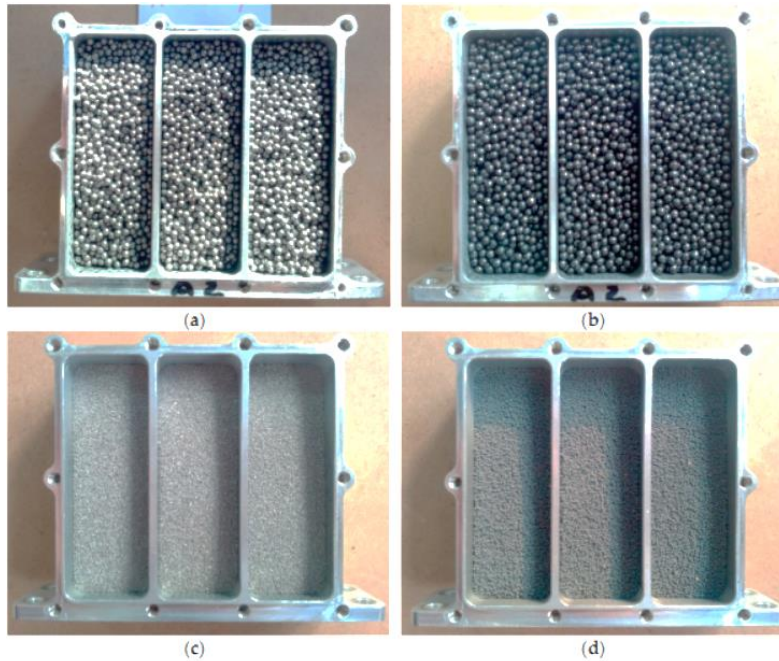


Figure 2-4: Particle filling: 2mm stainless steel particles (a), 2mm lead particles (b), 0.048mm stainless steel powder (c), 0.5mm tungsten carbide powder (d) (Ye, et al., 2019)

The damping effectiveness is compared between the same volume of particle, but from different materials (2mm stainless steel particles, 2mm lead particles, 0.048mm stainless steel powder, and 0.5mm tungsten carbide powder) and different layout of the cavity (up to two layers in the horizontal excitation direction, and up to five in the vertical direction). The total mass of the particle damper is always under 1 kg, which corresponding to a mass ratio of 8.8%.

The study concludes that more than 50% of the vibration can be damped, with the most effective material is tungsten carbide powder, at two filling layers in the main excitation direction. Layering the cavity in this direction can improve the damping effectiveness, especially when the vibration in this direction is large enough.

In the field of automotive, several researchers are investigating the effectiveness of particle damper. In 2017, Koch et al. has applied PD to the oil pan of a combustion engine. With an attached honeycomb structure filled with sand attached to the bottom, the more filling material there is, the damper the vibration becomes, this also leads to a reduction in sound. Up to 10 dB of vibration speed can be damped at 1095 g of sand filling, and the most effective vibration reduction per mass is found at 310 g. Regarding sound reduction, 2 dB can be removed at half-load condition, which shows certain promises for future application.

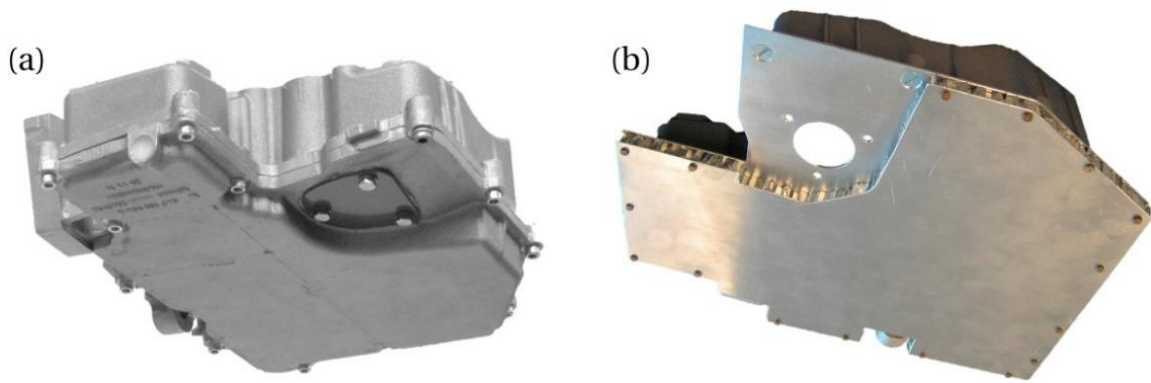


Figure 2-5: (a) the original oil pan bottom and (b) the structure partially filled with sand (Koch, et al., 2017)

An earlier work in 2011 by Xia, et al. also sees the effectiveness of PD in reducing the noise and vibration of a brake drum. In this study, the selected brake drum is 866 mm in diameter, 240 mm in width, and 16 mm in wall thickness is experimented on. The material chosen for this study is 3 mm spherical steel particles, and the study would compare experimental and simulation results. The conclusion shows that the simulation result matches with the experiment, proving a correct algorithm and parameter selection. Further, at the first natural frequency, the most effective filling ratio would be 70%, while for the second mode, the damping effectiveness increase with the filling ratio. The size and the number of cavities are also related to the damping ratio, the larger and the more holes available, the more damping is reached.



Figure 2-6: Brake drum with cavities on the wall for application of particle damping (Xia, et al., 2011)

PD has also been applied to various work tools. In one letter to a scientific journal's editors in 2004, Xu, et al. drilled multiple holes in diameter on the plates and the shafts of the banknote processing machine, then filled them up with 0.5 mm tungsten carbide particle. Application of PD on all positions leads to a damping of over 40 dB in the response of the structure in the frequency range of 4 to 6 kHz. The effective noise reduction is 6 dB(A), decreasing from 89 to 83 dB(A).

Another work is carried out later by Heckel, et al. in 2012, where PD is used to reduce the vibration of an oscillator saw. In the experiment, the saw is suspended by strings in a solid metal frame with accelerometers being attached next to the blade and on the top of the handle to evaluate the strength of the vibration. Two dampers are used in this experiment, each consists of 46 cavities, and each cavity contains 9-23 steel balls of diameter 2 mm. The weight of the saw (without damper) is 1 kg with the total mass of the damper is 180 g.



Figure 2-7: An oscillatory saw with prototype particle dampers attached (Heckel, et al., 2012)

The experimental result shows that the dampers are more effective in damping than a solid body of the same mass. The root-mean-squared acceleration can be reduced from  $1 \text{ m/s}^2$  to 0.75 with 2 dampers used, compared to 0.95 by using a single solid of the same mass. Furthermore, peaks of the power spectrum in the frequency domain can be reduced by 10 dB.

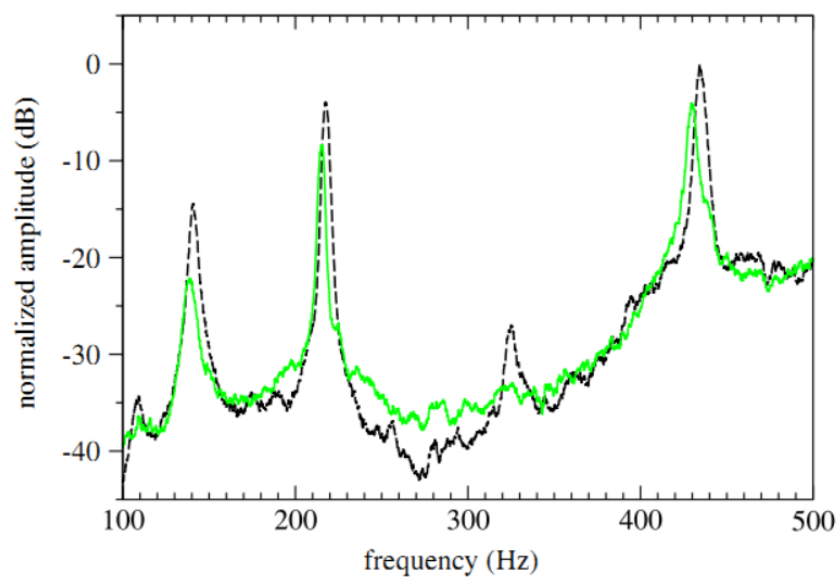


Figure 2-8: Power spectrum of the oscillatory saw at high power, with (green solid line) and without (black dashed line) particle damper applied (Heckel, et al., 2012)

Within the field of civil engineering, PD has also been studied in several studies, including for wind turbines, both on-shore, and off-shore, as well as other marine-related structures. In 2015, Zhang et al. applied a variant of PD, named Pounding Tuned mass damper to damp the vibration of a subsea jumper pipeline, typically used in the oil industry. Instead of multiple small particles, this system uses a single mass block.

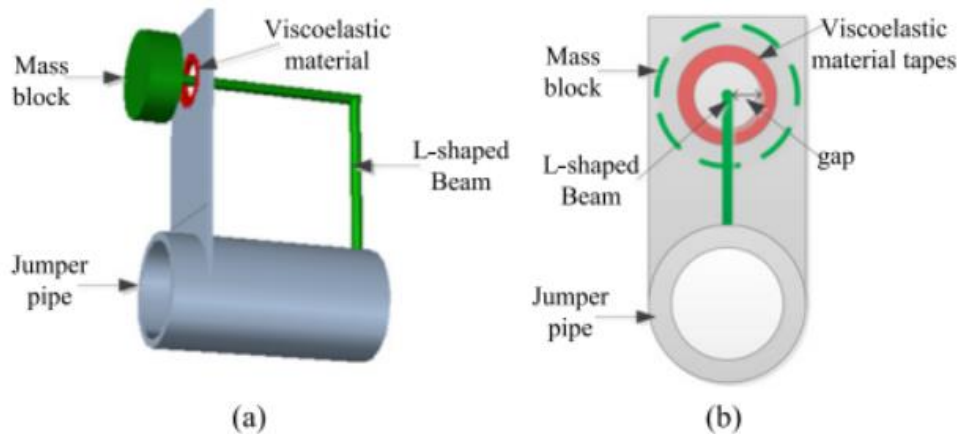


Figure 2-9: Pounding tuned mass damper (Zhang, et al., 2015)

The study is done from both simulation and experimental approaches, where the results match each other quite well. The data shows that increasing the pounding stiffness from 5000 to 50000  $\text{Nm}^{-3/2}$  would increase the damping effectiveness by 50%, and when the mass ratio of 2% can reduce the vibration by nearly 90%, showing a highly promising potential of this damper.

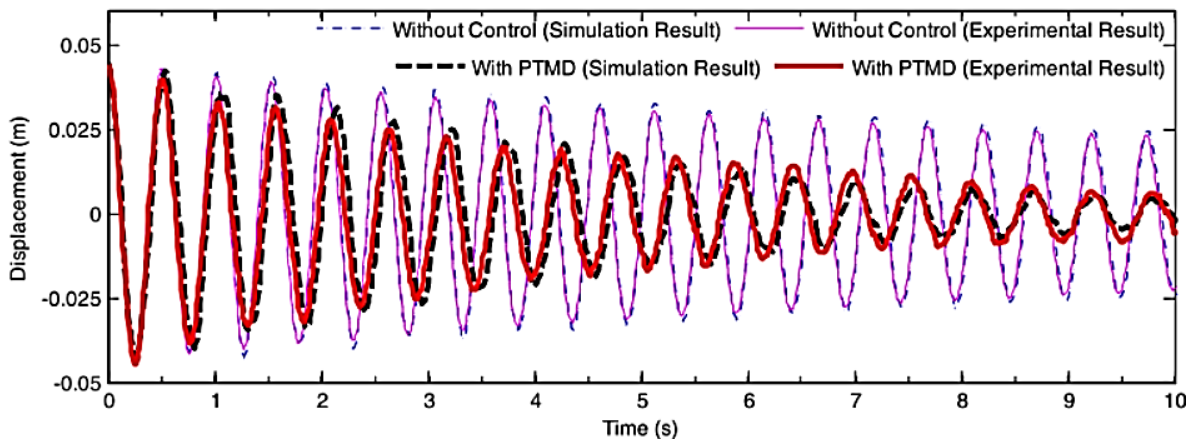


Figure 2-10: Displacement of the jumper in the free vibration test (Zhang, et al., 2015)

Earlier in 2013, Chen and Georgakis also used this Tuned mass damper variant in their study. The damper consists of one or multiple steel balls rolling in a container. Due to the restriction of laboratory size, a scaled model of 1/20 of a wind turbine is used. The damper would contain either a single large steel ball (4.1 kg) in a spherical container or multiple smaller balls (0.716 kg) in two

hemispherical of the same radius. The low-frequency range (around 1 Hz) is of specific concern in this study.

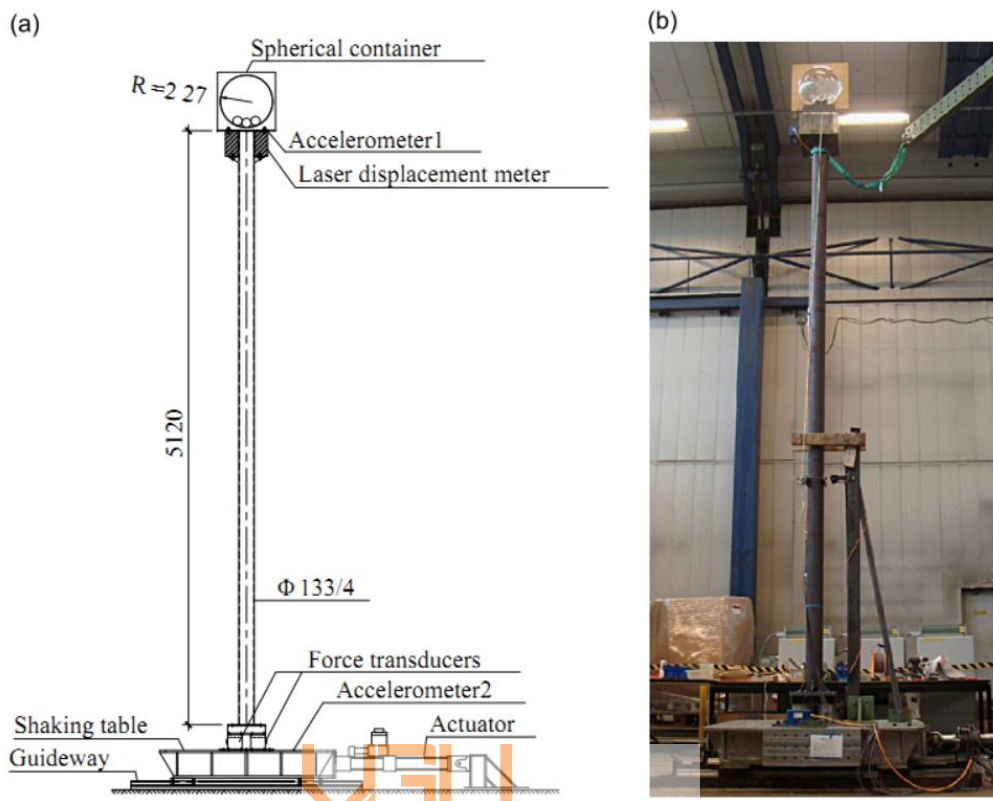


Figure 2-11: Shaking table setup in scheme (a) and actual view (b) (Chen & Georgakis, 2013)

The result of the experiment shows that for harmonic forced vibration, the ratio between the max displacement at the top and the amplitude of the excitation can be significantly reduced, from off-the-chart reading to a factor between 10 and 16 times. The study also concludes that this damper can work in all horizontal directions, making it a good candidate for off-shore wind turbines, and the best control effectiveness can be achieved with three small balls in a single layer of the container.



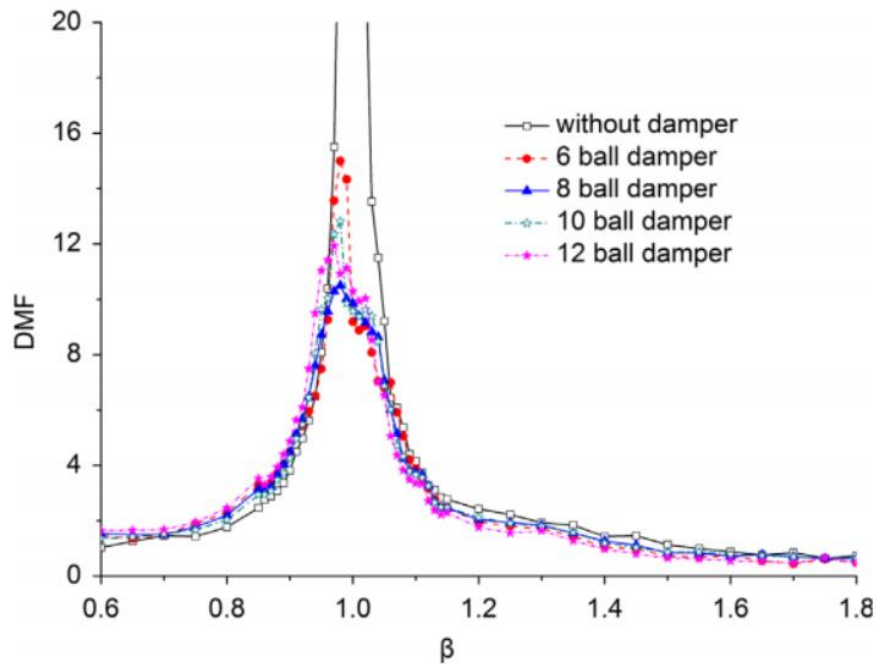


Figure 2-12: Displacement frequency response of the model without and with damper (Chen & Georgakis, 2013)

Recently, a few more works have been done using the traditional definition of PD, including a work done to study protection against earthquake on a marble temple column by Papalou, et al. in 2015, and another by Sandanshiv and Chavan in 2019 investigating the effect of damping on a wind turbine.



Vietnamese-German University

Papalou, et al. considered using PD within a multi-drum marble column (where the column is not a monolithic piece), using two different sizes of steel spherical particles: 20 and 50 mm. In the figure below, the 50 mm particles are being used. A model of scale 1:3.3 from a temple column is used, 2992 mm in height and 1707 kg of weight. The top drum is 445 mm in diameter, and 584 mm for the bottom one. Each of the 11 drums has the same height of 272 mm. PD would be applied to the 7<sup>th</sup> or the top drum. The mass ratio of the damper would be compared between 0.7%, 1%, and 2%.



*Figure 2-13: Experimental set up to study the seismic protection of PD (Papalou, et al., 2015)*

Two main excitation forms are used in this study: random and earthquake-like excitation. Under random excitation, PD can effectively reduce the response when it is put above mid-height level, especially when the particles have enough space to move and there is a sufficient amount of particles inside the drum. Generally, a filling ratio of 40 to 60% and a mass ratio between 1 and 3% would lead to a considerable reduction in the vibration. In this scenario, there is no appreciable difference between using 50 or 20 mm steel particles. The most effective scheme is to use 32 50-mm-in-diameter particles in the top drum (1% mass ratio). This scheme is used in the next part of the study, where under the earthquake excitation, the vibration can be reduced by 40% compared to the original column. The damping ratio is also increased from 2.6% to 4.8%. Further work in the study also simulates the degraded condition of the column by inclining it to 2%. The experimental result shows that the vibration reduction is even higher, at 50%. These results show promising leads to applying PD into civil engineering, especially within the topic of conservation of historical sites.

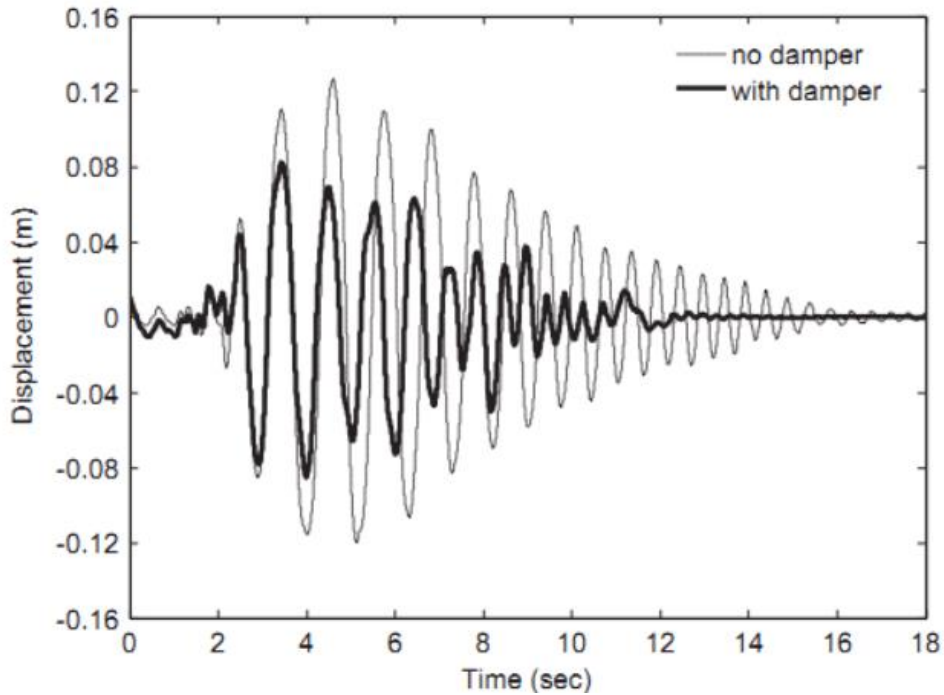


Figure 2-14: Displacement of the column under earthquake excitation (Papalou, et al., 2015)

In 2019, Shandanshiv and Chavan attached a particle damper on the wind turbine blade to study the damping effectiveness. The particle being used in this study has a diameter of 9 mm and is used in a plastic cylindrical container with a diameter of 48 mm and a height of 28 mm. An actual small-scale wind turbine (1 kW) is used in this study. The damper would be attached at different distances from the tip of the blade, and the vibration suppression effectiveness would be compared at different rotational speeds of the rotor.

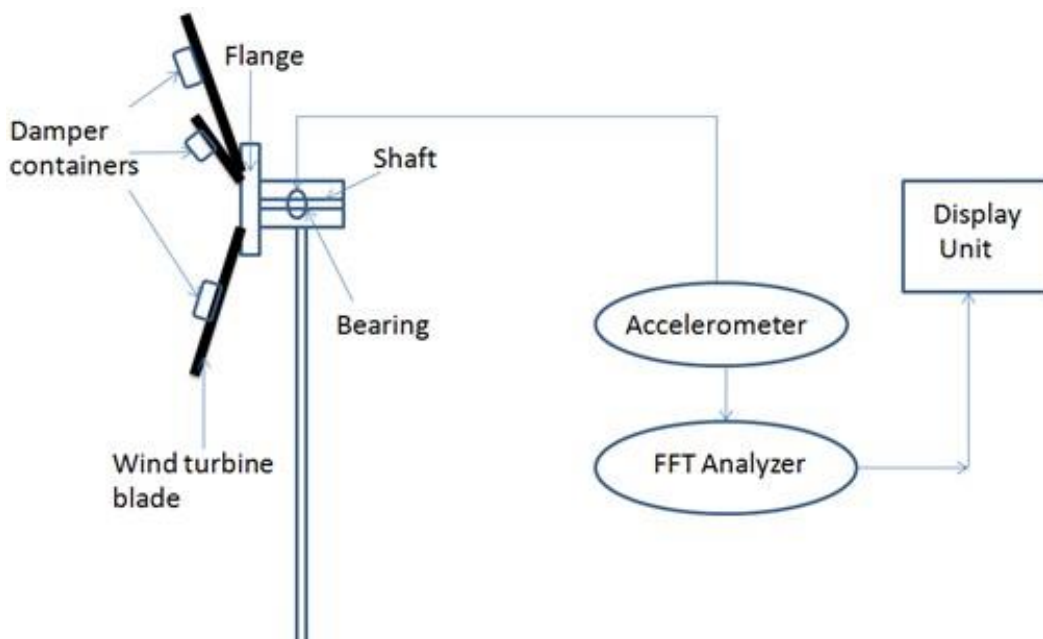


Figure 2-15: Experimental scheme of attaching the particle damper on turbine blade (Sandanshiv & Chavan, 2019)

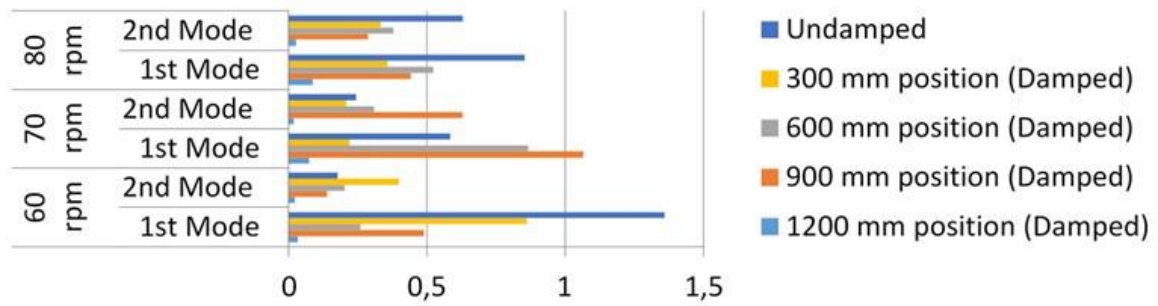


Figure 2-16: Combined results of undamped and damped cases (Sandanshiv & Chavan, 2019)

The result shows that by applying the particle damper 1200 mm from the tip (which is quite near the rotor shaft), the vibration of the turbine blade would be heavily suppressed and damped.

From the above studies, it can be said that particle damping is an effective damper, requiring no power yet still yield considerable (and in many cases almost total) vibration damping effect.

# 3 Experimental method

This chapter would focus on detailing the method used to run the experiment. The sections would explain the basic working principle of the laser scanner (section 3.1), and how to set up the measurement parameters in the thesis (section 3.2).

## 3.1 Laser scanning vibrometry

### 3.1.1 Doppler effect

In this project, the vibration of the specimen (or to be more precise the vibration speed of the surface) would be measured by a laser, the scientific principle of this process is based on the Doppler effect (Polytec GmbH, 2011). Simply explaining, the Doppler effect is the shift of the wavelength when the source moving toward or away from the observer (eFunda, 2019). A brief description of the Doppler effect can be seen in the figure below:

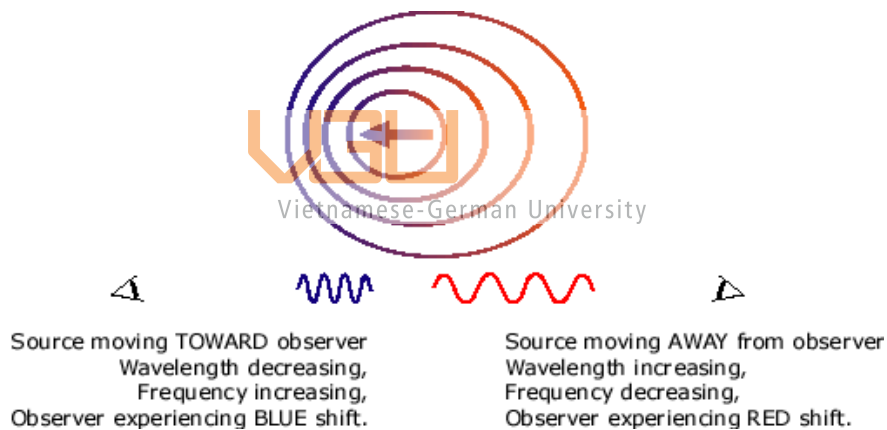


Figure 3-1: Doppler effect (eFunda, 2019)

In simpler term, the Doppler effect can be interpreted as follow. When the surface is moving toward the laser scanner, the reflected laser will have a shorter wavelength. The higher the speed, the more the difference will be. The shift here will be measured by the laser scanner, which allows the computer to calculate the current vibration speed of the specimen.

The measured frequency shift can be calculated with the following formula

$$f_D = \frac{2v}{\lambda} \tag{3-1}$$

in which:

- $f_D$  is the measured frequency shift

- $v$  is the vibration speed
- $\lambda$  is the wavelength of the emitted laser

To be able to conversely determine the velocity of an object, the (Doppler) frequency shift has to be measured at a known wavelength. This is done by using a laser interferometer.

### 3.1.2 Interference

The Laser Doppler Vibrometer works with the principle of laser interference, where two laser beams (reference and measurement beams in this case) overlap with each other (Polytec GmbH, 2011). The total intensity can be calculated by:

$$I_{\text{total}} = I_1 + I_2 + \sqrt{I_1 I_2} \cos \frac{2\pi(r_1 - r_2)}{\lambda} \quad 3-2$$

### 3.1.3 Scanner head

For a Laser scanning vibrometer, the system consists of three Beam splitters, one mirror, and one lens. Furthermore, it also has a laser source and an optical detector. The overall set-up can be seen in the figure below.

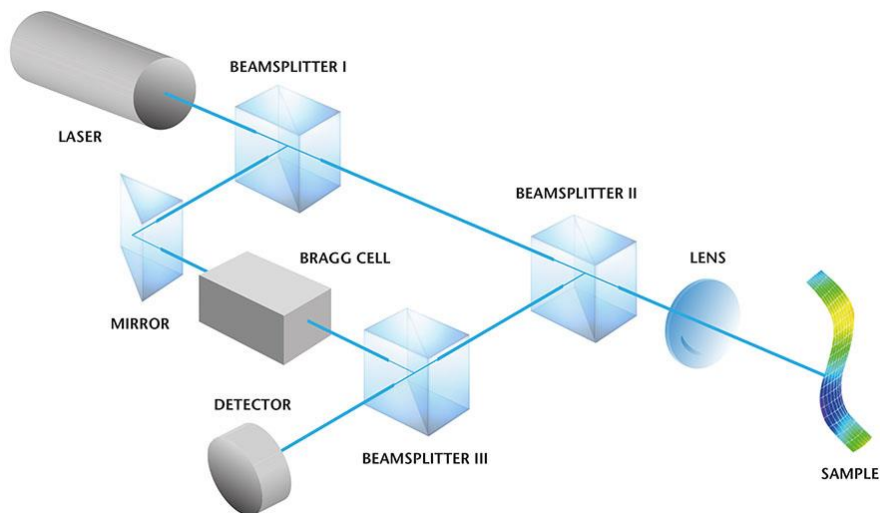


Figure 3-2: Overall structure of the Laser Doppler Vibrometer (Polytec GmbH, 2011)

Per the description from the manufacturer (Polytec GmbH, 2011), the system starts by having the Beam splitter I dividing the laser source into a reference beam and measurement beam. The reference beam is transferred to the optical detector with the help of the mirror, while the measurement beam is

sent toward Beam splitter II and the vibrating surface. From here, the beam is reflected back and finally merges with the reference beam on the detector.

The measurement before reaching the vibration surface would pass through a Bragg Cell, which would shift the frequency of the beam by 40 MHz. For comparison, the laser employed is a helium-neon laser, which has a frequency of  $4.74 \times 10^{14}$  MHz (or a wavelength of 632 nm). This would allow the direction of the movement to be detected.

Considering Equation 3-2, because the path of the reference beam ( $r_2$ ) is constant, the difference would only come from the variations of the path of the measurement beam ( $r_1$ ). This would lead to a changing of patterns of light/dark cycle on the photo-detector, and each of the cycles means that the vibration displacement is half of the wavelength used in the scanner (or 316 nm). The resulting interference here would be converted into an electrical signal by the photodetector and decoded into the controller unit.

## 3.2 Setting up the parameters

This section would detail the setting up process, namely why and how the experiment is set up. Various measurements are carried out to study the effects of parameters so that the final configuration can be chosen and set up.

### 3.2.1 General parameters

#### 3.2.1.1 Test specimen

As mentioned in section 2.2, there is one paper citing that mechanical noises have been greatly suppressed thanks to the more modern gearbox and generator designs. Therefore, this study should focus more on the turbine blade for the vibration suppression effectiveness of PD. However, it should also be noted that the usage of particle damper is broad and proven, as various cited researches have shown. In other words, if using granulated materials can reduce the vibration of a blade, then it can also do the same for a scaled model of the generator ring and the stator arm. Between the two types of specimen, the latter is easier for manufacturing, assembling, storage, and filling of granulated material.

The 3D rendered image (obtained from the CAD program) can be seen in the figure below. The grey section represents the generator ring, while the red part is the model of the stator arm. The two parts are connected via bolt connections, selected for ease of use and maintenance.

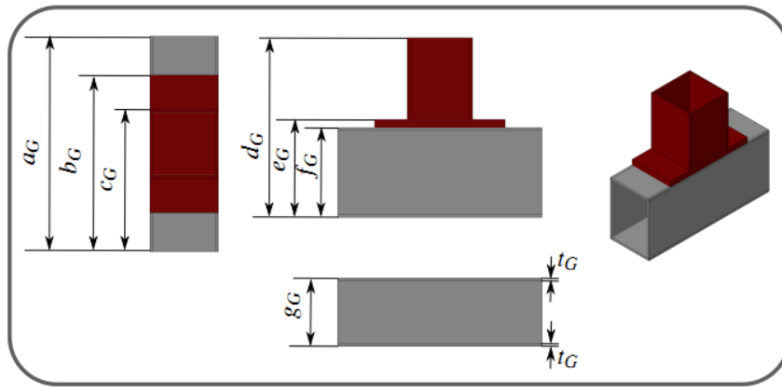


Figure 3-3: 3D visualization of the test specimen (Prasad, et al., 2020)

The value for each component is finalized as below:

Table 3-1: Dimensions of the test specimen

Dimension	Symbol	Value
Generator ring section length	$a_G$	30 cm
The distance from one end to the Stator arm's base on the other side	$b_G$	24.5 cm
The distance from one end to the Stator arm's side surface on the other side	$c_G$	19.5 cm
Overall height	$d_G$	27 cm
Generator ring profile height and Base of the stator arm	$e_G$	15 cm
Generator ring profile height	$f_G$	13 cm
Generator ring profile width	$g_G$	10 cm
Generator ring thickness	$t_G$	0.4 cm

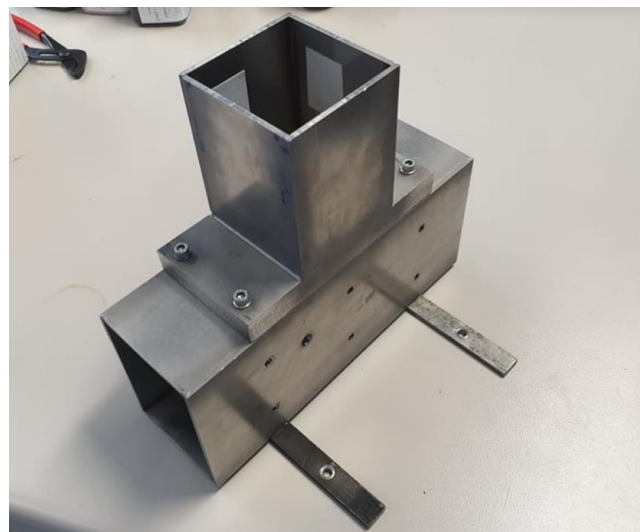


Figure 3-4: Assembled test specimen



The real image of the test specimen can be seen above. The two fangs at the bottom are the auxiliary components used to secure it into the test bench. The large hole on the side of the generator would be used to attach the force sensor to the test specimen. This would allow the usage of signals such as white noise or pseudo-random. However, for the actual experiment, an impulse (or a knock) would be given (see section 3.2.4.3 for the argument).

Due to the selection and construction of test specimen, the measurement of noise is not practical in this thesis. Here, only a scale model of the generator is built, which means that there is no functional component of any wind turbine. This means that there is no real noise level to be obtained as the base level to investigate the sound damping ability of particle damping.

### 3.2.1.2 Hardware used

For this thesis, the following equipment is used:

- A scanner head PSV-400 from Polytec GmbH
- The associate junction box, controller box, and software of the scanner head
- An electrodynamic TIRA shaker TV 50009 and its control module
- Different hammer tips (more detailed analysis in section 3.2.2.2)
- A force sensor
- A signal conditioner for the force sensor

The overview of the physical setup of the hardware involved can be seen in the figure below.

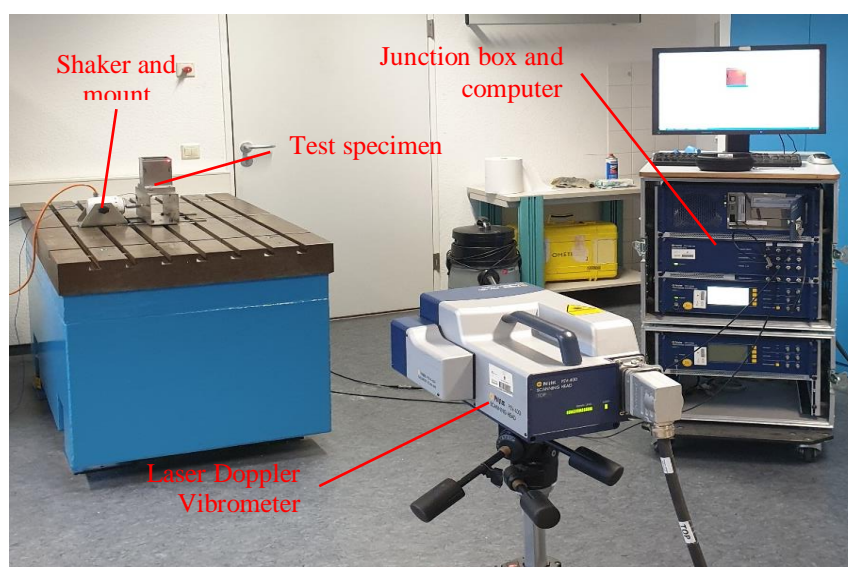


Figure 3-5: Overview of the hardware and equipment used



Figure 3-6: Signal conditioner for force sensor (left) and shaker controller (right)

### 3.2.1.3 Transfer function

As mentioned in section 1.2, this thesis aims to evaluate the effectiveness of using particle damping to damp transferred parts of excitation force within the test specimen. Thus, to clearly illustrate the effect, the transfer function is needed, which is defined as a ratio between the output and the input(s). Here, it is defined by the following formula:

$$\text{Transfer function } (H_{\Omega}) = \frac{\text{Output}}{\text{Input}} = \frac{\text{Surface vibrating velocity}}{\text{Input force}} \quad 3-3$$

The ratio between speed and force can be referred to as Mobility or Admittance (Brandt, 2011). It should also be noted that both the input and output here are calculated within the frequency domain. Thus, the transfer function would have the symbol  $H(f)$  and referred to as the “Frequency response function” in certain literature (Brandt, 2011; Nilsson & Liu, 2015). However, some materials cite that the two terms would have the same meaning (SIMCENTER, 2020), and can be used interchangeably. A normal transfer function would have two subplots, one for magnitude and the other for phase. However, the main concern within this thesis is on vibration reduction, thus only the magnitude plot would be used.

Both quantities (input and output) are given in the standard unit, which means m/s for the velocity (output) and N for the force (input). Thus, the unit for the transfer function would be m/s/N. However, a direct representation in this type of unit would have its trouble, namely the disappearance of small signals. For example, on a 10 cm screen, a distortion of 0.1% of the signal would lead to a harmonic of 0.1 mm only. This would lead to difficulties in measuring and analyzing. Therefore, the logarithmic scale is needed, which would compress large signals and

expand small signals. An example of this could be seen in Figure 3-7 below. The 0.1% distortion is now converted to a peak of -60 dB, occupying a quarter of the screen instead of a thousandth.

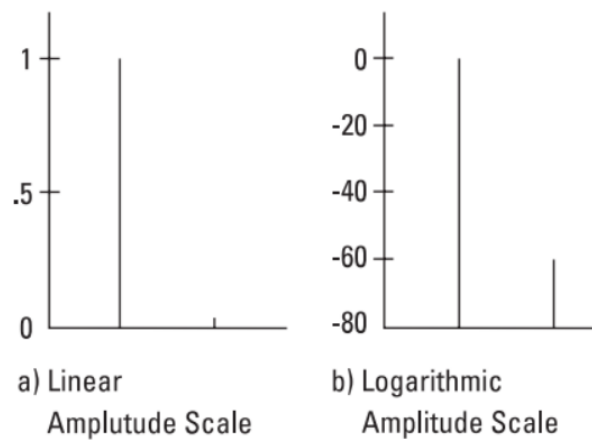


Figure 3-7: Measuring in linear scale (a) and logarithmic scale (b) (Hewlett Packard, 1989)

The formula to calculate dB is generalized as:

$$\text{dB} = 10 \log(\text{Power ratio}) = 20 \log(\text{Voltage ratio}) \quad 3-4$$

For this thesis, the transfer function is converted from linear scale (in m/s/N unit) to logarithmic scale (in dB unit) with the following formula, where the Reference value of the Transfer function is set at  $1 \times 10^{-6}$  m/s/N.



$$\text{dB} = 20 \log \left( \frac{\text{Numerical value of the Transfer function}}{\text{Reference value of the Transfer function}} \right) \quad 3-5$$

### 3.2.1.4 Frequency domain, Fourier series, and Fourier transforms

In this thesis, the vibration measurement (or to be more precise, the transfer function as concluded by section 3.2.1.3 above) would be observed in the frequency domain. There are two main reasons for this: the frequency domain can illustrate the distribution of the signal's energy over a range of frequency (The MathWorks, Inc., 2015), and shows a small wave in the presence of a large signal (Hewlett Packard, 1989). Visually, both of these reasons can be represented by having different amplitudes for different peaks in the frequency spectrum.

The main goal of using the frequency domain is to obtain the major characteristic of the vibration, including the frequency (how frequent or how fast vibration is) and the amplitude (how far or how long a vibration is moving). This information cannot be obtained from the time domain data, at least for a complex vibration like the one shown by the test specimen here. To solve this problem, it has to be broken down into simpler components, which could be done via the mathematic principle

developed by Jean Baptiste Fourier (1768 - 1830). Fourier's theorem states that any periodic function can be represented by an infinite sum of sines and cosines. Its mathematical representation is referred to as the Fourier series (Weisstein, 2008). An illustration can be seen below:

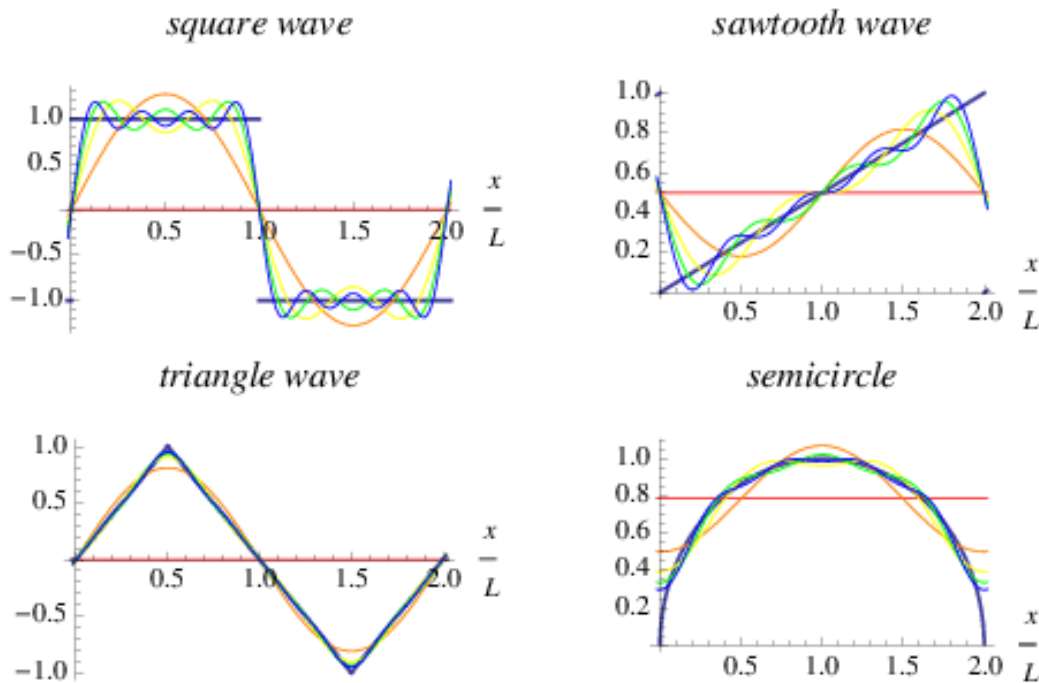


Figure 3-8: Using Fourier series to represent different signal waveforms (black line) (Weisstein, 2008)

In the above figure, the original signal in the black line is approximated using various numbers of trigonometry terms. The more terms being used, the more accurate the real signal being sampled and reconstructed. However, when there is a sharp transition (most evident in the square and sawtooth wave), the signal cannot be fully recreated with some ringing artifacts being made. This will play a role in choosing parameters (especially within section 3.2.3.3).

Concerning signal processing (both in general and with the specific application in vibration), the mathematical principle, represented by the Fourier series, is used to convert the signal from time to frequency domain. The Fourier series can be written in the form below:

$$f(t) = \frac{a_0}{2} + \sum_{k=1}^{\infty} \left( a_k \cos\left(\frac{2\pi kt}{T}\right) + b_n \sin\left(\frac{2\pi kt}{T}\right) \right) \quad 3-6$$

Due to the unknown time period T and the discrete sampling process, and  $a_k$  and  $b_k$  coefficients would be found via finite sums (a summation over the sample) (Hartin & Belanus, 1997). They are calculated as followed:

$$a_k = \frac{2}{N} \sum_{i=1}^n x_i \cos\left(\frac{2\pi ki}{N}\right) \quad 3-7$$

with  $k \geq 0$

$$b_k = \frac{2}{N} \sum_{i=1}^n x_i \sin\left(\frac{2\pi ki}{N}\right) \quad 3-8$$

with  $k \geq 1$

The magnitude and the phase at each discrete frequency (which can then be used to calculate the frequency response), can be calculated from these coefficients:

$$c_k = \sqrt{a_k^2 + b_k^2} \quad 3-9$$

$$\phi = \tan^{-1} \frac{b_k}{a_k} \quad 3-10$$

In addition, per Euler's formula, the connection between trigonometry and the complex number is also proven. Therefore, to illustrate the frequency effects in a system, one can also use complex numbers. This applies to DFT (Discrete Fourier Transform) and FFT (Fast Fourier Transform) algorithms below.

$$e^{ix} = \cos x + i \sin x \quad 3-11$$

Vietnamese-German University

This formula (and its variations) allow the Fourier series to be re-written in form of complex numbers. For convenience, it is assumed that the original signal is periodic, and the interval is from  $-T/2$  to  $T/2$ :

$$f(t) = \sum_{n=-\infty}^{\infty} c_n e^{i2\pi nt/T} \quad 3-12$$

$$c_n = \frac{1}{T} \int_{-T/2}^{T/2} f(t) e^{-i2\pi nt/T} dt \quad 3-13$$

Complex numbers are generally used in vibration analysis (or signal processing in general) because they are more effective and do not involve complicate trigonometry rules, this leads to easier data manipulation (Brandt, 2011; Shin & Hammond, 2008).

For application into this thesis, the signals (the vibration speed of the test specimen and the input force) can be converted from the time domain to the frequency domain via the mathematical principles of the Fourier series. However, in practice, only a limited measurement time is available and the data is sampled discretely (not continuously), the DFT method would be used instead of the

direct Fourier series (Kulkarni, 2016; National Instruments Corp., 2019). A more in-depth investigation and research on the differences between the two (and other related mathematical expressions) are out of the scope of this thesis.

While DFT is the practical application of Fourier series into signal processing, in realistic conditions FFT would be used, rather than DFT. This method is considered a simpler way, allowing the system to complete the task in a shorter time (National Instruments Corp., 2019). Assume that the original signal in the time domain can be divided into  $N$  equal periods (or  $N$  data blocks,  $N$  samples), DFT would take a processing time in the scale of  $N^2$ , while FFT only take a multiplication of  $N \log_2 N$  (Smith S. W., 1999; Shin & Hammond, 2008; Brandt, 2011). The effectiveness of this can be seen by comparing multiply and add operations in both processes, such as in the figure below.

Table 3-2: Number of multiply and add operations, FFT versus DFT (Shin & Hammond, 2008)

$N$	$N^2$ (DFT)	$N \log_2 N$ (FFT)	$N^2 / (N \log_2 N)$
16	256	64	4.0
512	262 144	4608	56.9
2048	4 194 304	22 528	186.2

Usually, the number of sample points  $N$  in the time domain would be a power of 2. The reason for this is that using an integer power of 2 would be simpler (Brandt, 2011). The software used in this thesis also follows the same principle.

For reference purposes, the formulas for DFT (Equation 3-14) and FFT (Equation 3-15) are cited here. However, this section and this thesis will not attempt to analyze the mathematical process behind them or go into in-depth analysis. Here, the formulas are written in exponential form and not trigonometric form, thanks to the application of Euler's formula:

$$X(k) = \sum_{n=0}^{N-1} x(n) e^{-\frac{i2\pi kn}{N}} \quad 3-14$$

$$X(k) = \sum_{n=0}^{N-1} x(n) (W_N)^{nk} \quad 3-15$$

where  $W_N = e^{-\frac{i2\pi}{N}}$

Using the above knowledge, the square wave signal (the black line in the top left part of Figure 3-8) can be converted into the following frequency ramp via FFT.

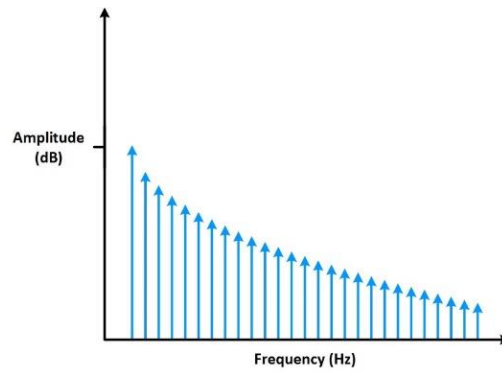


Figure 3-9: The frequency spectrum of a square wave (National Instruments Corp., 2019)

In addition, converting the signal from the time to the frequency domain can also help with validation and troubleshooting. For example, adding two similar sine waves would lead to an almost perfect new sine wave in the time domain. However, instead of a single peak within the frequency domain, one might observe one or a few smaller peaks, which indicates noises. From this, the conclusion is that the obtained sine wave is not as pure as expected, and thus the circuit or system can be re-worked to eliminate the noise source.

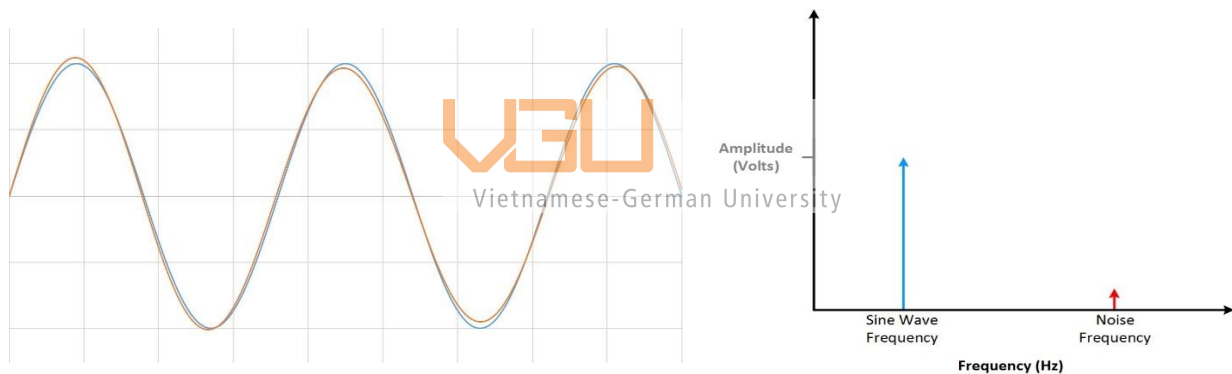


Figure 3-10: An apparently perfect sine wave in the time domain (left) and in the frequency domain (right) (National Instruments Corp., 2019)

In short, using FFT to convert the complex vibration speed function from the time domain to the frequency domain is a simple, fast, and efficient way to observe and analyze its characteristics. A rough scheme for conversion between the time and frequency domains could be seen below

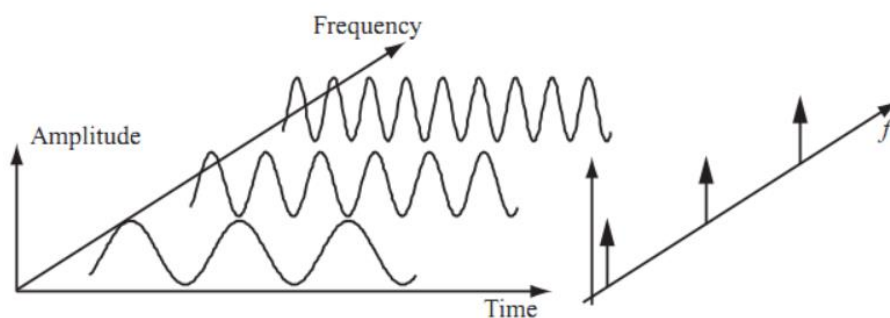


Figure 3-11: Conversion between time and frequency domains (Brandt, 2011)

However, using FFT would lead to its own issues and problems, such as noises being included (solved in section 3.2.3.1), aliasing or the resolution of the result (discussed in section 3.2.3.3), and leakage (analyzed in section 3.2.3.3.1).

## 3.2.2 Experimental set-up

### 3.2.2.1 Securing the test specimen and the shaker to the test bench

For this thesis, the bolt connection is used to secure items onto the test bench, this list includes

- Between the shaker and the shaker's mount
- Between the shaker's mount and the test bench
- Between the stator arm and the generator ring (to produce the assembly/test specimen)
- Between the assembly (or test specimen) and the test bench



For this thesis, the bolts between the stator arm and the generator ring would be tightened with a torque of 7 Nm. The main goal of this is to ensure there is no unknown element of uncertainty left in the system, which allows the reproduction of the measurement result. The remaining bolts are tightened by hand and as strong as possible. This would remove any free and uncontrollable vibration of the test specimen structure, further increasing the precision of the measurement and reproducibility.

### 3.2.2.2 Choosing hammer tip

For this thesis as well as other experiments in the field of vibration analysis, there are various ways to excite the system. One of the most common ways is to use a knocking force (either with a hammer or with a shaker), where the hammer tip plays quite an important role in establishing the spectrum. A few other examples include Pseudo random or White noise. However, this thesis fails to obtain reproducibility with those signals (see section 3.2.4.3) while it is possible with an impulse (see section 4.1). Thus, an impulse signal would be used for the input signal to drive the shaker, and therefore, the effect of the hammer tip must be investigated.



Table 3-3: Different hammers available for the experiment

Hammer type	Image
Red Hammer	
White Hammer	
Black Hammer	
Metal Hammer	

Because each of these hammers has a different height with differences by a few millimeters, it is very hard to maintain precisely the same gap between the hammer and the test specimen. However, as stated in section 3.2.1.3, the input is defined as the input force. Therefore, the shaker mount and the signal would be adjusted so that the recorded force is as close to each other as possible. The recorded value for the force sensor is as below:

Table 3-4: Hitting forces for different hammer

Hammer type	Hitting force (N)
Red Hammer	116
White Hammer	113
Black Hammer	104
Metal Hammer	103

With the input forces being closed to each other, the analysis on the effect of the hammer would have a higher degree of accuracy. Investigate the impact force, the following graph is obtained with the reference force as 1 N.

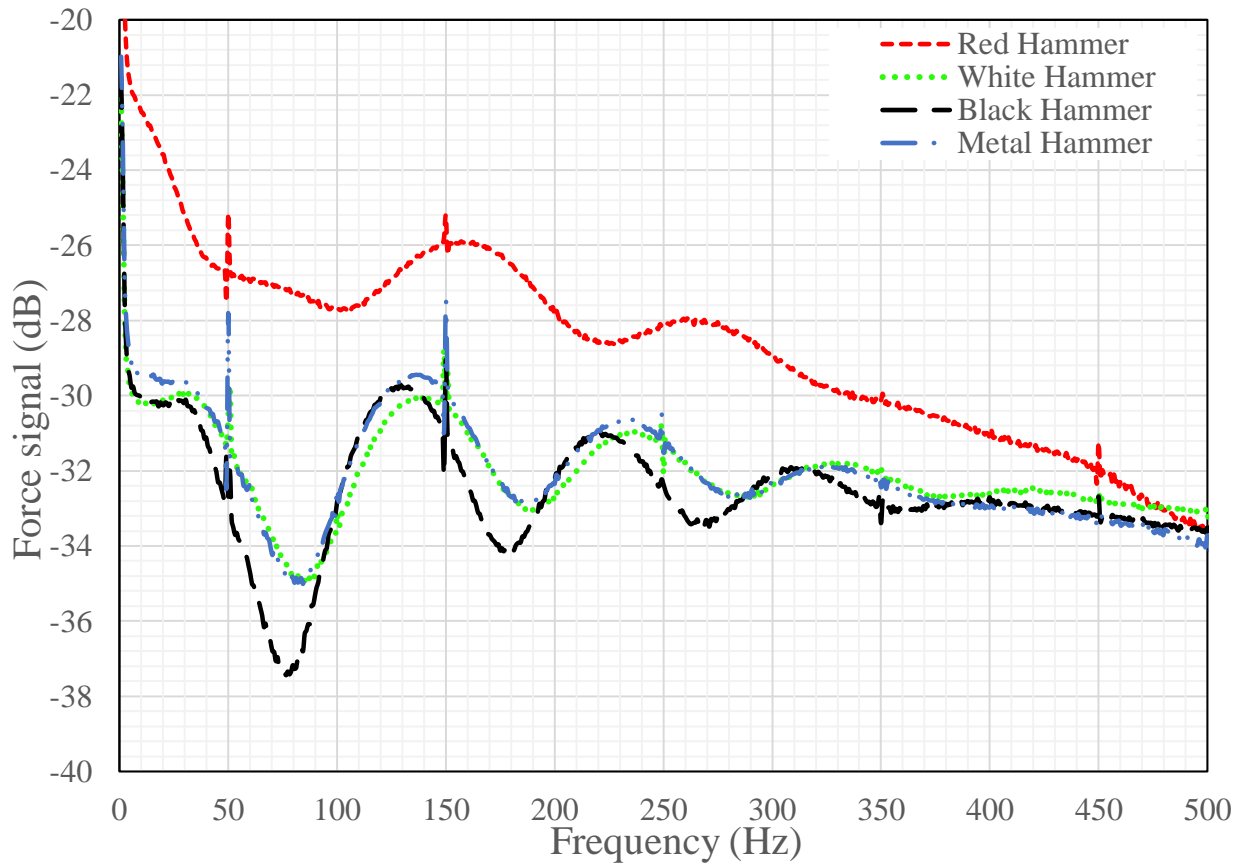


Figure 3-12: Input force signals with different hammers

As can be seen from the graph, all input force signals generated by different hammers would generate spikes at 50, 150, 250, 350, and 450 Hz. The presence of these spikes can be attributed to the electronic artifacts of the powerline (which is rated at 50 Hz in Germany). Further experiments and testing show that these spikes can be removed by switching to a different excitation point. This effect will be shown from section 3.2.4.2 onwards.

Table 3-5: Spikes' heights seen by using different hammer tips

Hammer \ Frequency (Hz)	Red	Black	White	Metal	Average
50	2.308 dB	1.759 dB	2.103 dB	4.570 dB	<b><u>2.685 dB</u></b>
150	0.788 dB	3.040 dB	1.728 dB	3.453 dB	<b><u>2.252 dB</u></b>
250			0.944 dB	1.017 dB	<b><u>0.981 dB</u></b>
350		0.629 dB			<b><u>0.629 dB</u></b>
450	0.867 dB	0.676 dB			<b><u>0.772 dB</u></b>
<b>Average</b>	<b><u>1.321 dB</u></b>	<b><u>1.526 dB</u></b>	<b><u>1.592 dB</u></b>	<b><u>3.013 dB</u></b>	

It is seen that, while on average, the relative spike heights obtained with the red hammer are the smallest, it might not be the best fit here. The reason for this is the material, the red hammer tip is

made with softer material. This leads to the input spectrum dropping off significantly, and the hammer can only be used to analyze the low-frequency range. One document even cites that a soft tip hammer like the red hammer should be used when all resonance frequency is under 200 Hz (SIMCENTER, 2019; Forrest, 1985), which is not the case here. For example, the Transfer functions show three clear peaks at 250, 300, and 330 Hz.

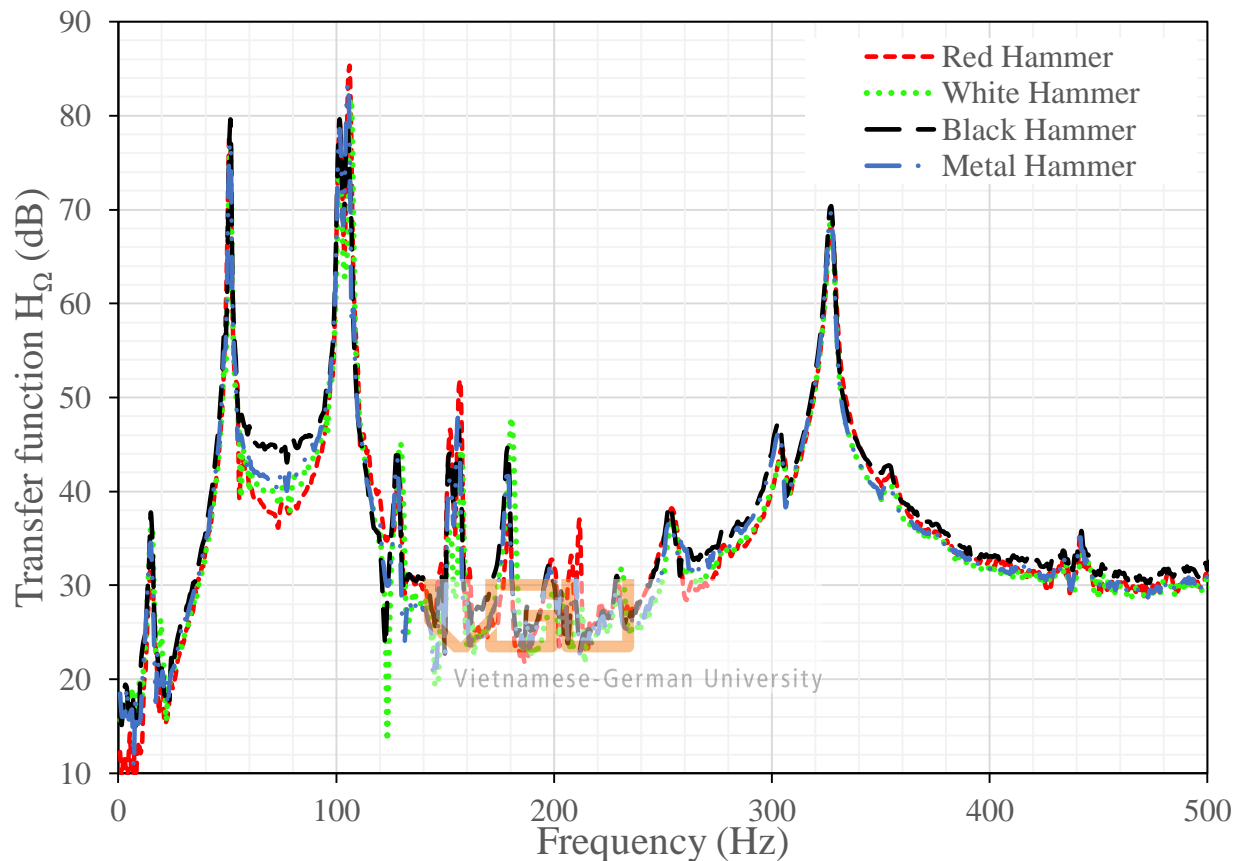


Figure 3-13: Transfer functions for different hammers

Considering the remaining three choices, the differences between the three force signal spectrum are much more moderate, and they make little practical deviations from each other. However, for realistic usage in the thesis, the white hammer is the most comfortable. It requires only a moderate amplitude of the shaker stroke due to its highest length. In addition, due to personal bias and subjective perspective, the noise made with the white hammer is the most tolerable among the three. For this reason, the white hammer would be chosen for the thesis.

### 3.2.2.3 Choosing distance of measurement

The frequency of the laser, both the reference beam and measurement beam, is independent of the distance (Polytec GmbH, 2011). Therefore, the evaluation process would not be influenced by the

space between the measurement surface and the laser vibrometer. This theory would be verified with a preliminary experiment.

The experiment studies the effects of distance between the laser scanner and the measurement surface (in this case the stator arm). In this parameter study, the measurement surface would be the side of the stator arm. The result is summarized in the chart below.

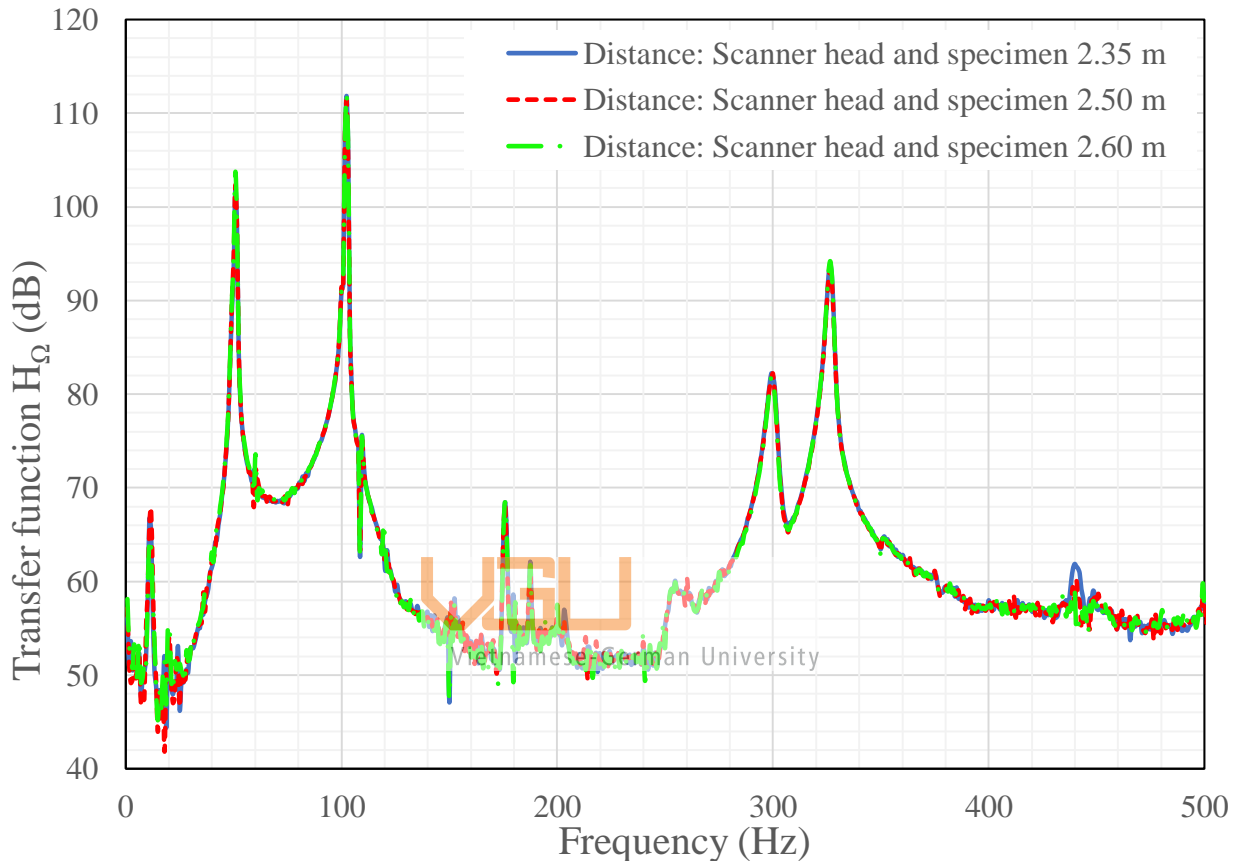


Figure 3-14: Transfer functions for measurements at different distances

It is confirmed and validated that within the scope of this thesis, the distance between the measured surface and the laser vibrometer does not affect the evaluation process. Therefore, the scanner would be put at the most convenient places (to prevent space cramping and accidents during off-time). In practical and real conditions in the lab, this translates to a distance of 2.65m from the laser scanner head to the specimen, or 1.95m to the test bench.

### 3.2.3 Parameter set-up

#### 3.2.3.1 Signal averaging

Measurement in real-life is easily influenced by noise, defined as modifications of signals that are unknown and generally unwanted. These alterations may be made during measurement, capture, transmission, processing, or conversion (Tuzlukov, 2010). In order to reduce the effect of noise, one can do signal averaging (Polytec GmbH, 2018; Hewlett Packard, 1989).

Because the data would be interpreted in the frequency domain (selected with arguments provided in section 3.2.1.4), the averaging of signal would also be done in this domain. In this process, different sequences of time traces, synchronized with the help of a trigger, are collected. Each time traces would have the same number of samples and converted to the frequency domain by FFT, where each converted time sample would have the same number of FFT lines. Here, the averaged spectrum is obtained by doing the average overall values at each frequency (Polytec GmbH, 2018).

As mentioned above, there is a mathematical connection between frequency, trigonometry, and complex number (via Euler’s formula in section 3.2.1.4), thus, the average here is done in complex number form (also referred to as complex average). The formula for this is:

$$\bar{S} = \frac{1}{N} \sum_{n=1}^N S_n = \frac{1}{N} \left( \sum_{n=1}^N \text{Re}(S_n) + j \sum_{n=1}^N \text{Im}(S_n) \right) \quad 3-16$$

Here “Re” stands for the real component, and “Im” is the imaginary component of the number. An illustration of the process (with 2 numbers being averaged) can be seen below

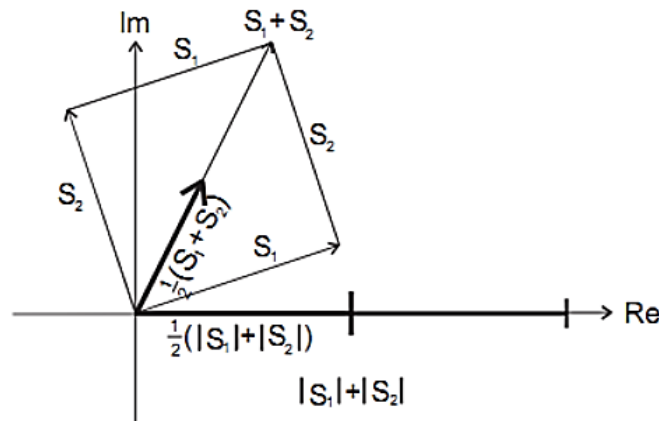


Figure 3-15: Complex and magnitude averaging of signals  $S_1$  and  $S_2$  (Polytec GmbH, 2018)

For this thesis, the signal averaging parameter is studied by comparing the result of having no averaged value to having different averaged complexes. It should have understood at one complex is

equivalent to one measurement, or “6 complexes averaged” means that for each scanned point, the measurement is repeated 6 times.

Overall, the time taken for each signal average is concluded as followed. As can be seen, the more averaged measurements taken, the longer it needs to finish the whole process.

Table 3-6: Evaluation time using different numbers of averaged samples

Number of averaged complexes	Time (mm:ss)	Number of averaged complexes	Time (mm:ss)
0	00:40	8	04:57
3	01:53	9	05:33
4	02:30	10	06:10
5	03:07	11	06:46
6	03:44	12	07:24
7	04:20		

An in-depth study of different signal averaging parameters is as followed:

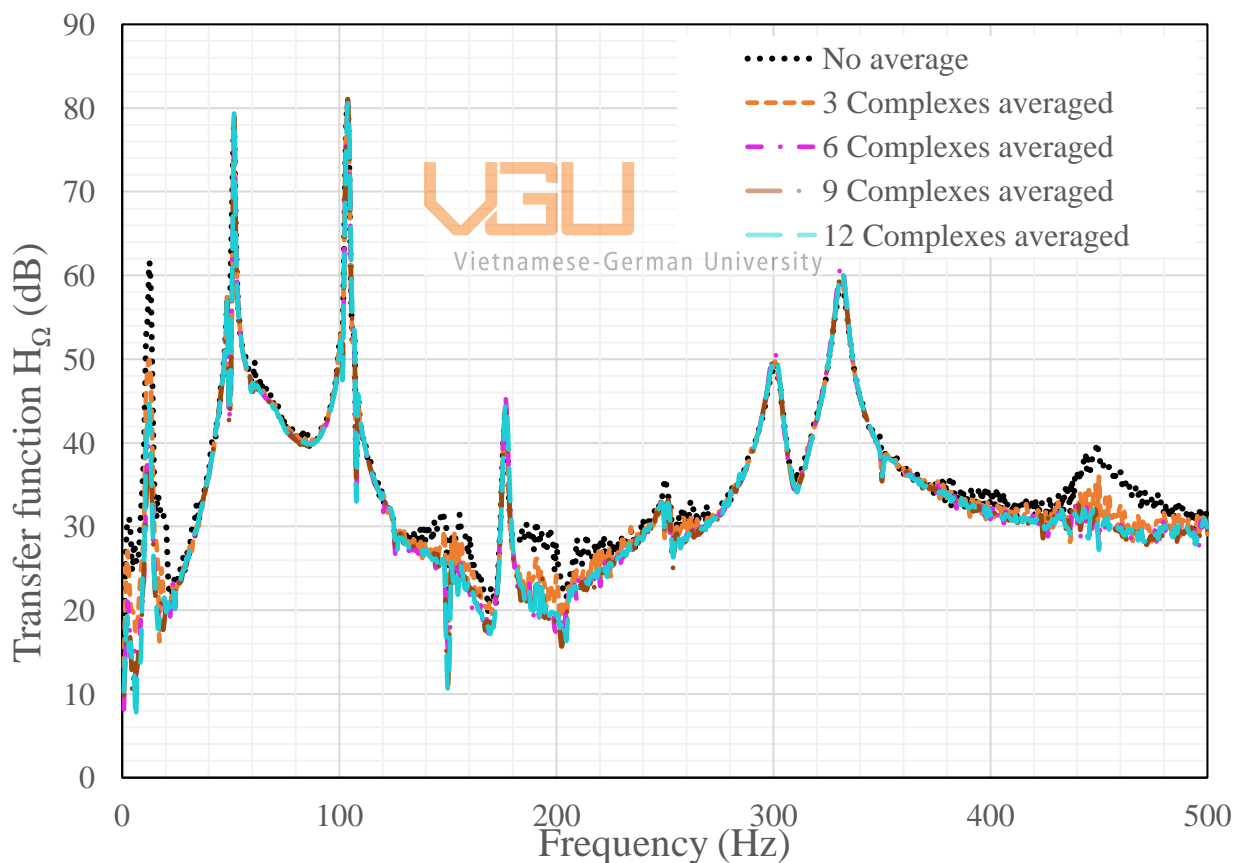


Figure 3-16: First study on signal averaging

As it can be seen from the graph, there are significant differences in the spectrum obtained with the “no average” and “3 complex averages” options compared to the rest. This suggests the effect of noises is not truly eliminated until the 6 complex averages option is used. Thus, choosing from 6 to 12 average complex values would be considered from this point onward. Next on the topic is to

consider using a high count of averaged complexes, here defined as having from 9 to 12 averaged values. As can be seen, there is no noticeable or significant difference within the frequency spectrum of these options for signal averaging. In other words, there is no point in using more than 9 averaged complexes. The remaining choices for signal averaging consist of choosing between 6 and 9 averaged complex values. This is carried out in the next part.

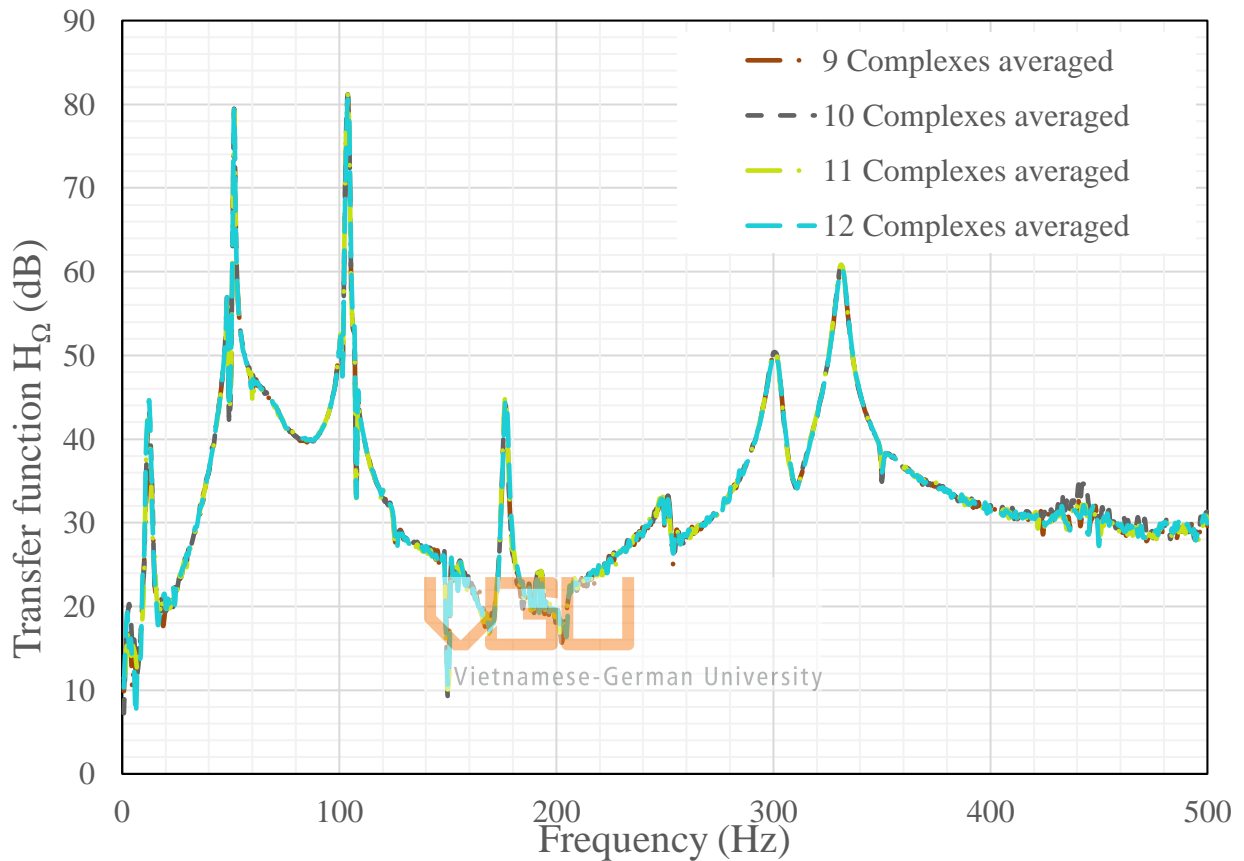


Figure 3-17: Second study on signal averaging

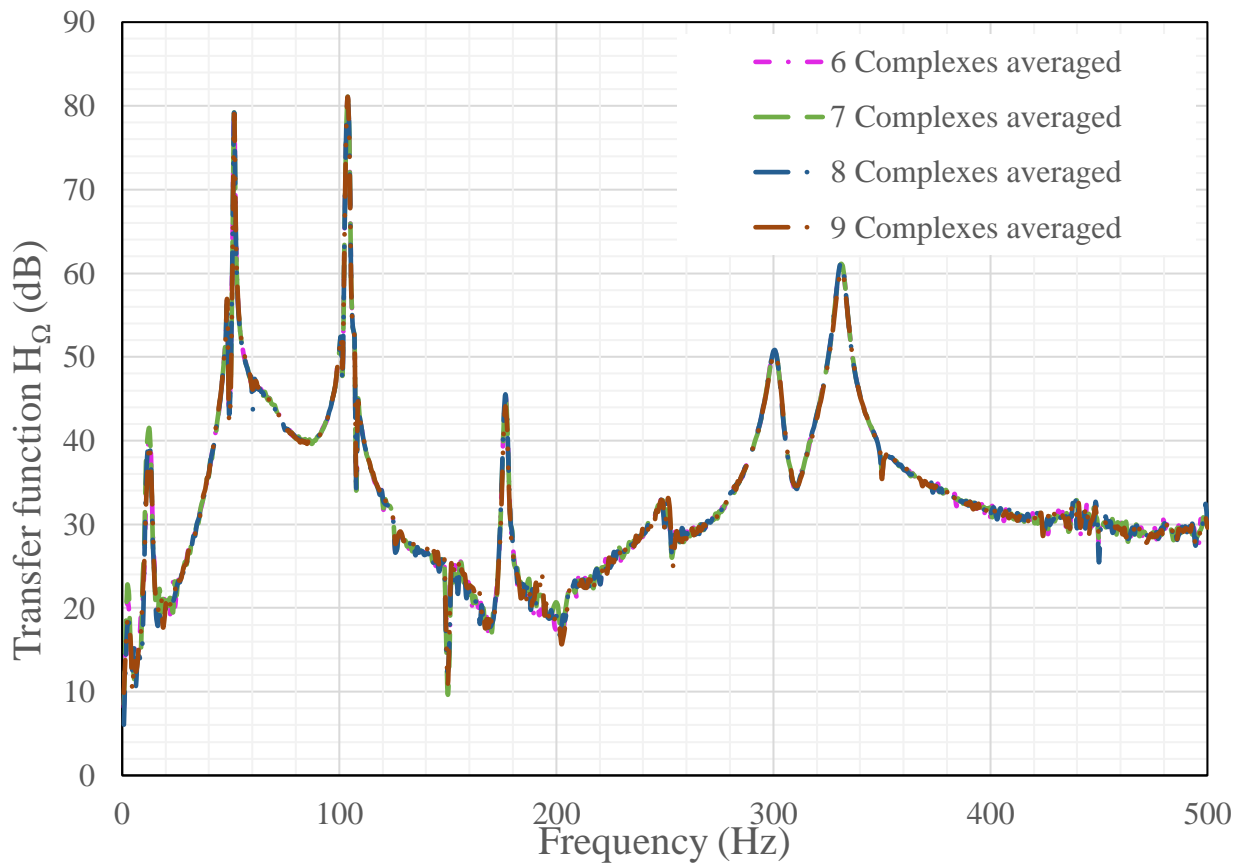


Figure 3-18: Third study on signal averaging

For the third study, the differences are only noticeable at very low frequency, especially at 2.3Hz- and 12.5Hz-peaks, where the options of using 7 averaged complexes yield higher peaks (differences of up to 2 dB). Thus, to fully ensured that the noises are fully eliminated from the evaluation process, this thesis would average the signal over 9 complex values.

### 3.2.3.2 Filter

Within the scope of this thesis, “filter” is understood as a digital filter, of which the general mathematical formula is:

$$a_0 y_n = \sum_{k=0}^{N_b} b_n x_{n-k} - \sum_{l=1}^{N_a} a_n x_{n-l} \quad 3-17$$

The filter used in the system is a Finite Impulse Response (FIR) digital filter (Polytec GmbH, 2018). This is obtained by setting  $N_a$  in the equation above as 0. In other words, an FIR filter would only use old inputs to compute the output (Brandt, 2011).



$$y[n] = \sum_{i=0}^N b_i x[n-i] \quad 3-18$$

As the vibration of the specimen is originally measured in the time domain, the concerned range of frequency can be covered by other signals. Thus, filters should be investigated to see if there are any effects on the evaluation process. The general characteristic of the low-pass digital filter (in terms of signal strength) used here can be observed in the figure below. Under cut-off frequency (blue line), there is no damping for the collected signal, this region is called the passband. The next region is called the transition band, where the signal strength would drop rapidly. The last region is the stopband, where the damping level would plateau at -60 dB. According to Figure 3-7, this damping level is equivalent to reducing the signal strength to 0.1% of the original signal.

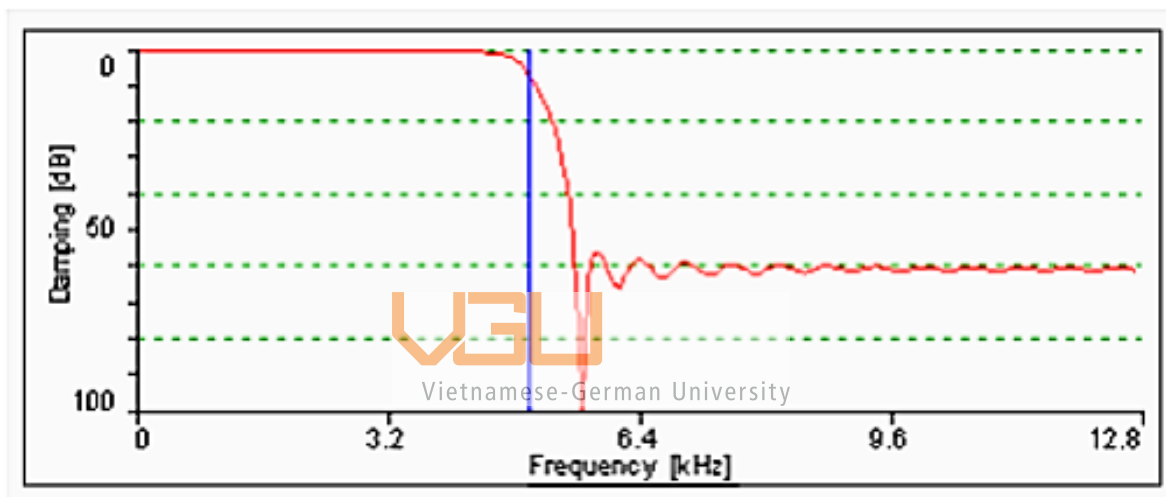


Figure 3-19: Filter characteristic (Polytec GmbH, 2018)

The frequency range of concern is from 0 to 500 Hz, which means on the lower end of the spectrum. Thus, a Low-pass filter (such as in Figure 3-19 above) will be used and compared. The result of this study can be seen below.

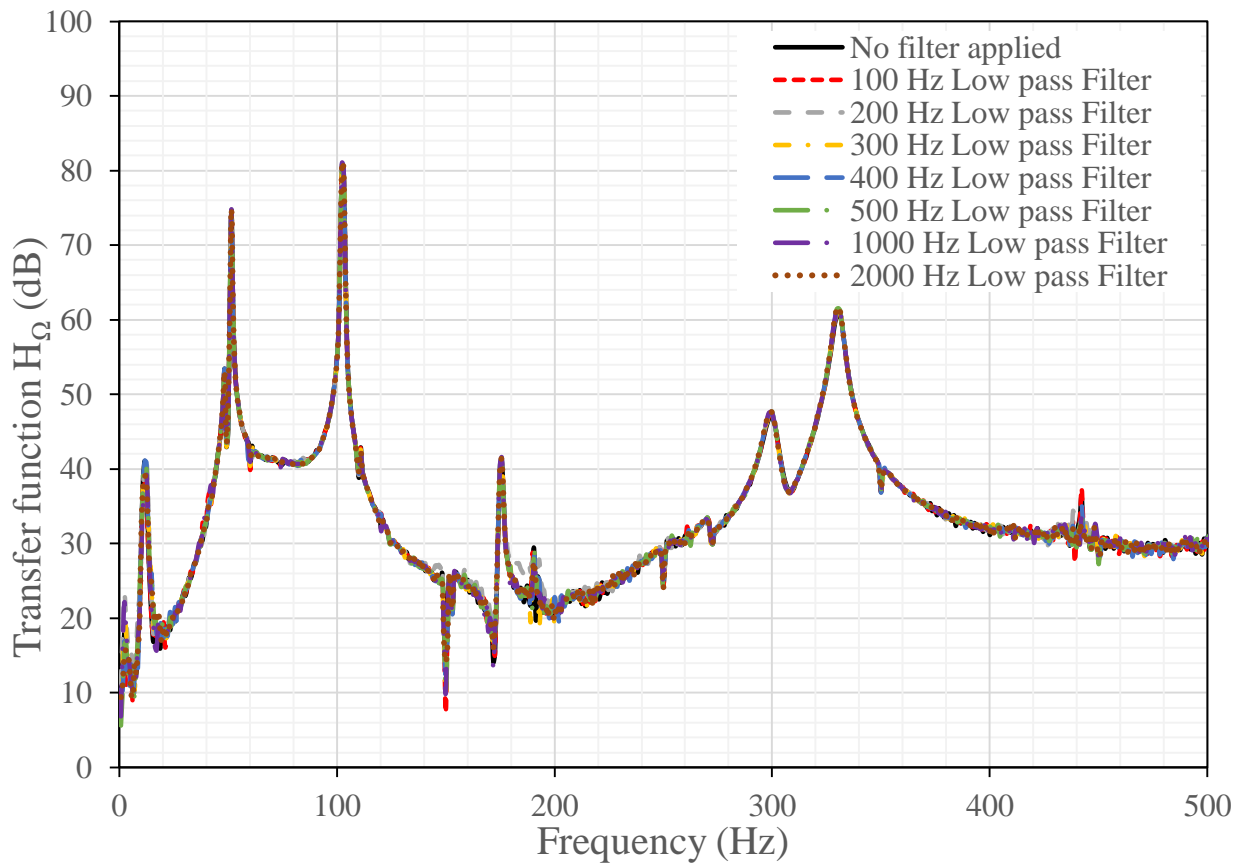


Figure 3-20: Transfer functions with different filters applied (logarithmic scale)

As seen from the chart above, there are no discernible differences with regards to the spectrum of different Transfer functions using different filters. The reason for this is two-fold. First, both the input (impulse force) and output (vibration speed) are filtered by the same mathematical function. Thus, the damping ratio would be the same for both of them, and the basic quotient rule would cancel out the modification. This means that the final value for the Transfer function would be the same. A simple math expression, written below, would illustrate this. The symbol  $\eta$  illustrates the damping ratio due to the (digital) filter being applied.

$$\frac{\text{Output} \times \eta}{\text{Input} \times \eta} = \frac{\text{Output}}{\text{Input}} = \text{Transfer function}$$

The second is that, after being filtered, the signal would decay by 20 dB for every decade (with a decade is an increase of 10 times for the frequency) (Brandt, 2011). Even for the lowest frequency setting for the filter (at 100 Hz), the concerned frequency ranges (up to 500 Hz) might not be clear enough to show the signal strength drop.

While using filter has no clear effect on the Transfer function within the concerned frequency range (0 to 500 Hz), a low pass filter is still used here, with the cut-off frequency set at 2 kHz. The main purpose of this filter is to act as an anti-aliasing filter (explained in section 3.2.3.3.1 below).

Furthermore, the cut-off mark of 2 kHz is much higher than the highest frequency of concerned (500 Hz), making sure that as little change as possible would be made within the concerned range of frequency.

### 3.2.3.3 The sampling rate, FFT lines, and Bandwidth

With the software provided by Polytec, two parameters can be changed with regard to frequency setting, including bandwidth and FFT lines. Other parameters would be automatically calculated from these two settings. This section will first analyze all related parameters before finally choosing the appropriate combination.

#### 3.2.3.3.1 Sampling rate

A related definition to bandwidth is sample rate (also known as sampling rate or sampling frequency)  $f_s$ , defined as the number of data samples acquired per second (SIMCENTER, 2020). Usually, the sample rate is defined as twice the value for BW, or:

$$\text{Bandwidth} = f_{\max} = \frac{1}{2} f_s \quad 3-19$$

This is an application of the Nyquist sampling theorem, where the required sample rate should be two times higher compared to the signal bandwidth (National Instruments Corp., 2019). The application of a high sample rate is to avoid aliasing, defined as distortion from the true signal due to a low sample rate. The illustration can be seen below. The original signal in red in the time domain is sampled at a low rate, which will produce the final (and false) signal in blue. Notice the acquired frequency (blue line) is much lower than the actual frequency.

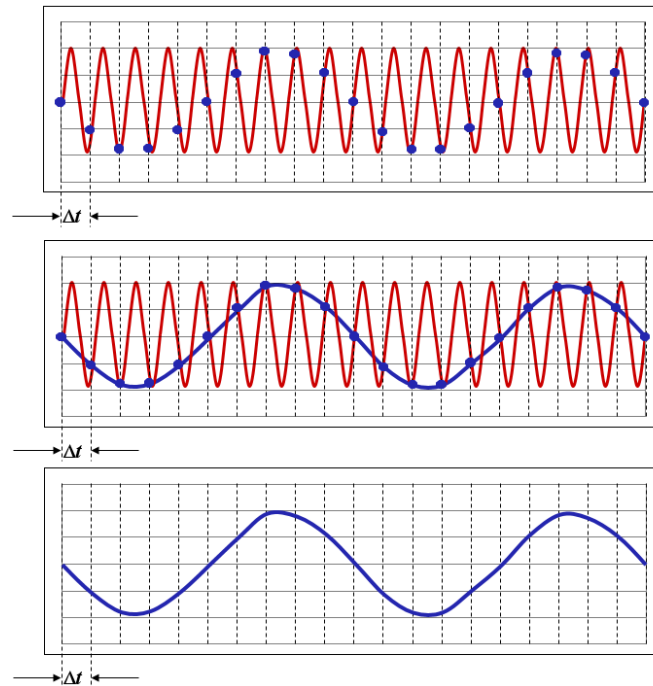


Figure 3-21: A low sample rate failed to replicate the original signal (SIMCENTER, 2019)

There is another consequence of using a low sampling rate. If the sampling frequency is less than twice the frequency of the sine wave, the result would be shown as a sine signal of a different frequency. For example, at  $0.4f_s$  and  $0.6f_s$ , both sine waves would return the same spectrum, or  $0.1f_s$  and  $1.1f_s$ . This is described as all frequencies are mirrored in the Nyquist frequency, defined as half the sampling rate. This phenomenon is also known as “frequency folding”. It should be noted that both terms (aliasing and frequency folding) describe the same effect of having a low sampling frequency. An illustration of frequency folding is seen below. The frequency axis (the horizontal) is cut at multiple of the Nyquist frequency, and the frequency spectrum is then folded over at these points (Brandt, 2011).

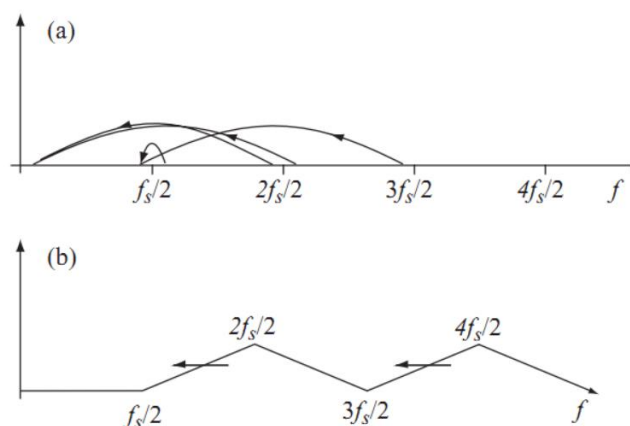


Figure 3-22: Alias (a), also known as Frequency folding (b) happens when the sampling frequency is low (Brandt, 2011)

Thus, the sampling rate must be sufficiently high (at least two times higher than the highest frequency component in the signal) to capture the original signal fully. Regarding the value of sample rate, Shreeve has proposed that it should be 2.56 times the signal bandwidth to comply with the computer world (Shreeve, 1995). This is also followed by Polytec, who also uses this number to automatically calculate the sample rate after choosing the bandwidth.

In addition, one assumption that must be made is that the captured signal (the vibration speed of the specimen and the impulse input) would have no frequency content higher than half of the sampling frequency. This is done by applying an anti-alias filter, of which cut-off frequency is lower than  $f_s/2$  (Brandt, 2011). For this thesis, the low-pass FIR filter with a cut-off frequency of 2 kHz (chosen in section 3.2.3.2) would fulfill this duty.

### 3.2.3.3.2 FFT lines

FFT lines, also referred to as Spectral Lines by certain documents (SIMCENTER, 2020), are the line that divides the bandwidth within the frequency spectrum. The more lines available, the better the frequency resolution gets. However, in return, for each measurement, more time would be needed. The number of FFT lines in the frequency domain is analogous or comparable to the number of sampling points in the time domain.



It should also be noted that there are equivalent terms for frequency resolution, including frequency bin or frequency increment. Within this thesis, all of these terms are considered to describe the same object: the frequency spacing between two consecutive FFT lines.

If the bandwidth is kept the same and more FFT lines are used, the frequency resolution would be smaller. This would lead to higher peaks within the frequency domain. There are two reasons for this. The first is at lower counts of FFT lines, the frequency range between two consecutive data points would be longer, increasing the chance for a peak to be missed. This is illustrated below, with 3200 FFT lines missing a peak in the middle. Using 6400 or 12800 lines would approximate the frequency value, and using 25600 lines would yield a much better value for the amplitude of the peak.

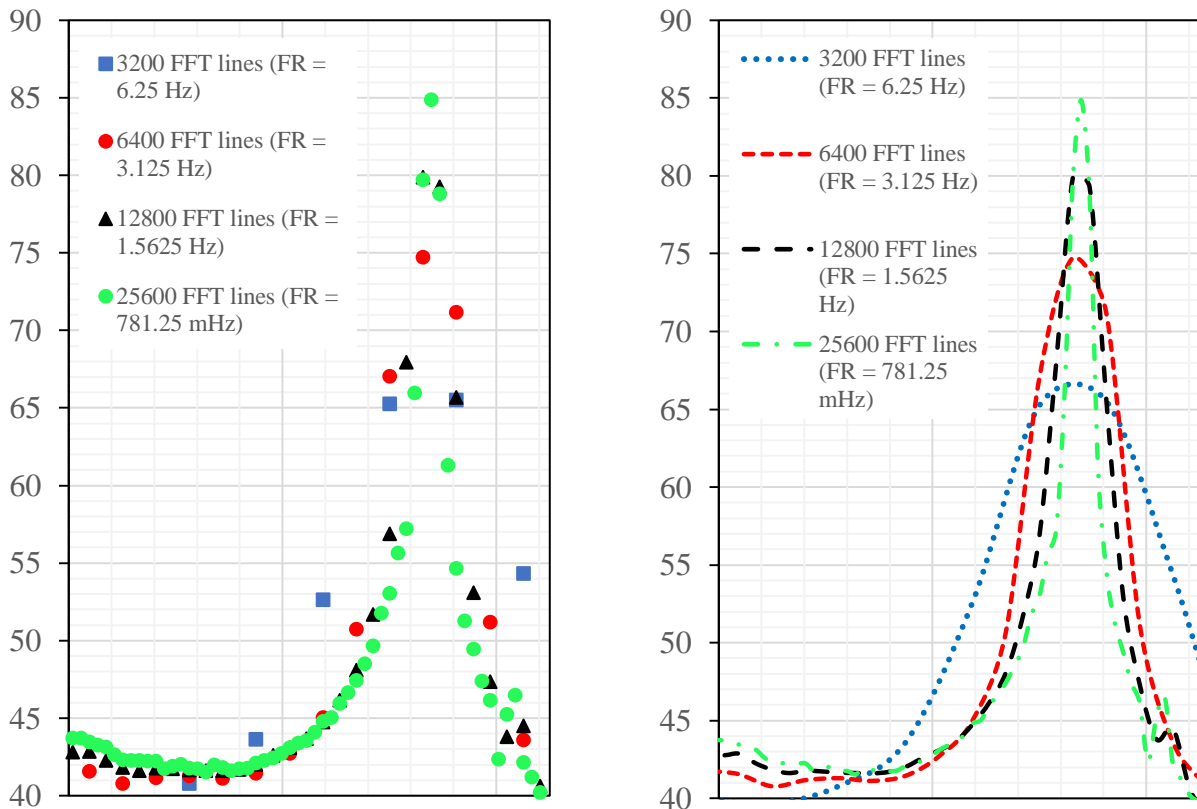


Figure 3-23: Effect of frequency resolution on the frequency spectrum (Left: discrete data points; Right: conversion into a continuous spectrum)

The other argument is due to the leakage effect (Cimbala, 2010). Visually speaking, leakage can be seen as a wide base at the end of each peak in the frequency spectrum. This can be seen on the right-hand graph of Figure 3-23. Leakage happens because the discrete data acquisition does not stop at the precise phase of the sine wave as it started. This would lead to some of the energy of the peak being distributed into the nearby frequencies, resulting in a net decrease of the peak. With more FFT lines being used, the frequency gaps between each of them would get smaller, leading to a smaller range of frequency where this energy distribution takes place. The result of using more FFT lines (for smaller frequency resolution) is that the peak would get higher. An example of this (albeit not in vibration analysis and the bandwidth is not kept the same) can be seen in the figures below. The input used here is a sine wave of 10 Hz frequency and amplitude of 10 V.

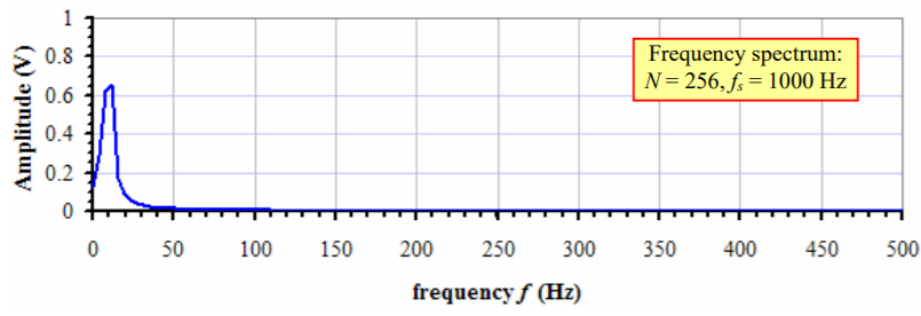


Figure 3-24: Signal captured with  $\Delta f = 3.91$  Hz (Cimbala, 2010)

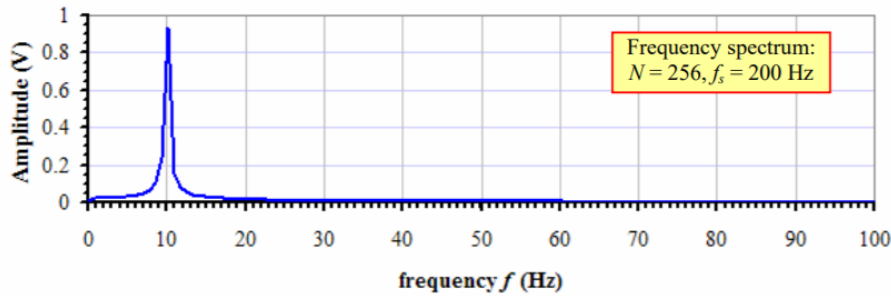


Figure 3-25: Signal captured with  $\Delta f = 0.781$  Hz (Cimbala, 2010)

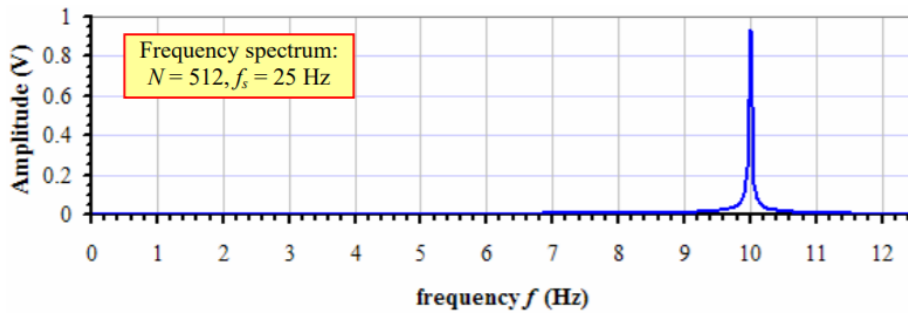


Figure 3-26: Signal captured with  $\Delta f = 0.0488$  Hz (Cimbala, 2010)

However, actual measurements for this thesis show that in practice, using smaller frequency resolutions does not always guarantee better results (see section 3.2.3.3.5).

### 3.2.3.3.3 Bandwidth

Bandwidth is the range of frequency in which the measurement will take place. There is no clear scientific or engineering proven theory on how to choose a bandwidth for evaluation on digital equipment, but it is quite self-evident that the bandwidth should be at least as high as the concerned frequency (500 Hz for this thesis).

In addition, there is a general rule of thumb (a guide based on practice rather than theory), that the measurement (or digitizer) bandwidth should be three to five times higher than the signal bandwidth, or bandwidth with at least two times the highest frequency component in the signal (National Instruments Corp., 2019). Another source (SIMCENTER, 2020) says that for the time domain, one should sample at 10 times the highest frequency to get the correct amplitude and 2.5 times (with accounting for anti-alias filter) in the frequency domain.

As mentioned above, the sampling rate is (at least) 2 times higher than the cut-off frequency of the anti-aliasing filter, and 2.56 times higher than the value of the bandwidth. Considering that the filter has been set at 2 kHz, the minimum applicable value for bandwidth in this thesis would be at least 1562.5 Hz. In practice, due to the design of the software, bandwidths of 2 kHz and above would be investigated.

### 3.2.3.3.4 Relationship between sample rate, FFT lines, and bandwidth

**Frequency resolution** (or frequency bin): the spacing between two consecutive data points (or two consecutive FFT lines) in the frequency domain.

$$\Delta f = \frac{\text{Bandwidth}}{\text{Number of FFT lines}} \quad 3-20$$

**Measurement time**: the period required to finish one measurement (or rather one sample), also known as the amount of time data collected to perform an FFT.

$$T = \frac{1}{\Delta f} = \frac{\text{Number of FFT lines}}{\text{Bandwidth}} \quad 3-21$$

**Total measurement time**: the total time needed to finish the whole measurement process, with T is the measurement time per sample as defined above.

$$T_{\text{total}} = T \times \text{Number of averages} \times \text{Number of scanned points} \quad 3-22$$

For N as the number of sampling point in the time domain, and within the context of digital sampling used in this thesis, the connection between the number of FFT lines and N is

$$N = \text{Number of FFT lines} \times 2.56 \quad 3-23$$

This formula is also independently verified in this experiment, comparing the data point available in the frequency domain (the number of FFT lines minus 1) and in the time domain (N).

**Sampling time**: the amount of time between data samples collected in the time domain. The smaller it is, the better the chance of measuring the true peak in the time domain. This value is also called sampling interval or time increment in some literature and online resources

$$\Delta t = \frac{T}{N} = \frac{\text{Number of FFT lines}/\text{Bandwidth}}{\text{Number of FFT lines} \times 2.56} = \frac{1}{\text{Bandwidth} \times 2.56} = \frac{1}{f_s} \quad 3-24$$

**Nyquist frequency**: the highest frequency that can be coded at a given sample rate to fully construct the signal, or half the sample rate (Weisstein, 2005):

$$f_n = \frac{f_s}{2} \quad 3-25$$

### 3.2.3.3.5 Choosing bandwidth and FFT lines

No clear literature or online resource is detailing the scientific process of choosing an appropriate frequency resolution (via setting bandwidth and the number of FFT lines). Either the explanation is made vague, or the choice should be done experimentally, which would be different in each case. For this reason, the selection of a correct frequency resolution would be carried out by the trial and error



method here, which is carried out over two steps. In the first step, the number of FFT lines would be kept the same, and the value for bandwidth would be varied. From this, the best-fit value for the bandwidth would be chosen. Then, in the second step, the chosen bandwidth would combine with different FFT lines count to choose the best frequency resolution. However, the choice of combination would be done fairly subjectively, dependent on personal opinion, and not a fully provable scientific, technical, or engineering theorem.

In the first step, 12800 FFT lines are used, and the values for bandwidth would be compared between 2, 5, 10, and 20 kHz. Lower values are not applicable due to the application of the filter (see section 3.2.3.3.3) and higher values are not strictly needed (four different values for bandwidth are sufficient for comparison).



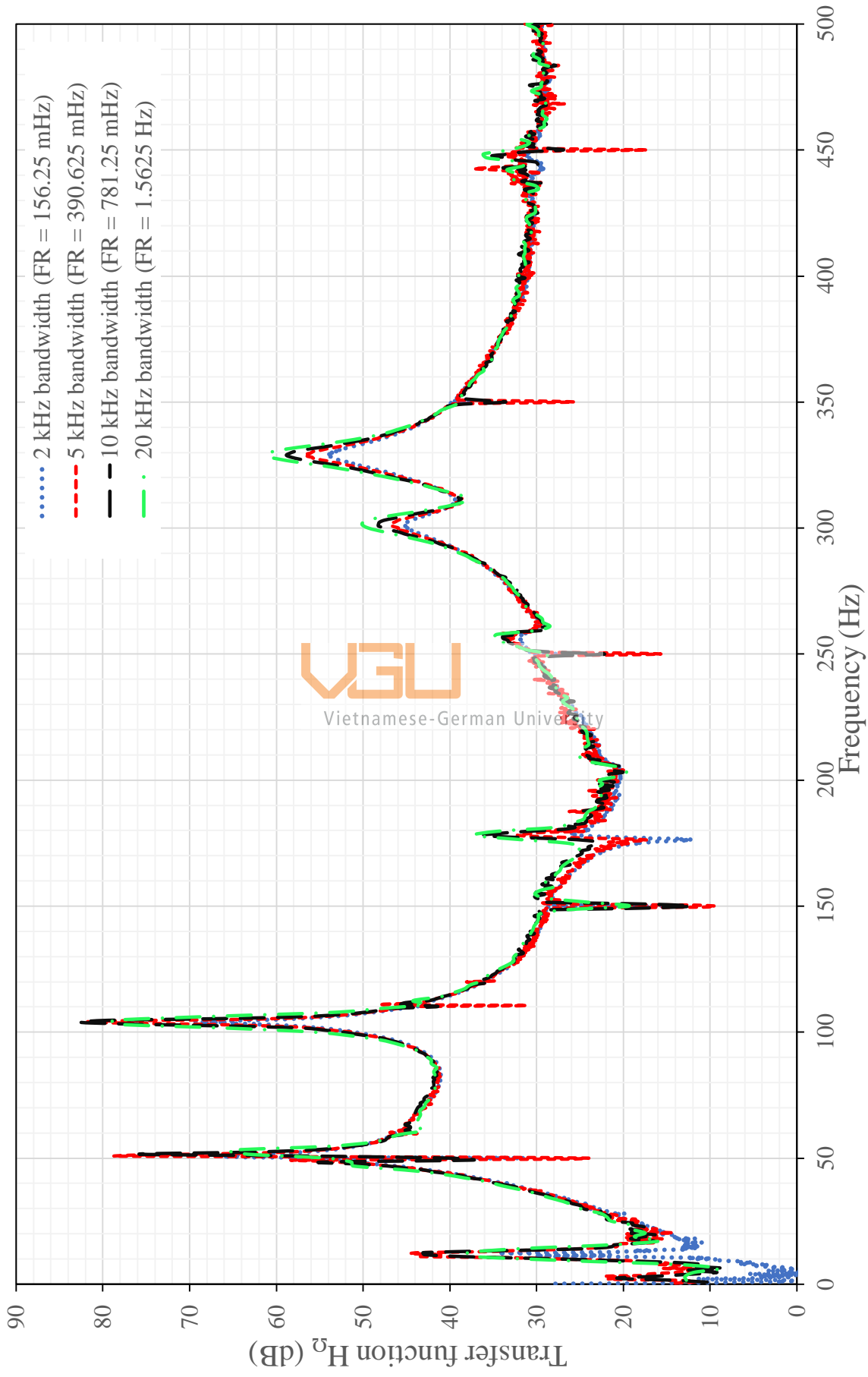


Figure 3-27: Transfer function  $H_{\Omega}$  for different bandwidth with 12800 FFT lines

As seen in the graph above, for all peaks, there are no major differences with regards to their widths. However, there are clear distinctions concerning their height. In particular, these heights mostly go against the idea of using smaller frequency resolution would lead to higher peaks. A possible answer can be found via interpreting the input (force) and output (vibration speed) individually.

The graph below represents the input force signal in different situations. It should be noted that the force collected in the time domain is the same (the shaker setting is maintained), with the only difference is different bandwidths. This would lead to different frequency resolutions being used. This leads to the four measurements having four spectra on different heights (albeit sharing the roughly same shape). This can be explained as each spectrum has its own distinct Fourier coefficients' magnitudes (Hartin & Belanus, 1997).

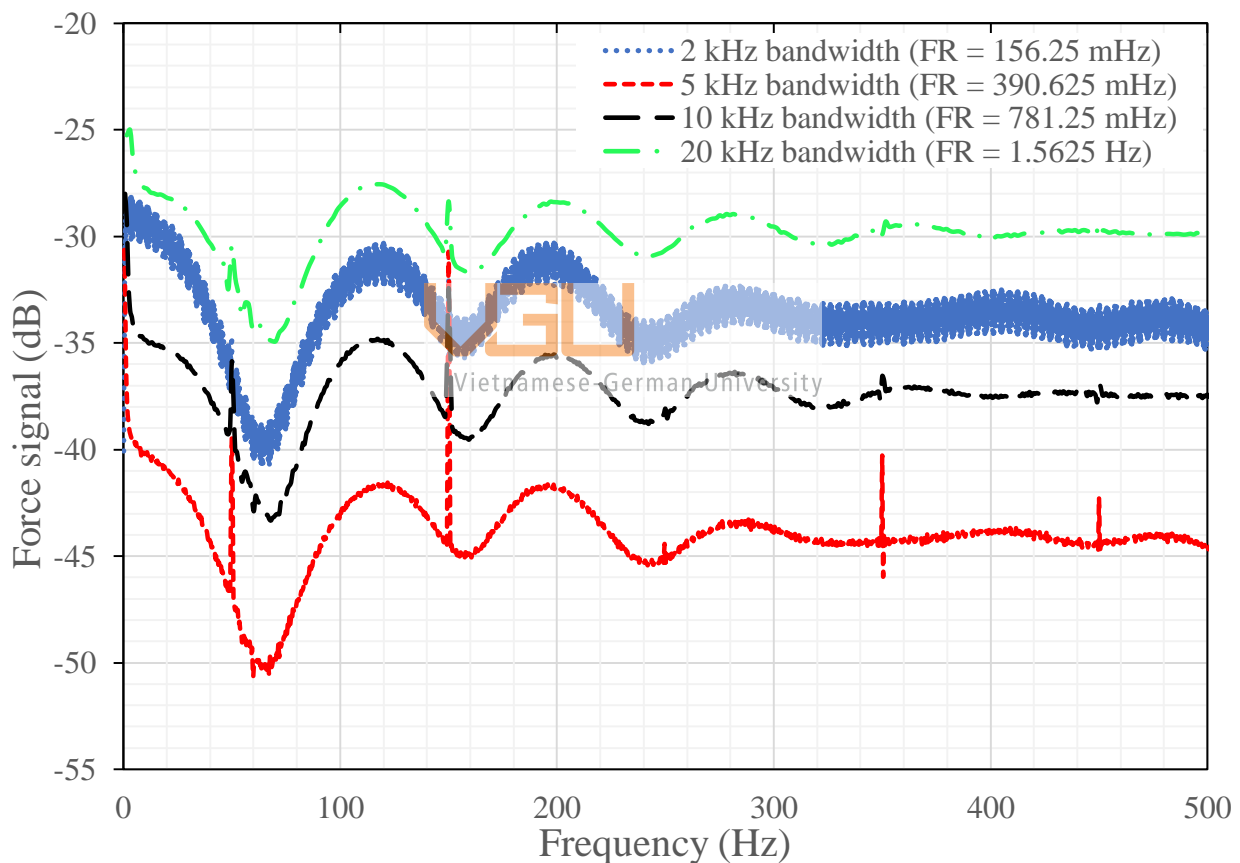


Figure 3-28: Input force signals in the logarithmic scale and the frequency domain, using 12800 FFT lines and different bandwidths

A more mathematical and detailed approach can be found via 3-13, as well as a combination with the relationship between related parameters (see section 3.2.3.3.4). With the same number of FFT lines being used, increasing the bandwidth would increase the sampling frequency and the width of the frequency bin. This would decrease the measuring time of one sample, and 3-13 shows that the measuring time is inversely proportional to the magnitude of the Fourier coefficient (and thus, the

amplitude in the frequency domain). Thus, a wider bandwidth would lead to an elevated spectrum in the frequency domain.

In addition, the signal obtained with 2 kHz bandwidth and 12800 FFT lines is heavily smeared. This is due to a very small frequency resolution in combination with the window function (more in section 3.2.3.4, and in this particular case, the Hann window function is used). Due to the design of the window functions (which is unavoidable), the signal strength of a certain frequency would be sampled into the neighboring bins. The smaller frequency resolution, the signal would be sampled into a shorter frequency range. In other words, if the increment between two consecutive frequencies is smaller, the resulting spectrum would be rougher. This would lead to a heavily smeared spectrum (as seen in the input signal using 2 kHz bandwidth) and the presence of sudden spikes for the remaining option.

Comparing the remaining spectrum (with 5, 10, and 20 kHz bandwidths) on the relative increase of the spikes, the following table is obtained. Here, the spike height is defined as the difference between the highest and the lowest point, and only spikes of 0.5 dB or more are considered. All values here are calculated to 3 decimal points.

Table 3-7: Spikes' height seen by using different bandwidths

<b>Frequency (Hz)</b> <b>Bandwidth (kHz)</b>	<b>50</b>	<b>150</b>	<b>250</b>	<b>350</b>	<b>450</b>	<b><u>Average</u></b>
<b>5 kHz bandwidth</b>	7.346 dB	13.883 dB	0.722 dB	5.599 dB	2.483 dB	<b><u>7.508 dB</u></b>
<b>10 kHz bandwidth</b>	4.157 dB	6.734 dB		1.089 dB	0.843 dB	<b><u>3.206 dB</u></b>
<b>20 kHz bandwidth</b>	2.283 dB	2.484 dB				<b><u>2.384 dB</u></b>
<b><u>Average</u></b>	<b><u>4.595 dB</u></b>	<b><u>7.700 dB</u></b>	<b><u>0.722 dB</u></b>	<b><u>3.344 dB</u></b>	<b><u>1.663 dB</u></b>	

As seen from above, the 20 kHz provides the smoothest spectrum, with the least amount of spike presence. This is preferable because a spike in the frequency spectrum of the input signal would lead to a sudden decrease in the spectrum of the transfer function, hindering the analysis process.

Furthermore, using a wider bandwidth would also lead to a smoother signal reconstruction in the time domain. As seen in the figure below, a shorter bandwidth will lead to more ringing effects before and after the main pulse. This ringing effect is termed the Gibbs phenomenon in mathematical term (Brandt, 2011). With wider bandwidth being used, the sampling frequency would also increase,

leading to more points being sampled in the same period (assuming the same number of FFT lines is used). The main impulse would last for about 1 ms, and thus, increasing the bandwidth means that more points within this period. And with more points being sampled (or the signal being approximated via Fourier series with more sine and cosine terms), the recorded data set would be smoother, reducing the ringing effect.

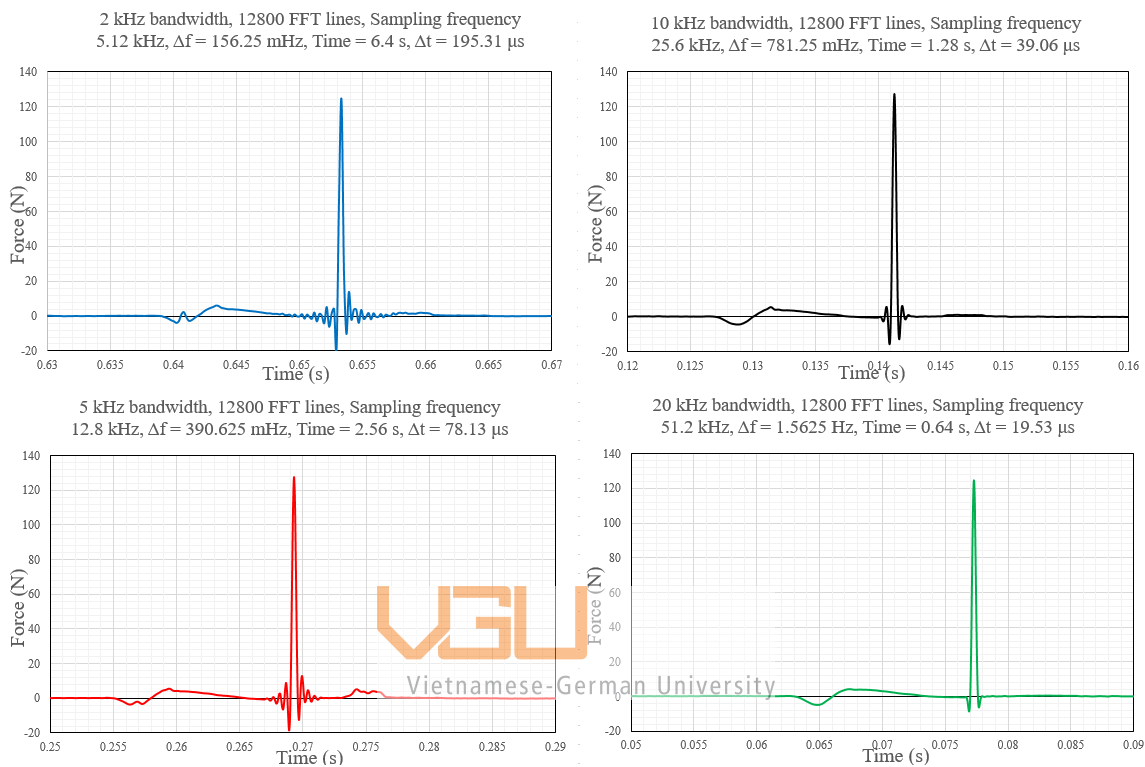


Figure 3-29: Time domain input force signals, obtained with different bandwidths on 12800 FFT lines

A simpler illustration can be seen below. The original signal is a square wave (in black), which is sampled with two different sampling frequencies (and thus, two different values for FFT lines). The red line represents 10 trigonometry terms while the blue line shows the result obtained with 200. As it is seen, the more terms being used (or more points being sampled in the time domain), the smoother the line will be, and the ringing effect will be minimized.

Strictly speaking, there is nothing wrong with the original signal, this is purely due to choosing the parameters for measurements. However, because the goal of this section is to choose the correct bandwidth, this effect must be put into consideration. The extra ringing effect would also be converted into the frequency domain by the FFT, which would falsify the final result. For this reason, the 20 kHz bandwidth would be chosen, as this would lead to the smoothest spectrum in the time domain. With the 20 kHz being chosen as bandwidth, the next step would be changing the number of FFT lines to study their effect. The spectrum of the Transfer functions can be observed in the graph below:

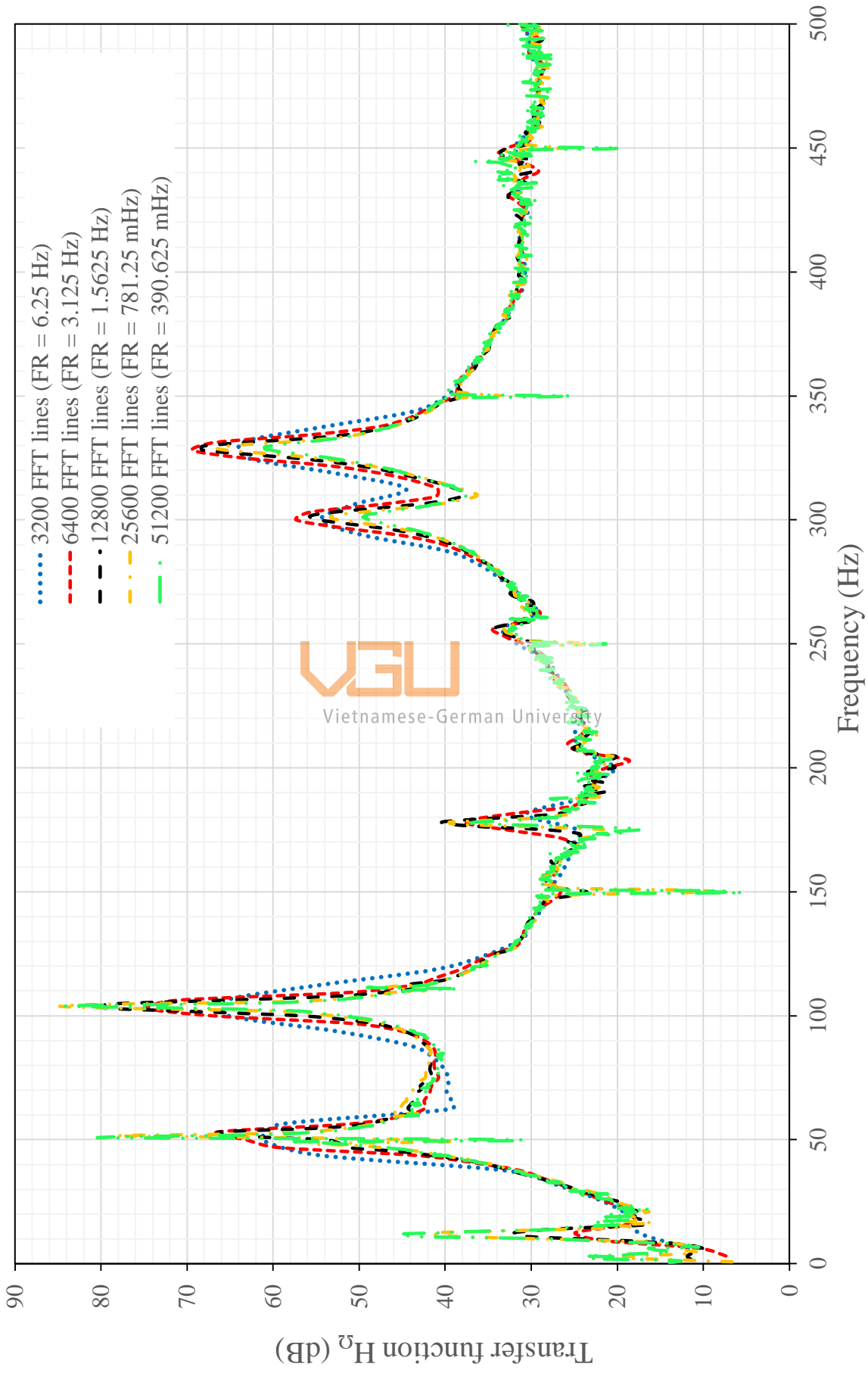


Figure 3-30: Transfer function  $H_0$  for different numbers of FFT lines on 20 kHz bandwidth

The figure above shows the Transfer functions, while the two below illustrate the input signals, and the vibration speed signals, obtained with different FFT line counts on the same 20 kHz bandwidth. By increasing the number of FFT lines, the frequency resolution would be smaller, and the general height of the spectrum (of both the input and output signal) would decrease. The reason is due to the computation of the Fourier coefficient as shown in 3-13. With fewer FFT lines, the frequency resolution would be larger, leading to a longer measurement time, and thus, lower the Fourier coefficients. This would finally result in the spectrum being lower with more FFT lines being used.

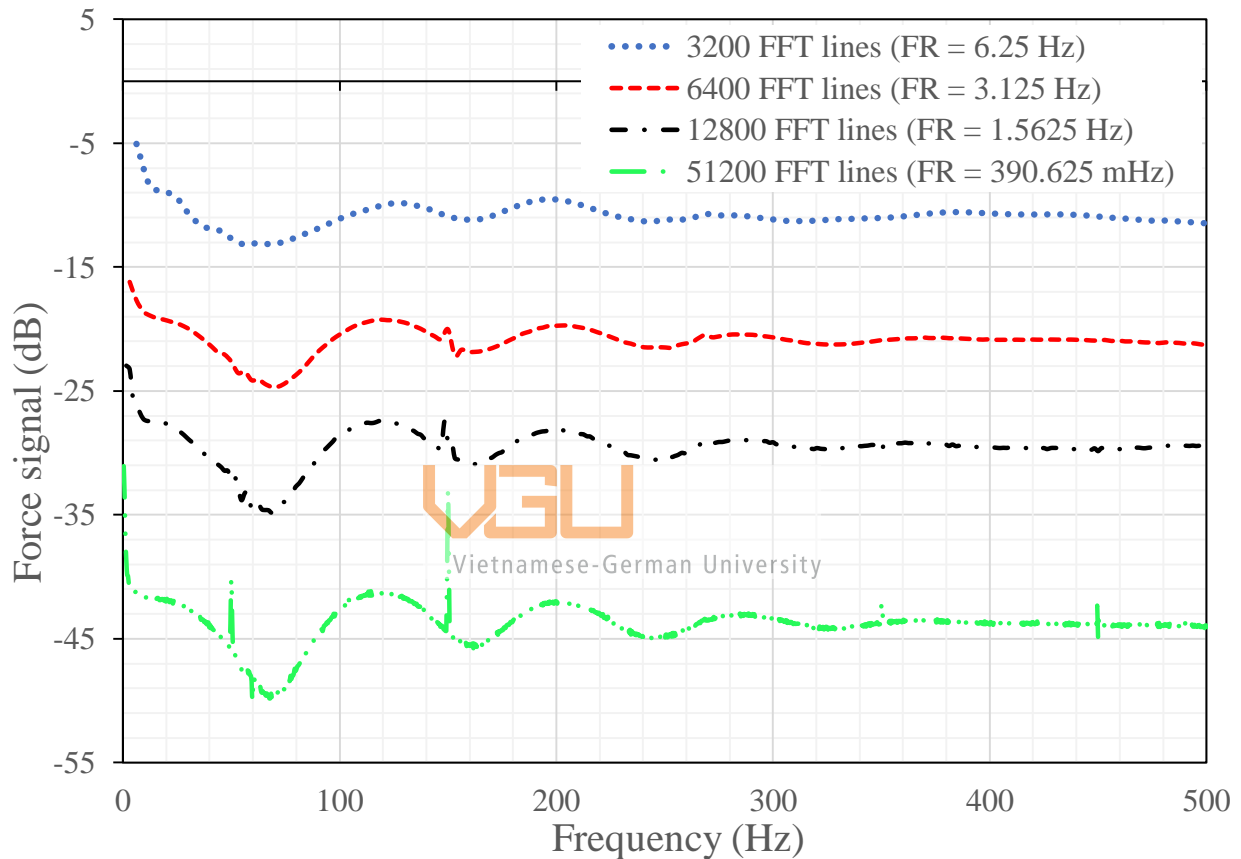


Figure 3-31: Force signals in the logarithmic scale and frequency domain, with 20 kHz bandwidth and different numbers of FFT lines

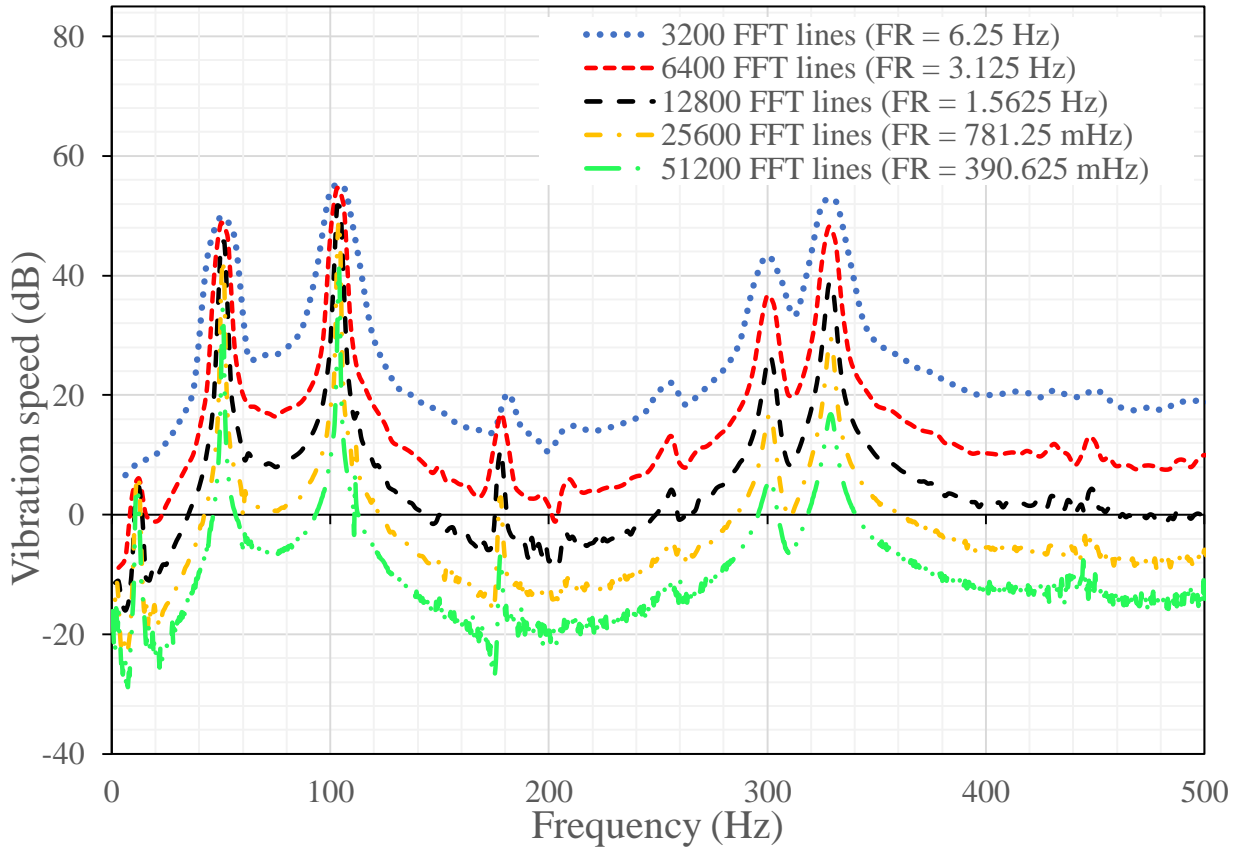


Figure 3-32: Vibration speed in the logarithmic scale and the frequency domain, with 12800 FFT lines and different bandwidths

Figure 3-31 shows that the smaller the frequency resolution, the more and higher spikes would be seen in the spectrum of the input. The peaks at multiples of 50 Hz can be attributed to the electronics effect (mentioned in 3.2.2.2). A more detailed comparison of these peaks is done within the table below. Note that only peaks with heights of 0.5 dB height or more would be considered.

Table 3-8: Spikes' heights seen with different numbers of FFT lines

Frequency (Hz) \ Number of FFT lines	50	150	350	450	Average
6400		2.109 dB			<u>2.109 dB</u>
12800		3.365 dB			<u>3.365 dB</u>
25600	6.796 dB	3.196 dB			<u>4.996 dB</u>
51200	6.340 dB	11.932 dB	1.346 dB	1.643 dB	<u>5.315 dB</u>
<u>Average</u>	<u>6.568 dB</u>	<u>5.151 dB</u>	<u>1.346 dB</u>	<u>1.643 dB</u>	

As it can be seen, a larger frequency bin would decrease (and eventually eliminate) the presence of sudden peaks within the spectrum of the force signal. However, simply choosing the option yielding the least amount of sudden peaks would not be fully effective. For example, using 3200 or 6400 FFT



lines would lead to a smooth spectrum for the input force signal, but the amount of spectral leakage in the vibration speed signal would be higher.

Furthermore, using a smaller frequency resolution would lead to a lower spectrum, for both the input force signal and the vibration speed. The reason might be because of lower Fourier coefficients due to longer measurement time as explained in this section above.

Among the 5 considered options, using 12800 lines is a comfortable compromise. There are still two visible sudden peaks in the spectrum, but they are fairly negligible and much smaller compared to using 25600 or 51200 lines. These peaks can be fully removed by adjusting the excitation point (illustrated in section 3.2.4.2). At the same time, the amount of spectral leakage is much reduced compared to using 3200 or 6400 lines. Another reason is that this thesis does not require a very fine frequency resolution. The frequency increment of 1.5625 Hz (obtained with 12800 lines on 20 kHz bandwidth) is deemed sufficient for the study.

Thus, for this thesis, the 20 kHz bandwidth would be used alongside 12800 FFT lines.

### 3.2.3.4 Window function

As mentioned above, the FFT algorithm is used in this thesis. The mathematics principles assume that the signals have an infinite circular topology. In other words, the two endpoints within the captured signal are assumed as being connected (having the same value) (National Instruments Corp., 2019). Therefore, one can try to perfectly capture a periodic signal, as seen below. In this case, there will be no leakage and thus no window function is needed.

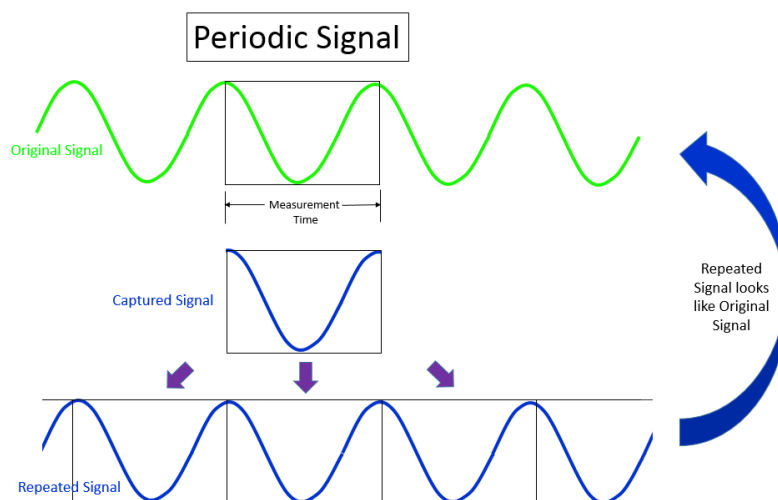


Figure 3-33: Example of a periodic signal (SIMCENTER, 2019)

Converting to the frequency domain, the spectrum would consist of a single line at the said frequency only:

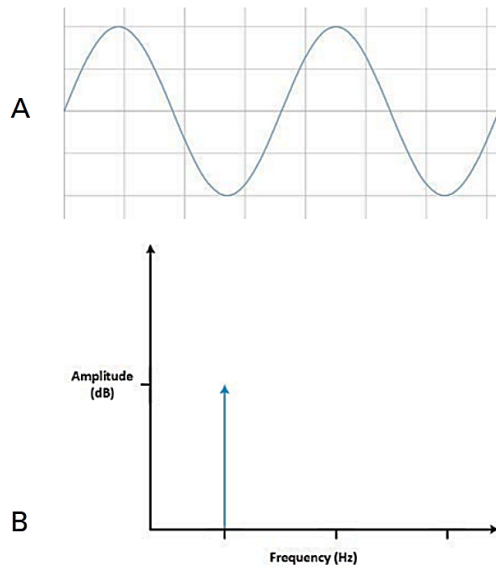


Figure 3-34: Converting a sine wave from the time domain (A) to the frequency domain (B) (National Instruments Corp., 2019)

However, in actual measuring conditions, the number of periods within the signal is not an integer, or the signal is not periodic, or the beginning and endpoints do not match each other, or the measured signal is captured in such a manner that the captured is no longer periodic. This means that the measured signal would be truncated into a new waveform with a different characteristic compared to the original. The repeated signal would show sharp transition changes or discontinuities within the spectrum. An illustration can be seen in the figure below:

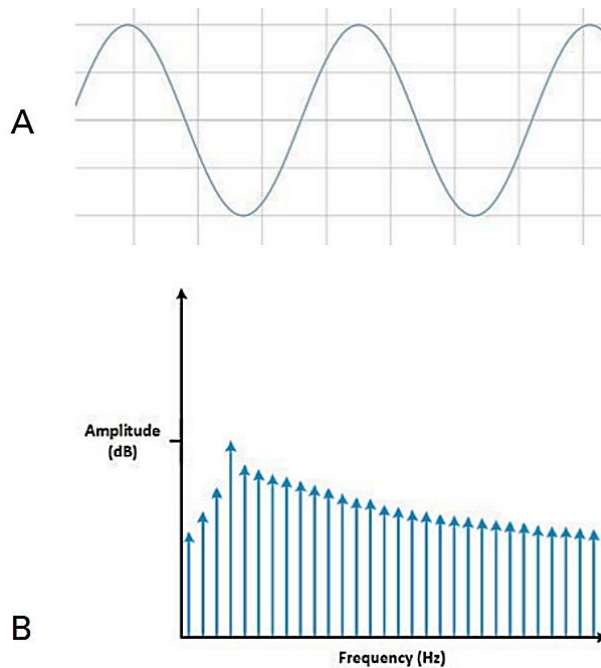


Figure 3-35: Measuring a non-integer number of periods (A) adds spectral leakage to the FFT (B) (National Instruments Corp., 2019)

Instead of a single peak at a set frequency, the spectrum is spread over a range of different frequencies. This mismatch is referred to as “spectral leakage”. A comparison of this effect within the frequency domain is summarized in the figure below. The original signal (in the time domain) is a sine wave.

To reduce the effect of leakage, the window functions would be applied. The most three famous (or commonly used) window functions are Rectangular, Hanning, and Flat Top (Hewlett Packard, 1989). It should be noted that the window function would be immediately applied after signal capture and before application of the FFT algorithm. An illustration of this process can be seen in the figure below.

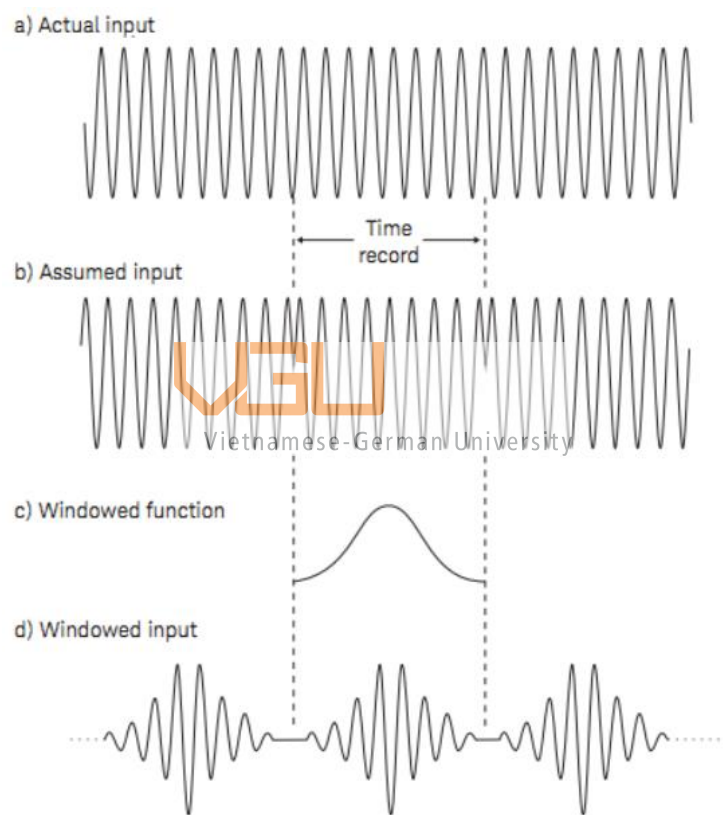


Figure 3-36: Application of window function in the time domain (Hewlett Packard, 1989)

One common characteristic of the window function is “lobes”, which can be observed while observing its frequency response (or within the frequency domain). There are two types of lobes shown within the frequency response: the main lobe and side lobes. A comparison of them could be seen below.

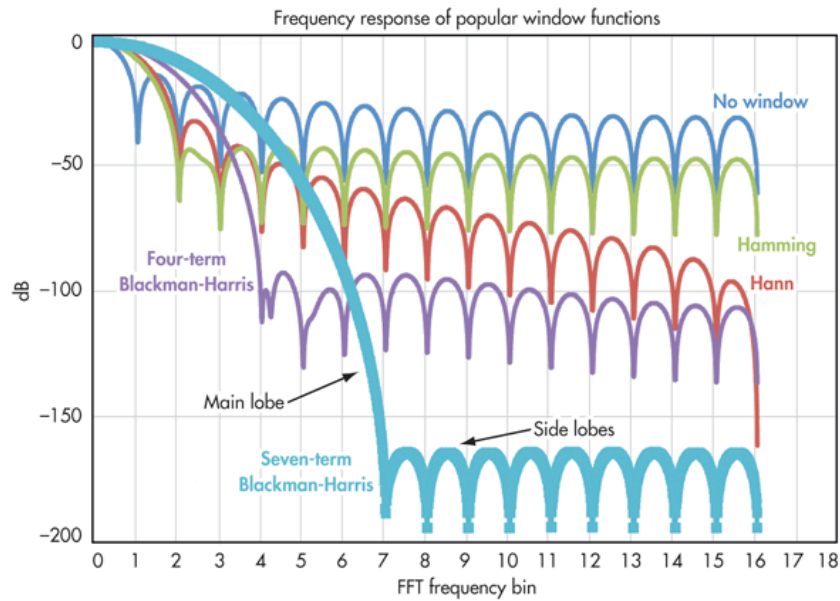


Figure 3-37: Main lobe and side lobes of a window function (frequency domain)

Generally speaking, a narrow main lobe (which will lead to a good frequency resolution) and a very low side-lobe level (resulting in having the signal being spread over fewer FFT bins) is preferred (Smith & Serra, 1987). However, it is not always possible to have both at the same time, and one must make the necessary trade-off, depending on the particular situation at hand.

Some related characteristic of a window function also includes 3 dB bandwidth (the frequency range where the signal is reduced by 3 dB compared to the reference, sometimes referred as half-power bandwidth), 60 dB bandwidth, the shape factor (ratio between 60 and 3 dB bandwidth) or noise bandwidth (width of an ideal filter with the same peak power gain). While these characteristics originate from the topic of filter, they are also adapted to describe window functions. Certain documents make no clear distinction between these two terms (Herlufsen, 1987; Shin & Hammond, 2008). Just like the main lobes and side lobes, these features representing certain compromises made within the window function design, and the user must make a certain trade-off in choosing the function.

The target of this section (section 3.2.3.4) is to study the effect of window functions and to determine which compromise has to be made. Thus, other than the three named functions above, available functions within the software would also be considered.

#### 3.2.3.4.1 Rectangular window function

The Rectangular window function is also known as the Uniform window function. This is a window function that weights every time records uniformly, or it can be understood as “no window function is applied” (Hewlett Packard, 1989; SIMCENTER, 2019). Some other names for this window

function include Flat, Boxcar weighting, or Rectangular Weighting. The general formula for this window function is:

$$w(t) = 1 \quad 3-26$$

The Rectangular window function is considered to be a poor function when a deterministic or harmonic signal is used, with a wide 60 dB bandwidth and large ripple up to 3.9 dB (Herlufsen, 1987). Furthermore, when the actual frequency of the sine wave falls in between the two frequency lines (determined by the FFT algorithm), the actual peak would drop by 36% and the effect of the leakage effect would be highly visible, this can be termed as the worst-case scenario in using Rectangular window function (Brandt, 2011; Herlufsen, 1987).

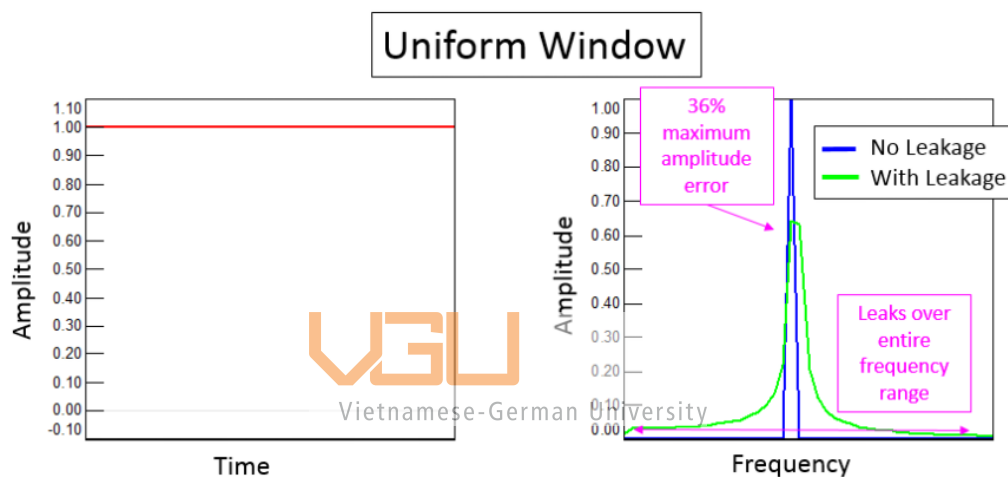


Figure 3-38: Left – Rectangular window function in the time domain. Right – "Worst case" of using Rectangular window function (SIMCENTER, 2019)

This effect can be explained by the slow fall-off rate of the side lobes, -13.3 dB for the first and -20 dB/decade for the subsequent ones (Shin & Hammond, 2008; Wickramarachi, 2003). However, when the signal is periodic (or when the frequency of the sine term lies precisely on the FFT lines, or "best-case"), this is a preferred window function. This Rectangular function is recommended for impact testing (hammer blow) with transient signal (Hewlett Packard, 1989; Herlufsen, 1987; Wickramarachi, 2003; Polytec GmbH, 2018). A more recent source (SIMCENTER, 2019) also recommends this window function if the impact measurements fully decay within the measurement time, which is also what is observed in the experiments.

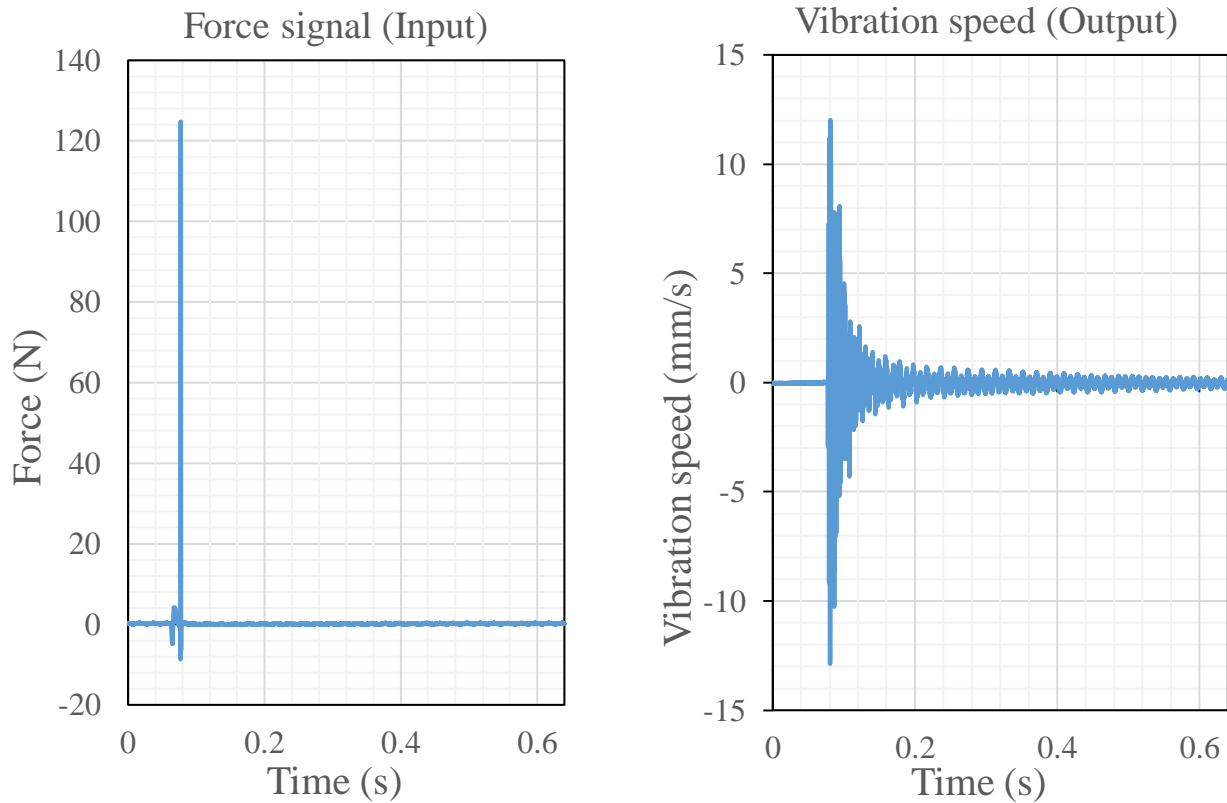


Figure 3-39: Collected data in time domain for input force signal and vibration speed

As seen from the figure above, both the input and output signals have mostly reduced to 0 at the end of the measurement time. Interpreting the numerical data from the exported file of the software shows that the

#### 3.2.3.4.2 Hann window function

Originally called Hanning, this is a good general-purpose window function and a commonly used function within the field of FFT (Shin & Hammond, 2008; Brandt, 2011; Herlufsen, 1987). One source even cites that the Hanning window is satisfactory for 95% of the situation (National Instruments Corp., 2019). Due to the presence of a similar name (Hamming window function, described below), the “Hanning” window function would be referred to as “Hann” in this thesis to avoid mistakes. The formula for this window function is

$$w(t) = \frac{1}{2} \left( 1 - \cos \frac{2\pi t}{T} \right) = \sin^2 \frac{\pi t}{T} \quad 3-27$$

Hann window function is capable of fixing certain issues of the Rectangular function, most particularly reducing the error if the frequency falls between two frequency lines (only 15% or 1.42 dB, compared to 36% or -3.92 dB of Rectangular function). If the said frequency is one-fourth of the frequency spacing, then the error would be 7.5% (Herlufsen, 1987; Hewlett Packard, 1989; SIMCENTER, 2019; Wickramarachi, 2003). Furthermore, the roll-off rate of the Hann window is

also better to the Rectangular, -31.5 dB for the first lobe and -60 dB/decade for subsequent ones (Wickramarachi, 2003; Shin & Hammond, 2008).

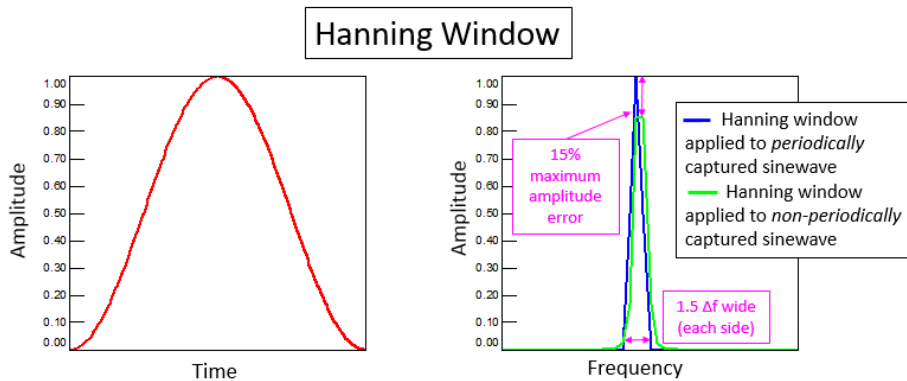


Figure 3-40: Left – Hann window function in the time domain. Right – “Worst case” of using Hann window function (SIMCENTER, 2019)

However, the cost of this is that the main lobe (in the frequency domain) of the Hann window is larger ( $4 \Delta f$ , double than that of the Rectangular window function), and the same can be said about the noise bandwidth ( $1.5 \Delta f$  compared to  $\Delta f$ ). The 3 dB bandwidth of the primary lobe is also increased from  $0.85 \Delta f$  to  $1.4 \Delta f$  (Wickramarachi, 2003). Due to differences in conventions, another source state the increase is from  $0.443 \Delta f$  to  $0.720 \Delta f$  (Prabhu, 2014). Eventually, the widening of the larger main lobe would lead to an increase in leakage when a sine wave is captured periodically

Vietnam-German University  
 Periodic Signal with and without Hanning Window

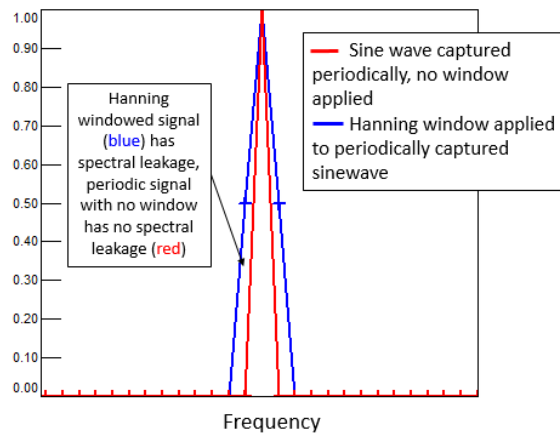


Figure 3-41: The periodically captured sine wave with the Hanning window (blue) is wider in frequency than the original signal (red) (SIMCENTER, 2019)

This tradeoff is accepted when the analyzed signal is not periodic or being random, illustrated by the figure below

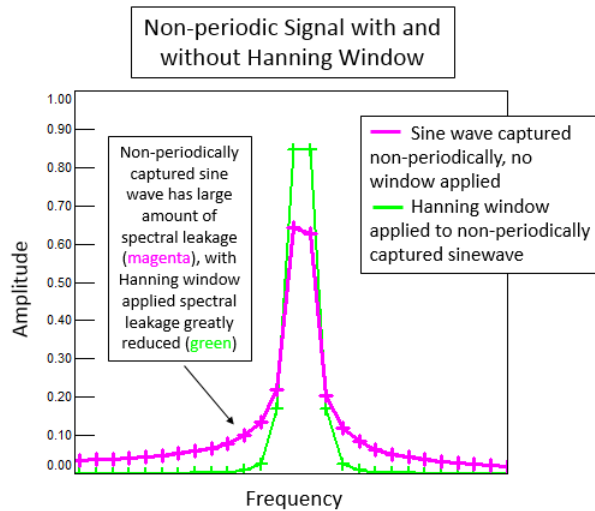


Figure 3-42: A non-periodically captured sine wave (magenta) has a spectral leakage over the entire bandwidth, applying a Hann window minimized the leakage (green) (SIMCENTER, 2019)

### 3.2.3.4.3 Hamming window function

Hamming is fairly similar to the Hann window function (National Instruments Corp., 2019). Visually speaking, while both Hann and Hamm functions have a sinusoidal shape, only the Hann function reaches 0 at both ends.

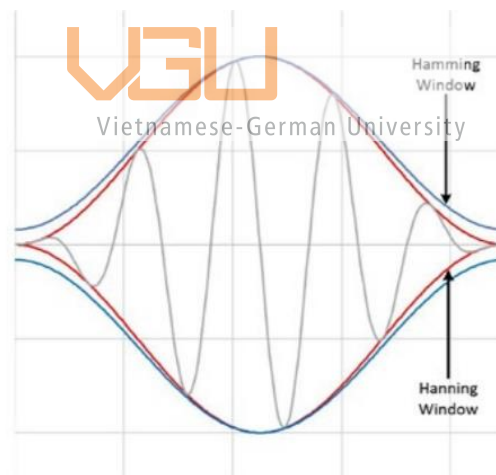


Figure 3-43: Hann and Hamming window functions in the time domain (National Instruments Corp., 2019)

The formula of Hamming function is given as:

$$w(t) = 0.54 - 0.46 \cos \frac{2\pi t}{T} \quad 3-28$$

This formula gives a good suppression on the nearest lobe (-43 dB) at the expense of other lobes (rolling off at -6 dB/octave, same as the Rectangular window function). The noise bandwidth of Hamming function is slightly better than Hann (1.363  $\Delta f$  compared to 1.5  $\Delta f$ ), and the same thing can be said about the 3dB bandwidth (0.651  $\Delta f$  compared to 0.720  $\Delta f$ ) (Prabhu, 2014).



Thus, this function is suited for analysis requiring good frequency resolution while moderate side lobes are not a problem (Shin & Hammond, 2008; National Instruments Corp., 2019). However, when the measured signal is noisy, this function is not recommended (Polytec GmbH, 2018).

### 3.2.3.4.4 Flat Top window function

Generally used for calibration purposes (Herlufsen, 1987; Polytec GmbH, 2018), Flat Top (also referred to as Flattop) is a window that has a high amplitude accuracy, with the maximum error given is 1% (Hewlett Packard, 1989). Other materials give an even lower error, such as 0.1% (Wickramarachi, 2003; Brandt, 2011) or even 0.01% (SIMCENTER, 2019).

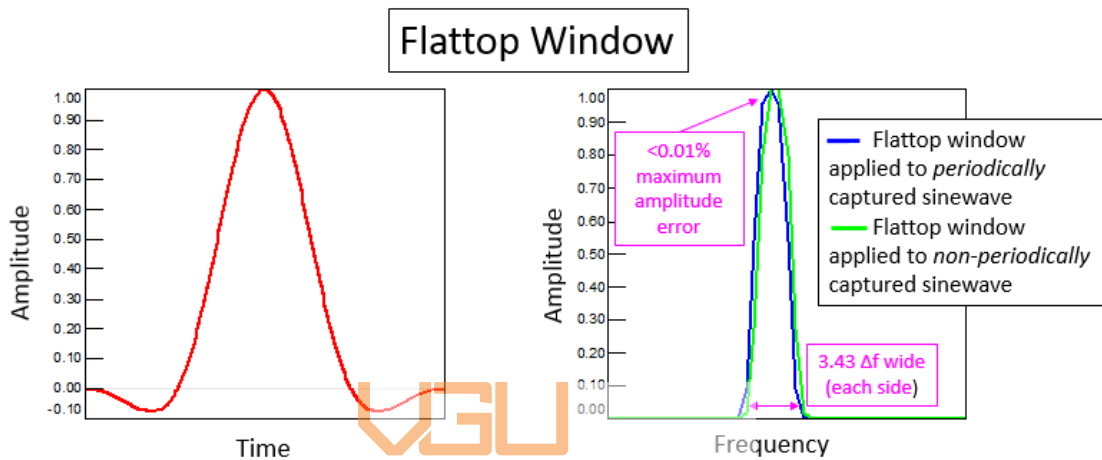


Figure 3-44: Left – The time-domain shape of Flat Top window, Right – Frequency domain effect of Flat Top window on periodic and non-periodic sine wave relative to measurement time (SIMCENTER, 2019)

There are a few variants for the Flat Top window function, the version used in the program has five terms arranged as below. The coefficients have been reduced to 5 decimal figures for ease of observation and writing.

$$w(t) = 0.21558 - 0.41663 \cos\left(\frac{2\pi t}{T-1}\right) + 0.27726 \cos\left(\frac{4\pi t}{T-1}\right) - 0.08357 \cos\left(\frac{6\pi t}{T-1}\right) + 0.00694 \cos\left(\frac{8\pi t}{T-1}\right) \quad 3-29$$

However, the trade-off is that this function has a very main lobe (up to 3.43 Δf) with no roll-off of the side lobes (Wickramarachi, 2003). This means that the peak width of this function would be considerably wider compared to others, such as Hann:

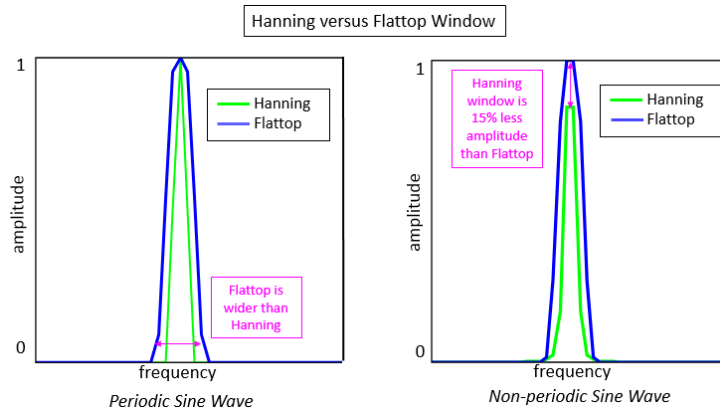


Figure 3-45: Differences between Hann and Flat Top window for periodic (left) and non-periodic sine wave (right) (SIMCENTER, 2019)

In addition, due to the wide main lobe (and thus more leakage), it is also plausible for this window function to miss out the peaks if they are very close to each other:

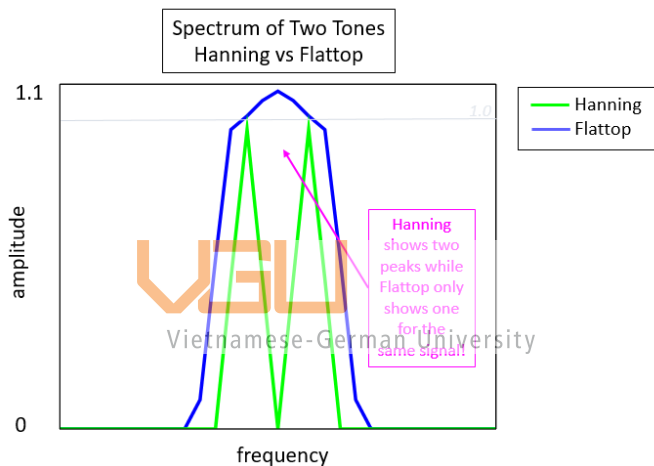


Figure 3-46: Spectrum of two periodically captured tones that are 4 Hz apart, Hann vs Flat Top functions (SIMCENTER, 2019)

Thus, the Flat Top function is recommended for calibration purposes, or when there is a clean periodic waveform to avoid the interested signal being lost in broadband noise. It can be concluded that this window function is not particularly fit for the experiment of this thesis.

### 3.2.3.4.5 Blackman-Harris window function

Blackman-Harris is another window function that shares certain similarities with Hann, other than Hamming function (National Instruments Corp., 2019). There are different variants of the function, but the one cited by the Polytec (and thus, the one used by the software in this thesis) has a side lobe attenuation of 92.1 dB (Polytec GmbH, 2018), making it a minimum four-term Blackman-Harris.

Thus, its formula is:

$$w(t) = 0.35875 + 0.48829 \cos \frac{2\pi t}{T} + 0.14128 \cos \frac{4\pi t}{T} + 0.01168 \cos \frac{6\pi t}{T} \quad 3-30$$

It is also called “Minimum Four-term Blackman-Harris”. This function has a fairly wide noise bandwidth (up to  $2 \Delta f$ ), which would lead to some degradation in frequency resolution, but it has a very good lobe suppression (-92 dB for the first lobe, and a decay rate of -6 dB/octave). It can also be considered as a general-purpose window function, alongside Hann and Hamming (Prabhu, 2014; National Instruments Corp., 2019). Thus, this is a function that can be used when good frequency resolution is needed or the measured signal is periodical, but it would be inappropriate when there is a great amount of noise (due to irregular attenuating behavior) or the signal is not periodic (Polytec GmbH, 2018).

### 3.2.3.4.6 Bartlett window function

Bartlett window function is a function that has the shape of an isosceles triangle in the time domain. It is considered to be a compromise between the Rectangular function and cosinusoidal ones (such as Hann, Hamming, and Blackman-Harris) (Polytec GmbH, 2018). It has the first sidelobe suppression of -26 dB, and a roll-off rate for further lobes of -6 dB/octave. The formula for this function is:

$$w(t) = \begin{cases} \frac{2t}{T}, & 0 \leq t < \frac{T}{2} \\ 2 - \frac{2t}{T}, & \frac{T}{2} < t \leq T \end{cases} \quad 3-31$$

### 3.2.3.4.7 Exponential window function

For tests such as the hammer blow, the vibration can die out within a few seconds of the impact. However, if the vibration lasts longer than the measurement window, then the signal analysis would need some extra damping to make sure that the signal is fully decayed by the end of the measurement time (Hewlett Packard, 1989; Fladung, 1997; Wickramarachi, 2003). One solution for this is called the Exponential window function, to force that to happen.

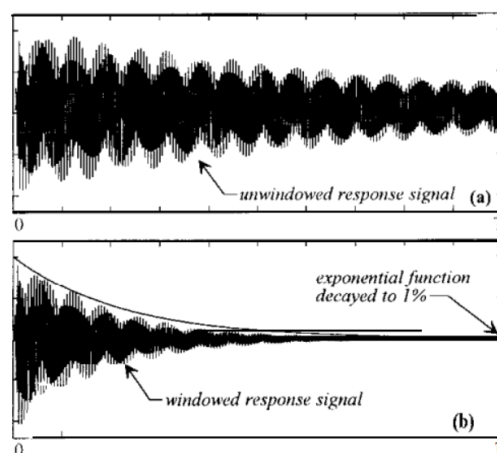


Figure 3-47: Usage of Exponential window function (Fladung, 1997)

The proposed formula for this function is:

$$w(t) = e^{-t/\tau} \quad 3-32$$

with tau ( $\tau$ ) as the time constant. However, according to the document provided by Polytec (manufacturer of the equipment used in this thesis), using the Exponential window would have the signal “attenuated to the e-th part ( $e=2.718$ ) of its initial value according to time constant  $\tau$ ” (Polytec GmbH, 2018). This means that the actual formula used in this thesis would be slightly different above. The proposed formula is

$$w(t) = e^{-\tau t/T} \quad 3-33$$

This function form is also found in one reference literature (Brandt, 2011). To test which formula is the one used in the software, two-parameter values would be chosen, with  $\tau=1$  and  $\tau=8$ .

This window function is recommended to use when the measured signal (excited by the hammer blow) is decaying weakly, however, it is unfit for measuring periodic signal (Polytec GmbH, 2018; Wickramarachi, 2003). One interesting feature of this function is that it does not attenuate the signal at the beginning of the measurement time, unlike other sum-of-cosines and triangular functions.

#### 3.2.3.4.8 Choosing a window function

Generally speaking, window functions are not fit for analyzing transient input, of which the vibration speed is an example. An illustration of this can be seen below

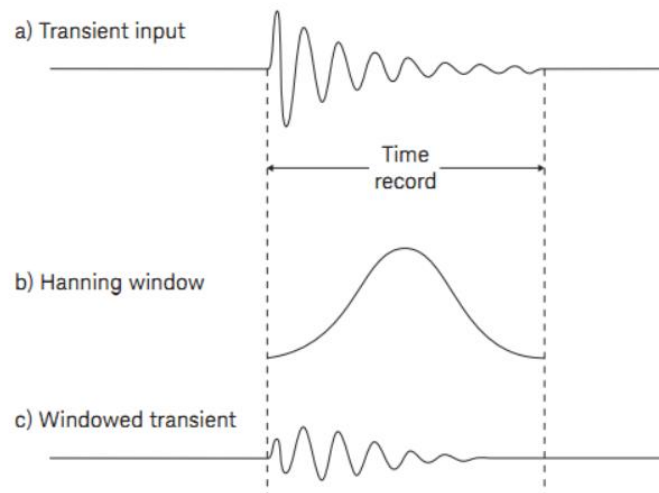


Figure 3-48: Loss of signal information due to using window function (Hewlett Packard, 1989)

This can be attributed to the formulas of the window functions. Most of the transient information or the vibration speed happens in the early section of the measurement time. However, this section is damped and lost due to the design of the window function. This effect can be seen in Figure 3-50.

In the figures below, the Rectangular window function is compared with the Hann function when the signal is a sum of 3 sine waves (Figure 3-49) and when the signal is transient (Figure 3-50).

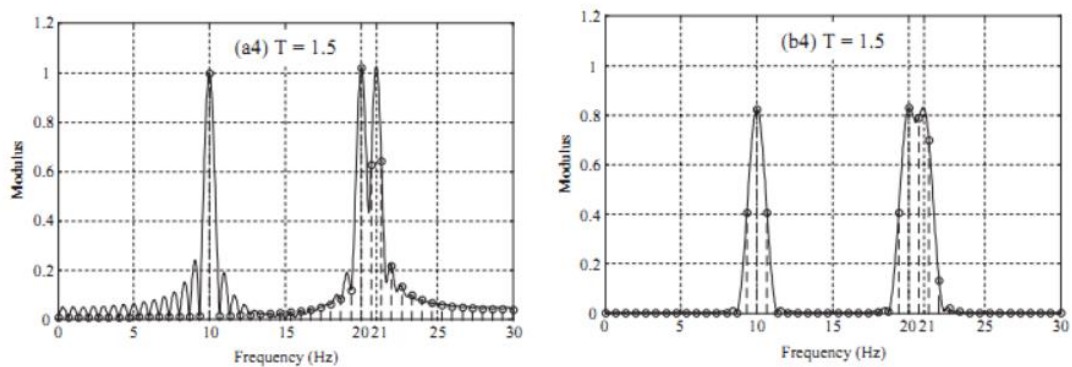


Figure 3-49: FFT of a sum of 3 sine waves, using Rectangular window function (left) and Hann window function (right) (Shin & Hammond, 2008)

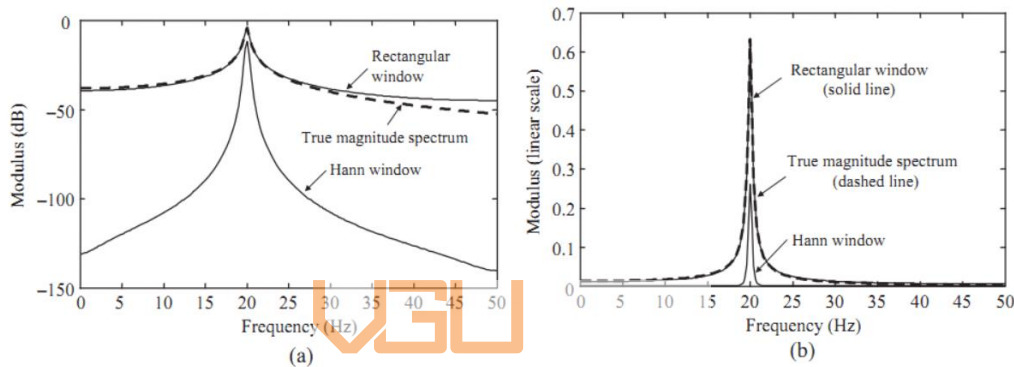


Figure 3-50: FFT of a transient signal, using Rectangular and Hann window functions (Shin & Hammond, 2008)

In both cases, the resonance frequencies are identified. However, using Rectangular would lead to a serious rippling effect in the spectrum (even if the magnitudes of the peaks are obtained correctly) when the signal is a combination of sine waves. However, when the signal is transient, the Rectangle function would lead to a spectrum staying close to the true spectrum.

A more general comparison between the four concerned window functions can be seen below, where the functions are plotted on the same graph in the time domain as below. The graph is obtained via the Octave program to best simulate the functions being used in actual conditions. As it can be seen, the Rectangular function has the highest magnitude, followed by (in descending order) Hamming, Hann, Blackman-Harris, and Flat Top. Thus, it is expected that, for individual signals, the magnitude of the signal obtained with the Rectangular function would be the largest.

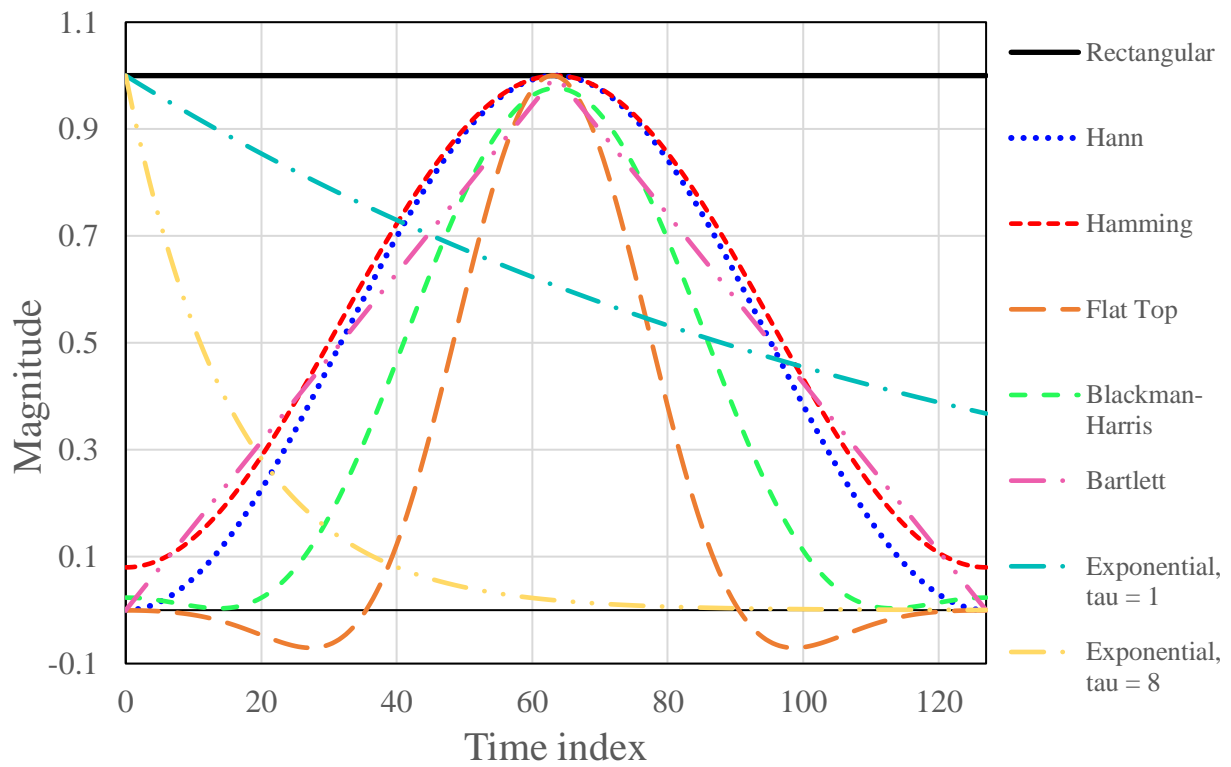


Figure 3-51: Window functions in the time domain

Further comparing the four window functions can be done via analyzing the graphs of the Transfer functions, the Input force signal, and the Vibration speed signal.



Vietnamese-German University

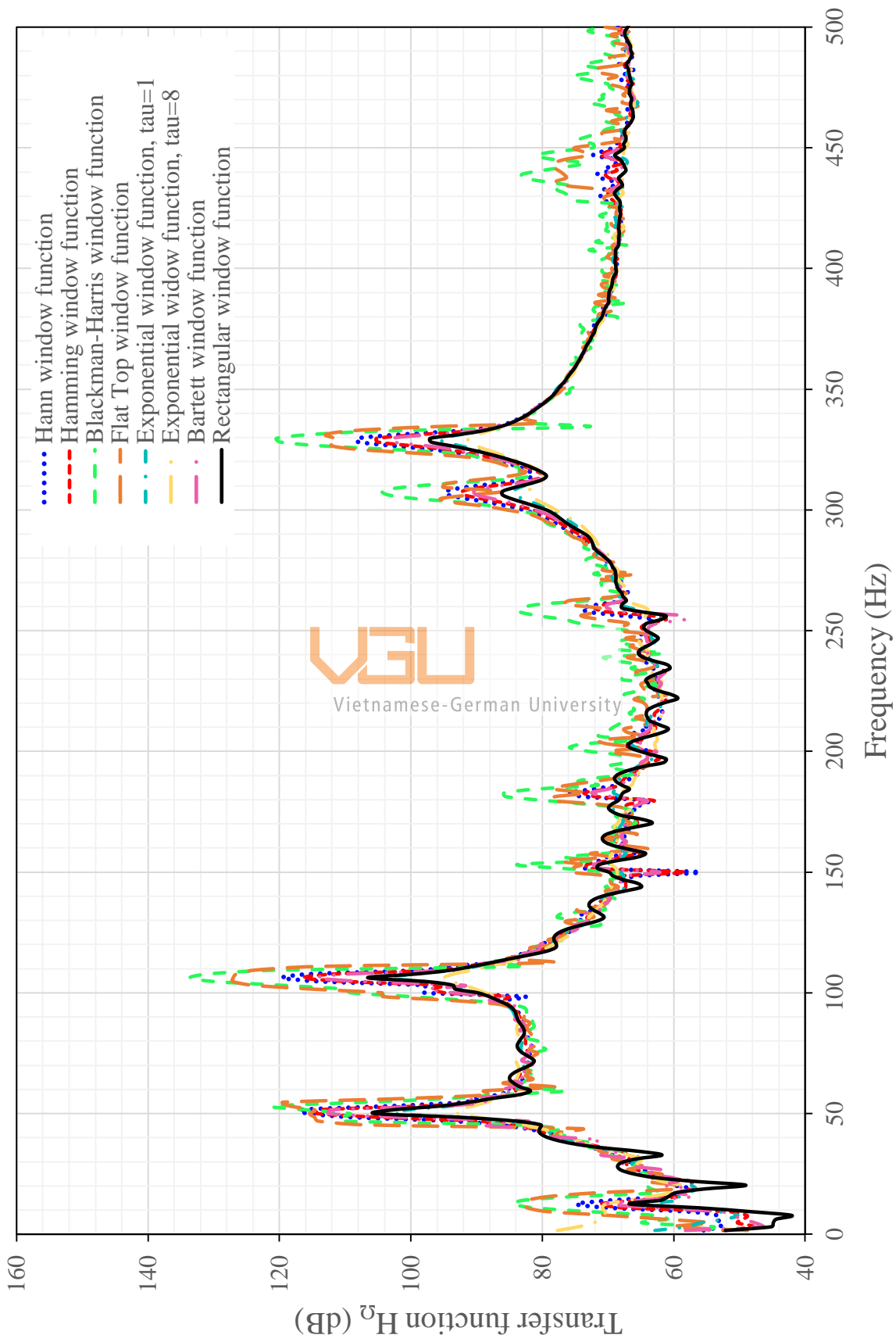


Figure 3-52: Transfer functions in the logarithmic scale and the frequency domain with different window functions

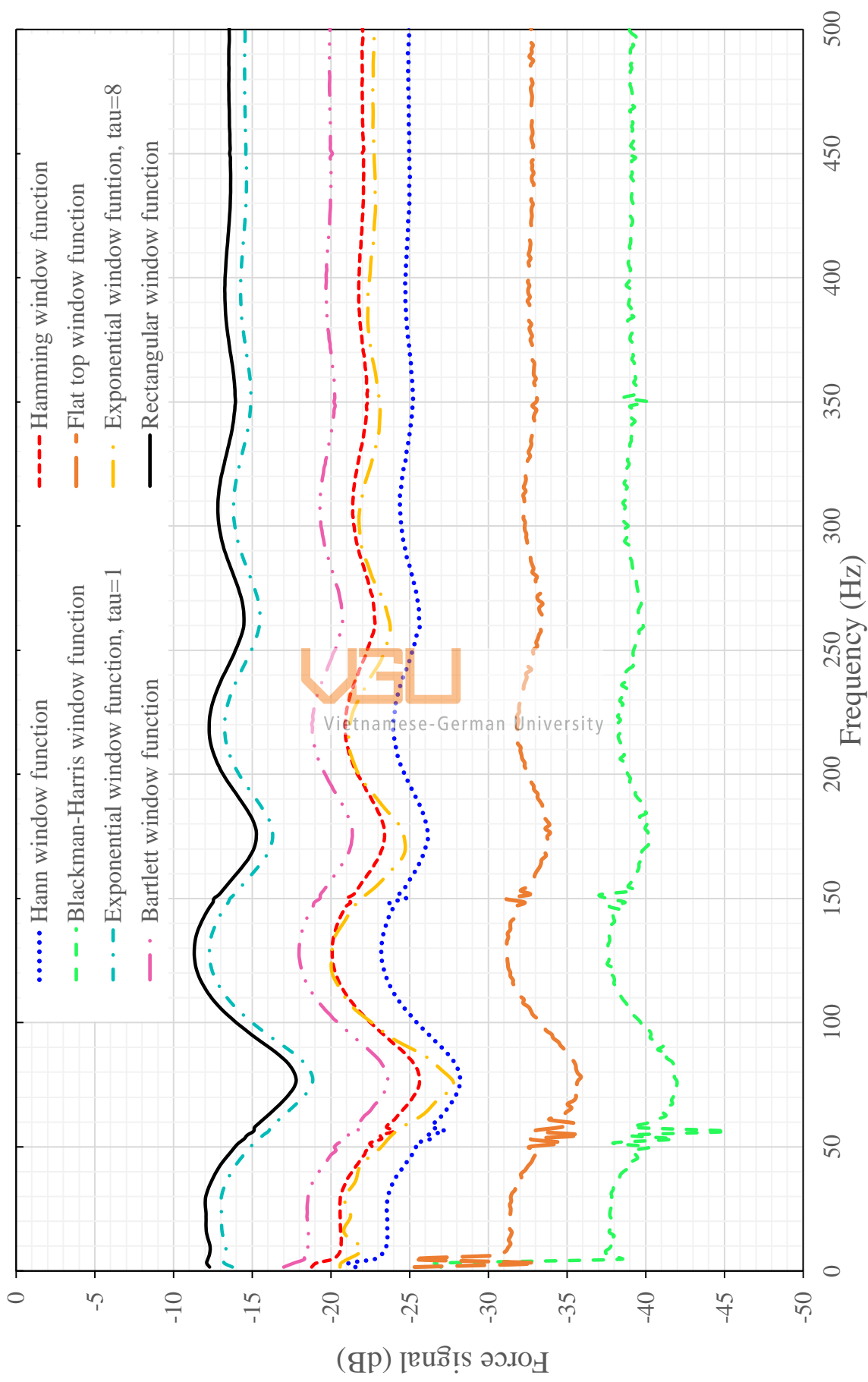


Figure 3-53: Input force signals in the logarithmic scale and the frequency domain with different window functions



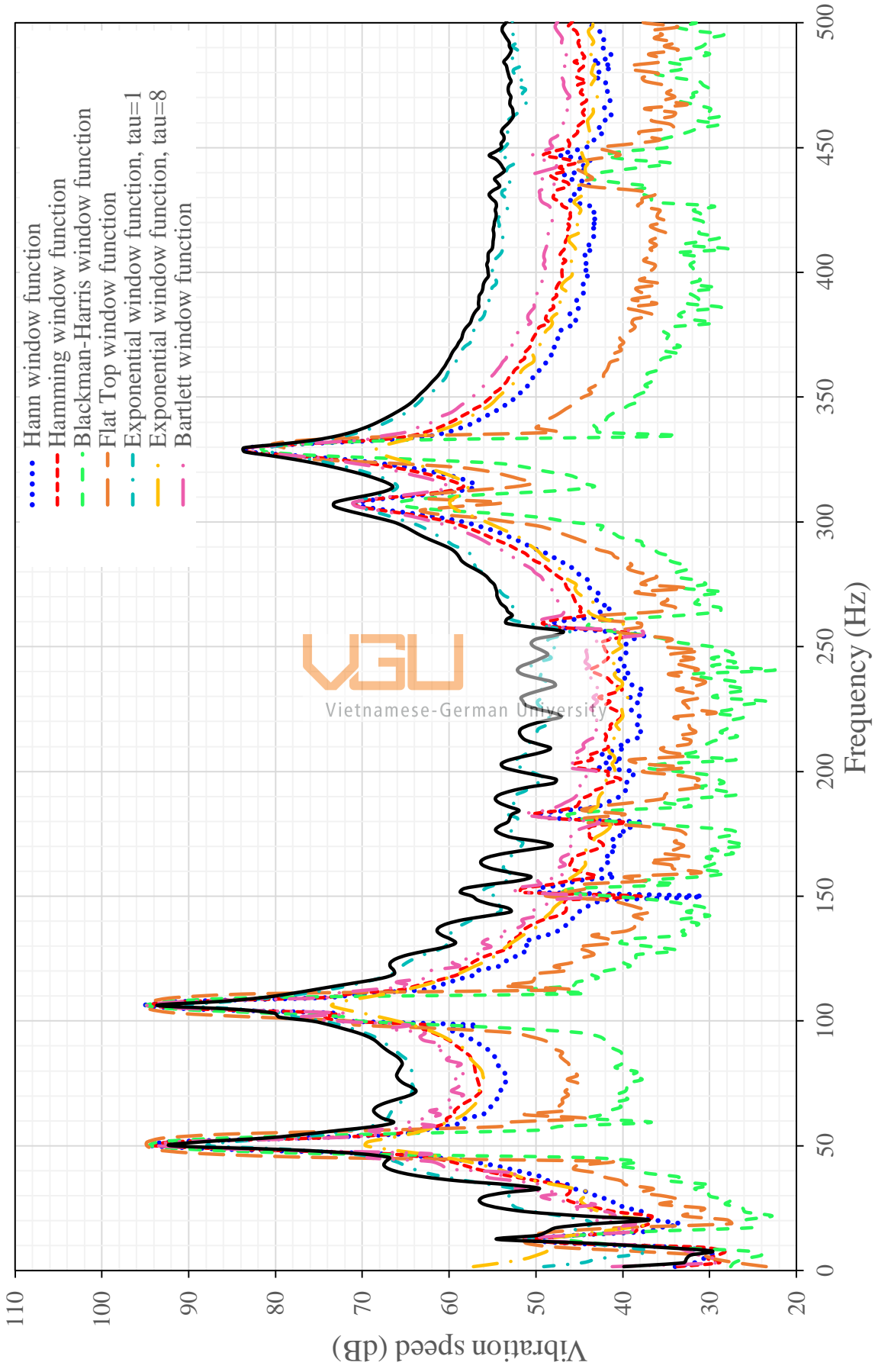


Figure 3-54: Vibration speed signals in the logarithmic scale and the frequency domain with different window functions

While considering the inputs and outputs individually, the Rectangular window function would lead to the highest spectrum. This is due to the nature of “no window” so the signal level would not be decreased, which is not the case for the remaining functions (each of which is a sum of cosines). Furthermore, using the Rectangular function would lead to the least amount of sudden jumps, resulting in a smoother spectrum for the Transfer function.

With regards to the two Exponential window functions (with different time constants  $\tau$ ), it is cleared that the signal is damped with  $\tau=8$ , while the effect is negligible with  $\tau=1$ . The benchmark for comparison is the spectrums obtained with the Rectangular window function. This proves that the proposed formula for the Exponential window function (3-33) would be the one used by the software, while the original formula (3-32) is not due to different definitions of the time constant  $\tau$ .

The general behaviors of the remaining window functions also fall within expectation. Due to the software setting, the impulse will be made when the measurement time has run 10% of its course. At these points in time, only the Rectangular and Exponential ( $\tau=1$ ) window functions have a sufficiently high magnitude (90% and more) to preserve the signal level. This would explain why the two spectrums obtained with these two functions are much higher compared to others. Figure 3-51 shows that Hann and Hamming have roughly the same graph, which leads to their spectrums being very close to each other. Bartlett function would lead to higher individual spectrums compared to these two, due to a higher magnitude at the first segment of measurement time. Flat Top and Blackman-Harris window functions would lead to the lowest spectrum due to their small magnitudes. However, the Flat Top function has a higher spectrum (despite having a lower magnitude on most indexes) because of its wider main lobe and less attenuation on the side lobes.

Comparing different window functions, it can be said that the general trend (increasing and decreasing) in the vibration signal is the same, suggesting that the amount of spectral leakage here is either minimum or the same on all functions. It should be noted that this is one major pitfall of the Rectangular window function. In addition, it also provides one of the smoothest spectrum (in all three graphs), leading to easier analysis. The “rippling” effect, while visible, falls within non-peak areas and generally has no effect on the current analysis.

From the theory and experiment data above, it has been concluded that the Rectangular window function preserves the most signal strength in this case. Therefore, this function would be chosen for usage in this thesis.

### 3.2.3.5 Conclusion for parameter setups

In summary, the parameter setups are as followed:

- Signal averaging is done over 9 points with the complex type
- A low-pass filter of 2 kHz is used
- A bandwidth of 20 kHz and 12800 FFT lines
- The Rectangular window function is used


## 3.2.4 Measurement parameters

### 3.2.4.1 Choosing measurement area

As the granulated material is only partially filled inside the stator arm, it is clear that the bottom part of the stator arm would be damped immediately. However, it is unverified if other sections are also damped. This section aims to answer that answer with the final goal is to pick a specific area for evaluation.

There are four measurement areas to compare for this topic, including a line at the top of the stator arm, an area at the top of the stator arm, the bottom part of the stator arm, and the profile of the generator ring. There might be differences in the evaluation result of these areas, so an investigation is needed. A comparison of the three possible sites is below. For easy reference, each area is designated with a short-handed name. It should also be noted that to see the bottom of the stator arm clearer, the image is slightly zoomed in compared to others.

Table 3-9: Different measurement areas being compared

Measurement area	Illustration	Short-handed name
A line at the top of the stator arm		Top Line

An area at the top of the stator arm		Top Area
The bottom part of the stator arm		Base
The profile of the generator ring		Bottom Edges

Each measurement area is compared between the blank (or standard/initial) state and with the granulated material filled in. The material is recycled and granulated plastic from the OvGU laboratory. The result (evaluated via Transfer function) is as followed:

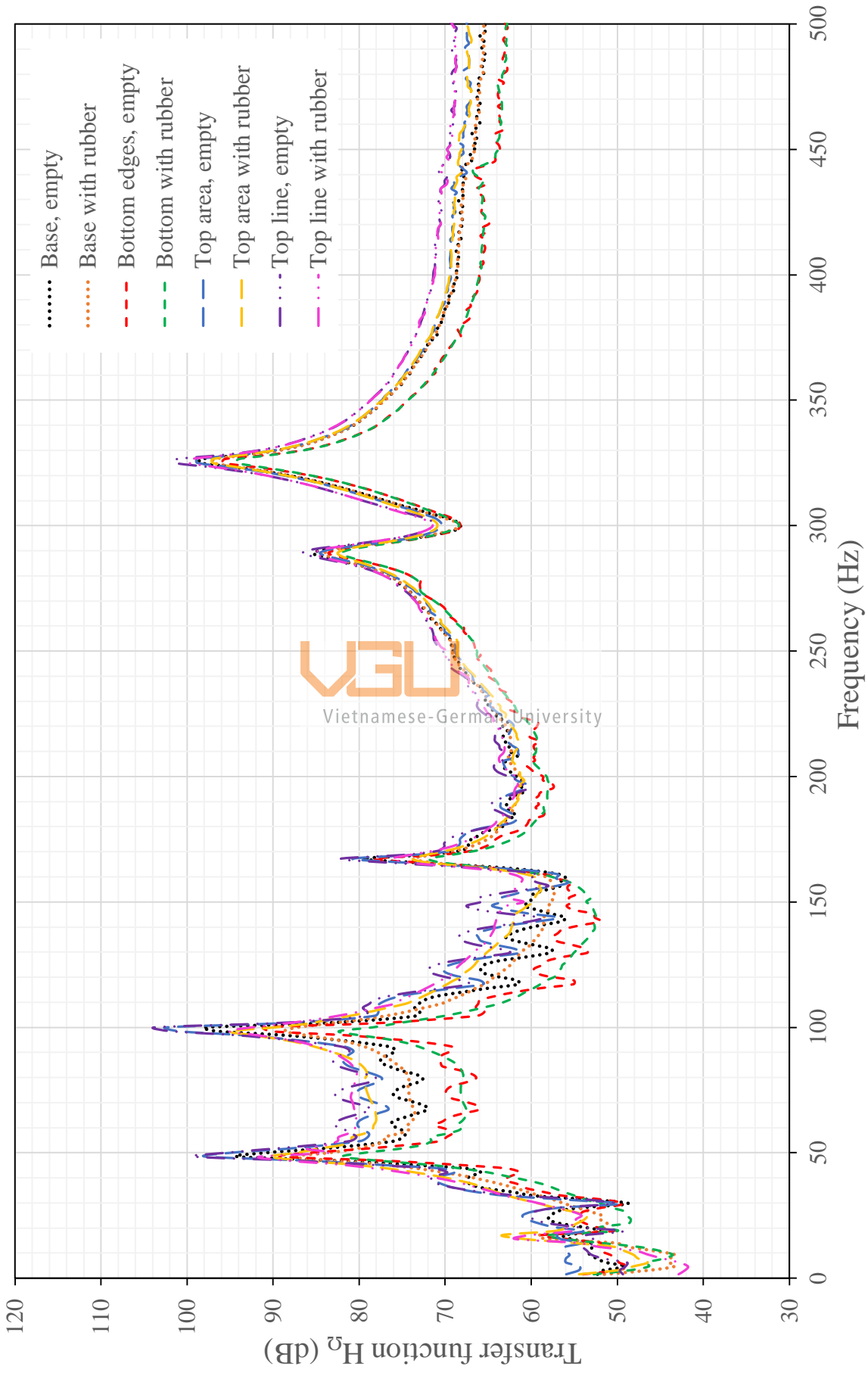


Figure 3-55: Transfer functions from different measurement areas

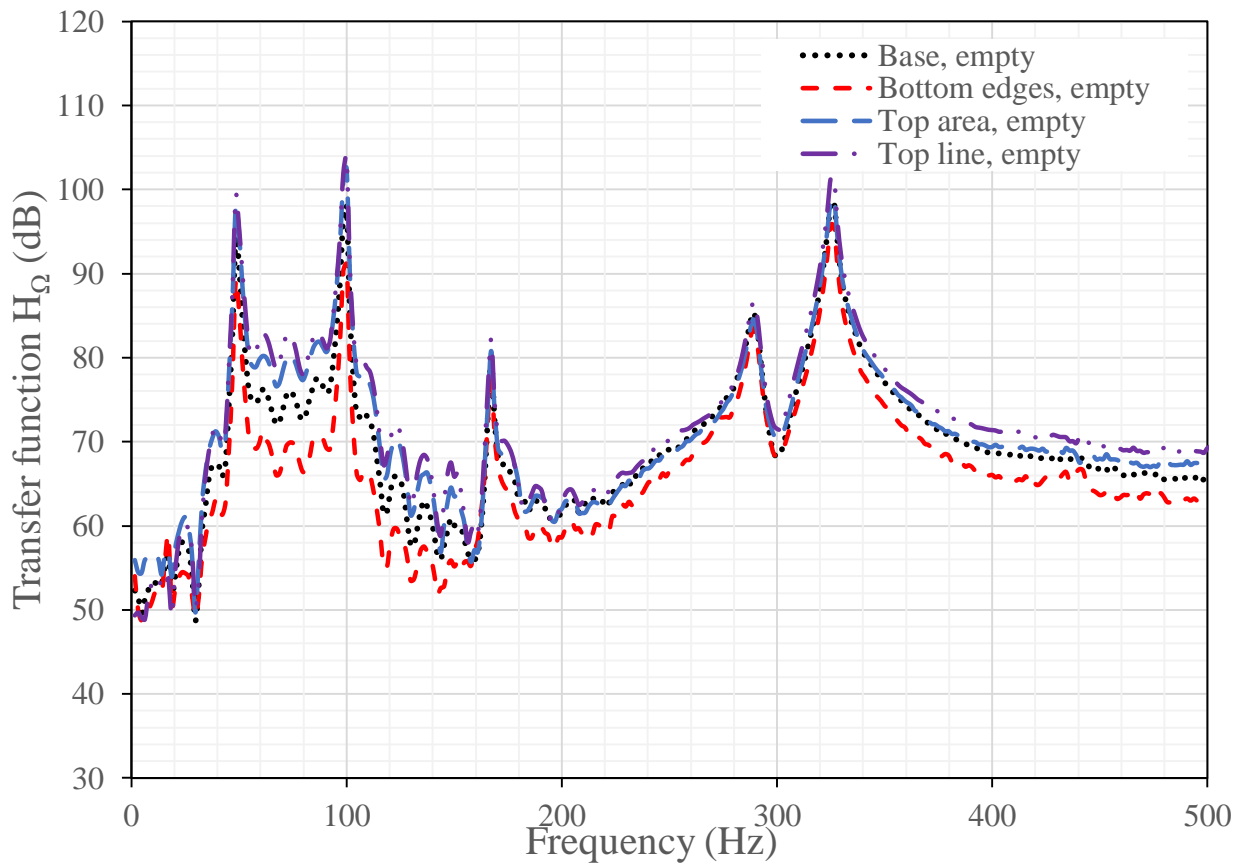


Figure 3-56: Transfer functions from different areas without granulated materials

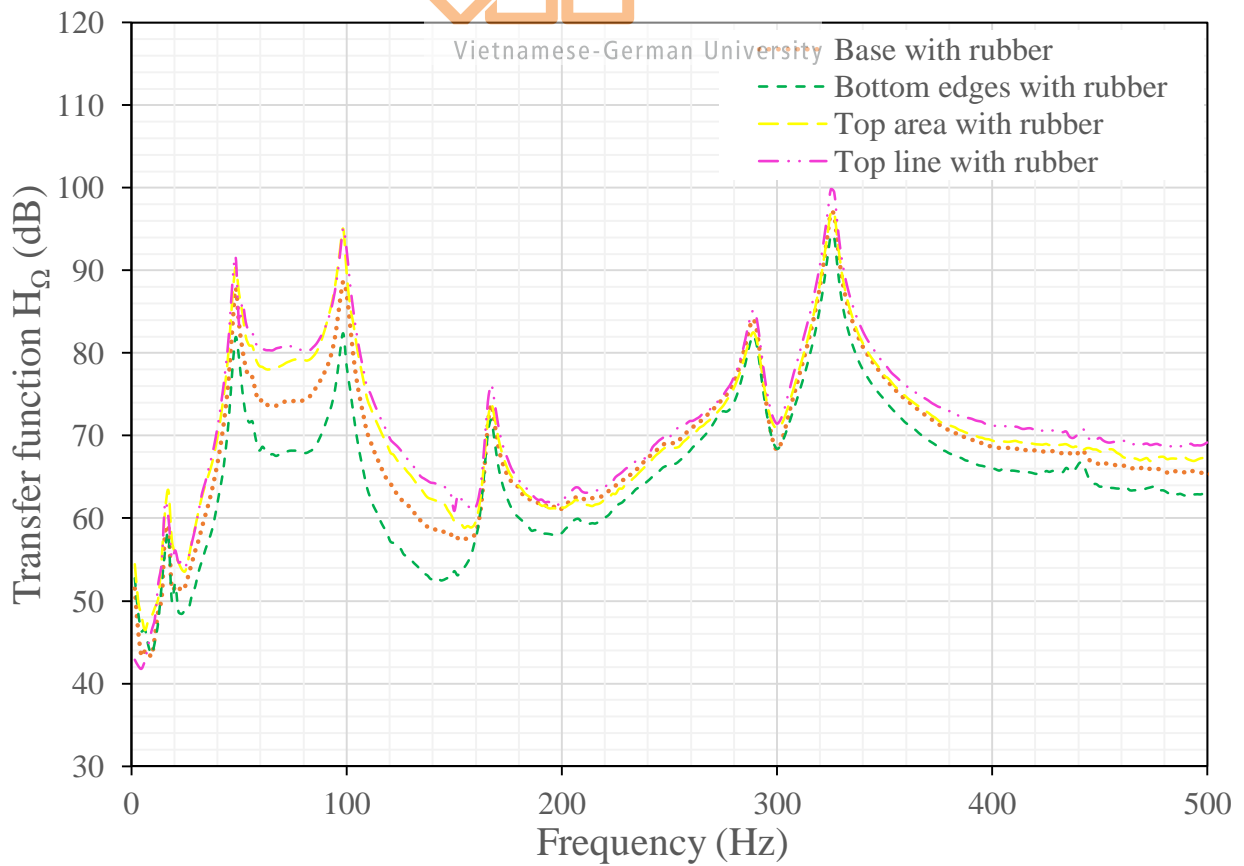


Figure 3-57: Transfer functions from different areas with granulated materials

As can be seen from the three graphs, the general shape of the transfer function is the same in the three cases. The frequencies where the peaks are shown (or natural frequencies) are the same for all measurement areas. Furthermore, there is no significant difference between the transfer functions of the line and the area at the top of the stator arm. The negligible difference here can be attributed to the definition of these measurement areas. The position of the “Top Line” is a part of the “Top Area”, and thus, both will share similar characteristics. Thus, between these two measurement areas, and within the scope of this thesis, the line at the top of the stator arm would be preferred. This area needs a shorter measurement time (due to having fewer measurement points) and yields the same result.

With regards to the other two measurement areas, the general trend and the positions of the resonance of the peaks are also the same as the first two. This can be explained as the structures (the stator arm and the generator ring) are fully bolted into each other, creating a final rigid structure. Therefore, the overall vibration would be homogeneous (in the sense that the general vibration characteristic would be the same). These two have lower peaks within the spectrum (compared to the “Top Line” or “Top Area”) due to having different vibration speeds, this is caused by a closer distance to the excitation point.

Furthermore, Figure 3-55 shows that regardless of the measurement area, the effect of the particle damping is noticeable and measurable. The reduction effect, considered at the

Therefore, the choice of measurement area would be based on the time required to complete the full evaluation. For this reason, the line at the top of the stator arm would be chosen to be assessed. Because the number of measurement points here is the least, the measurement time is also the shortest.

#### 3.2.4.2 Choosing excitation point

The scientific and engineering principles of choosing the correct excitation point are based on modal analysis, a more complex variant of vibration analysis used in this thesis. Due to limits in scope, this topic would only use basic knowledge, rather than in-depth analysis of the field.

Generally speaking, when the input force is set at natural frequencies, the specimen would vibrate at a “fixed” form, known as mode shape. Each frequency would yield a typical mode shape, and each mode shape is matched with the appropriate frequency. When this happens, there are interesting features in the shape, called nodes (stationary points) and anti-nodes (point vibrating with the

maximum amplitude). The positions of nodes are of particular importance, because if the excitation points are the same at these nodes, then some mode shapes will disappear. Concerning the Frequency response function (as we as the vibration speed signal), it means that peaks of certain frequencies will not be shown anymore (Hewlett Packard, 1986; Crystal Instruments, 2016).

This would make the analysis not being done fully and completely. In a broader sense, it would miss a few natural frequencies, which are seen as critical safety parameters in various fields of engineering. For this reason, the effect of different excitation points must be investigated, in order to prevent an accidental application of excitation during the main experiments of the thesis.

A total of four excitation points are investigated in this section. Their positions and their respective transfer functions are shown in the following two pictures.

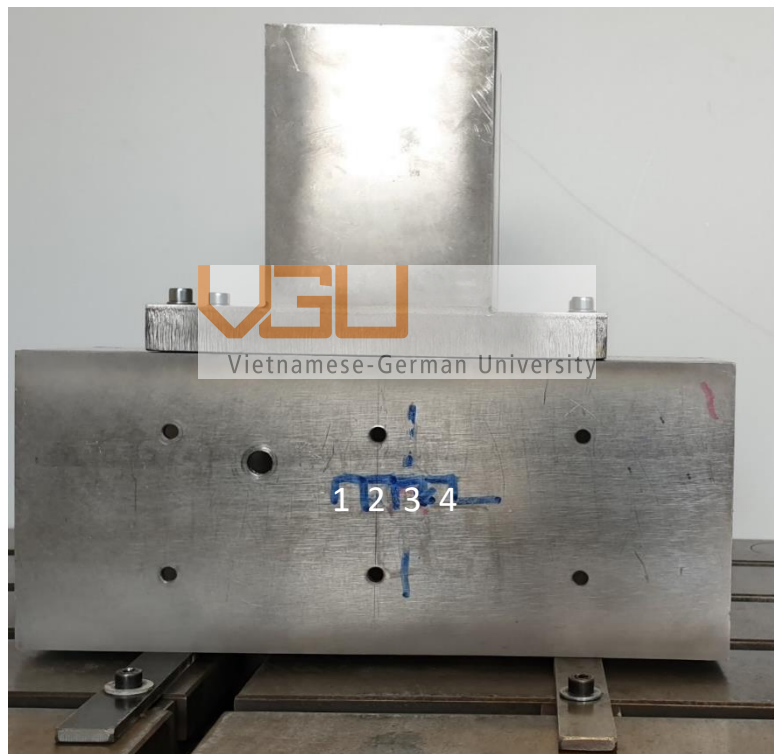


*Figure 3-58: Excitation points on the generator ring*



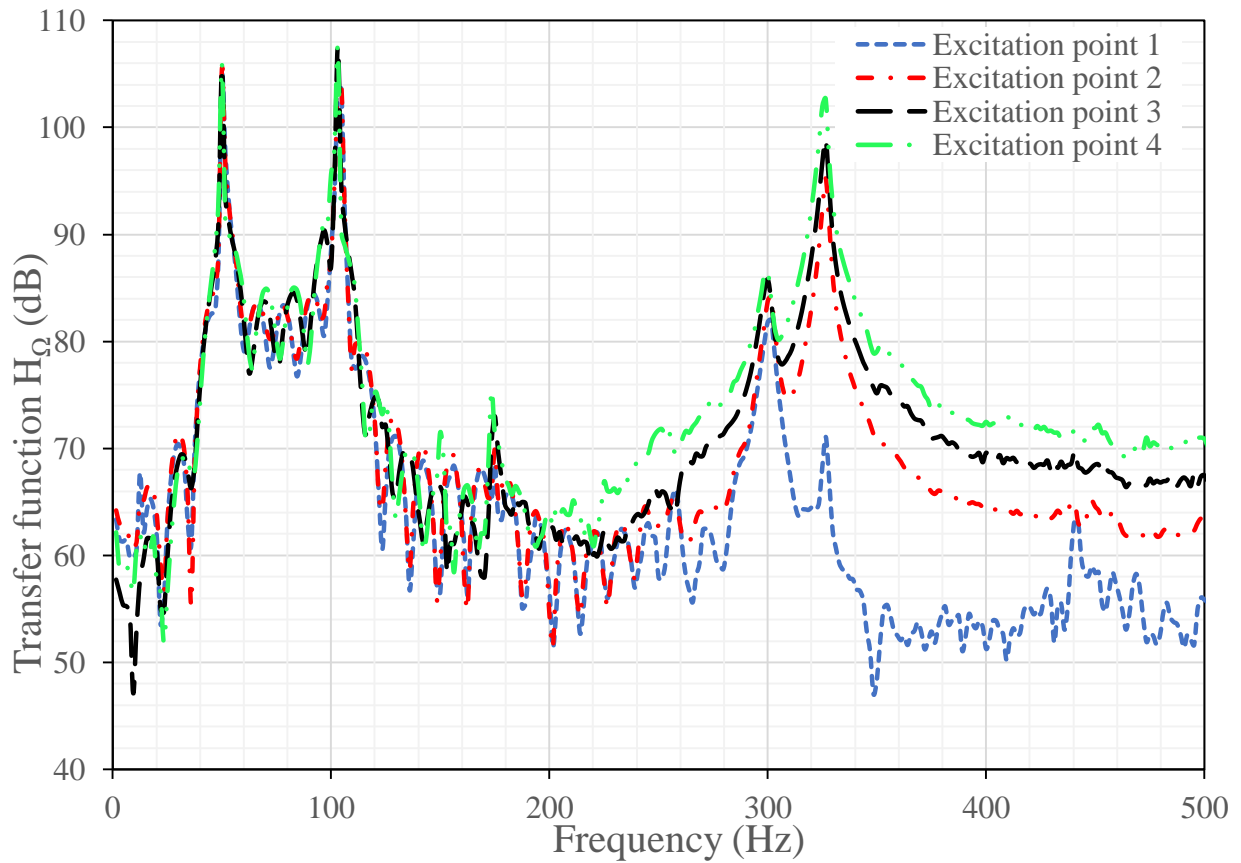


Figure 3-59: Transfer functions for different excitation points

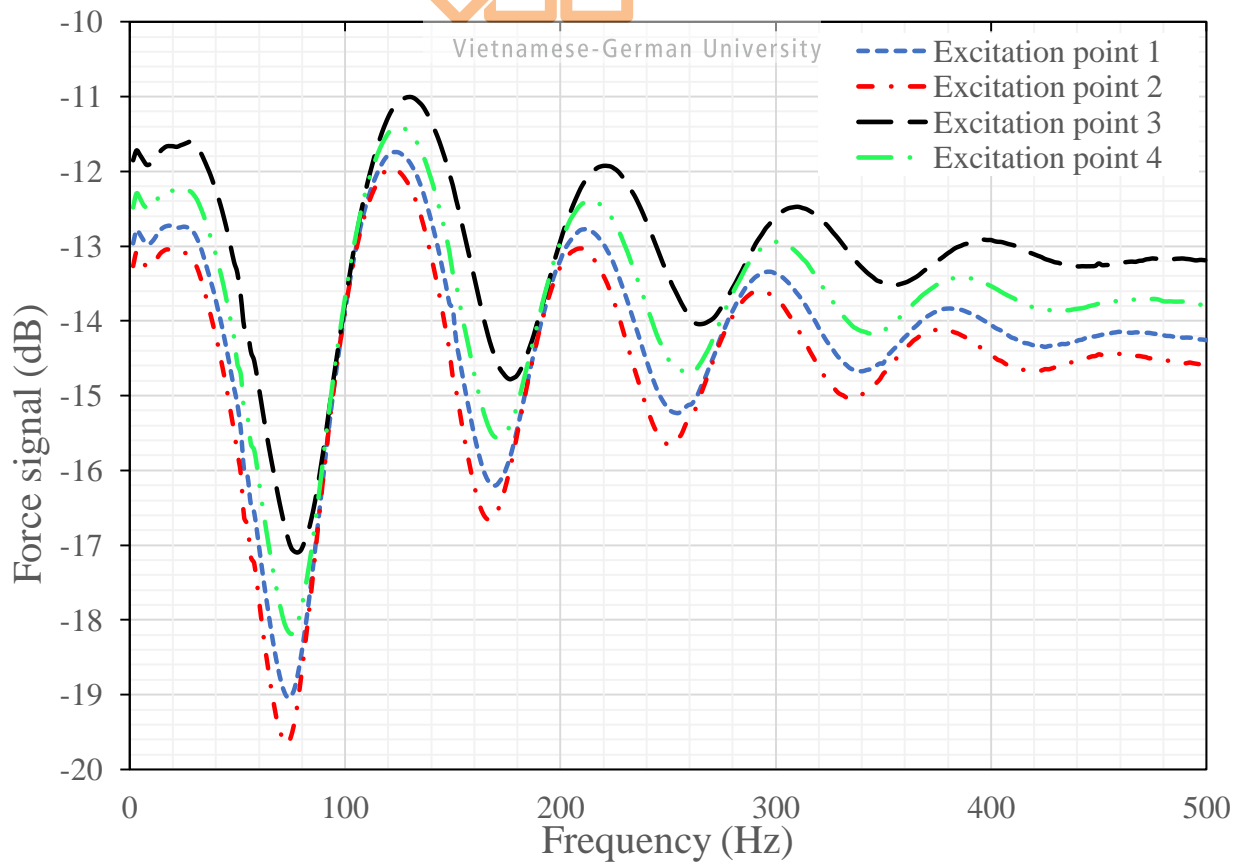


Figure 3-60: Force signal from different excitation points

From Figure 3-59, it is seen that if the impulse is delivered at Excitation point 1, the resonance frequency at 330 Hz has disappeared. This suggests the possibility that this is a node of the system. However, more tests would be required to verify this theory. This process is not a part of this thesis, so it will not be done.

Furthermore, Figure 3-60 shows that by using different excitation points, the spectrum would be slightly different from each other. The peaks at multiples of 50 Hz (shown in Figure 3-12, Figure 3-28, Figure 3-31, and partially in Figure 3-53) have also disappeared, confirming the idea put forth in section 3.2.2.2. Figure 3-59 shows that, by using Excitation point 3, the obtained spectrum is the easiest to observe. The peak at 170 Hz has a good difference compared to the surrounding zone, and the rippling effect (due to using the Rectangular window function) is less compared to others. Hence, Excitation point 3 will be used for the main experiments of this thesis.

### 3.2.4.3 Generator's signal

Section 3.2.2.2 above mentions that it is not plausible to achieve reproducibility with some form of signals. The particular signals being considered in this section are White noise and Pseudo random. The first form of signal is defined as a random signal, of which the spectrum is flat after being adapted to the concerned bandwidth. Meanwhile, Pseudo random is a signal being generated in the frequency domain, using a uniformly distributed random number (Polytec GmbH, 2018). An in-depth study about these two signals (as well as other signals available in the program) is not within the scope of this thesis, however.

In order to use these signals, the force sensor must be directly attached to the generator ring. An illustration of this can be seen in the figure below.

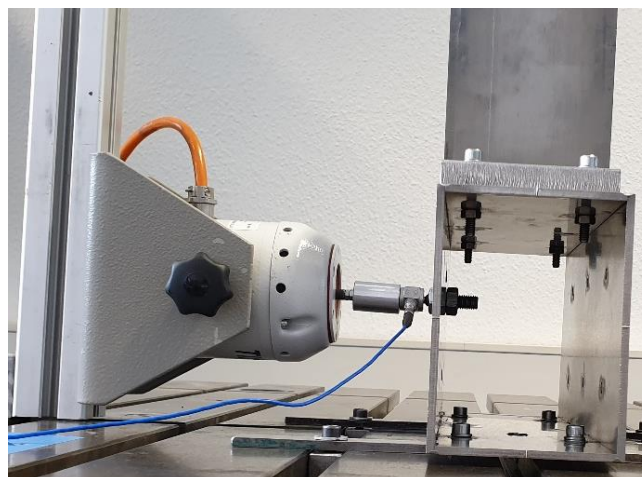


Figure 3-61: Fixing the force sensor on the generator ring

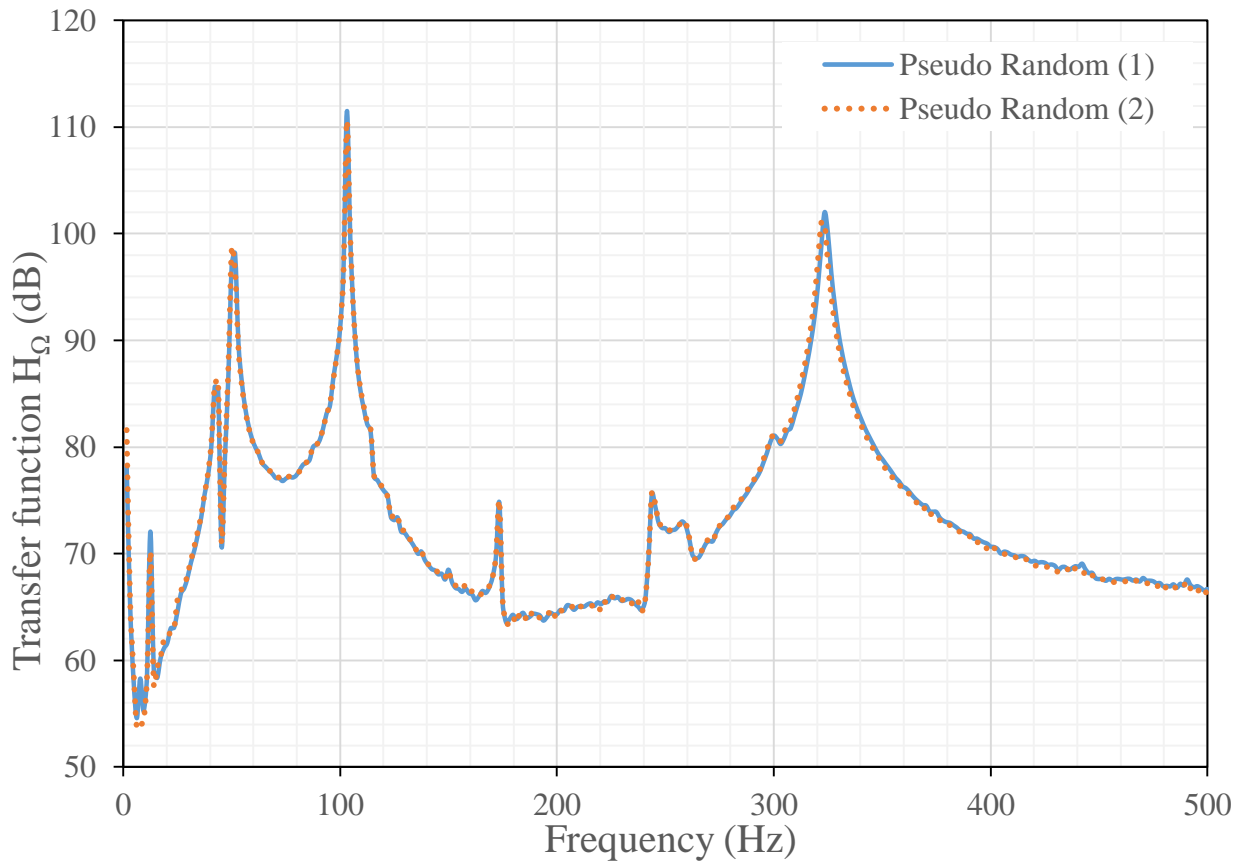


Figure 3-62: Inability to reproduce the result with the Pseudo random signal

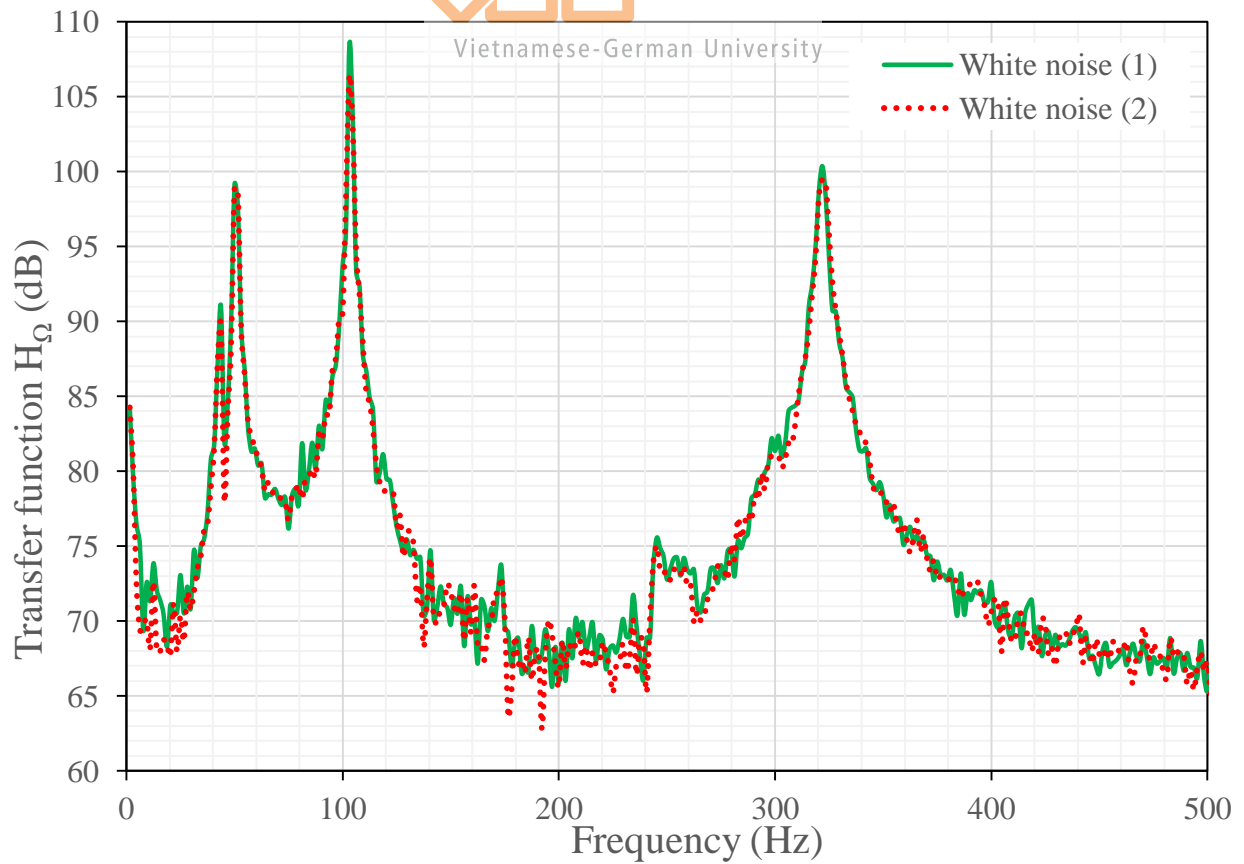


Figure 3-63: Inability to reproduce the result with the White noise signal

As seen from the two charts above, attaching the force sensor on the generator ring and using related signals failed to reproduce the result, here defined as having a difference of 1 dB or less for the peaks in the spectrum. Using Pseudo random signal, the difference of 1.1 dB is seen at 330 Hz and 0.9 dB at 50 Hz. While may not be a real peak, the peak at 12.5 Hz shows a variance of 2 dB. Using White noise signal, 2 dB and 1.2 dB differences are observed at 100 and 43.75 Hz respectively.

With no reproducibility being made, the measurement result would not be trustworthy, and therefore, these two signals as well as attaching the sensor on the generator would not be used in this thesis.

The reason why reproducibility is not obtained is not a target of this thesis. However, it is suspected that there are more uncertainty sources in this setup, including a not perfectly perpendicular shaker rod (especially where both ends are fixed), more components between the rod and the generator ring, as well as the randomness nature of the signals being used.

#### 3.2.4.4 1/3 Octave band

Octave band can be defined as a frequency range between two values, where the ratio between them is determined beforehand. The specific octave band used in the program is 1/3 Octave band, a form of bandwidth analysis (Polytec GmbH, 2018). Bandwidth analysis is quite useful when there are random or broadband vibration in the spectrum, where no sharp peak would be made. This is in contrast with constant or tonal frequencies, where peaks would be produced and they can be represented as a function of time (Amick & Bui, 1991).

In fields such as acoustics, instead of analyzing the frequency content on each individual frequency line (or FFT line in this thesis), the spectrum would be evaluated by parallel bandpass filters. The bandwidth would be either a full octave or 1/3 octave. For a full octave, the ratio between the highest and lowest frequency is approximately 2 times, and the bandwidth is approximately 0.70 the central frequency. The values for the 1/3 octave band are 1.2589 and 0.23 respectively (Brandt, 2011).

Ülgen, et al. summarised in their paper in 2016 that the 1/3 octave band can be used to simplify the vibration spectrum.

In this thesis, the values given on individual spectral lines within every octave band will be computed together to generate a characteristic value for the said band. On the one hand, it allows the charts to be observed much easier. On the other hand, the precise location and values of the peaks would be lost. This graph would be helpful to complement the normal graph of the frequency

spectrum, especially when there are multiple lines or when the effectiveness of particle damping is not so clear.

An illustration on the supportiveness of the 1/3 octave band chart can be extracted from the work of Amick and Bui:

### EXAMPLE FAB FLOOR VIBRATIONS - VERTICAL Converting Constant Bandwidth to 1/3 Octave Band

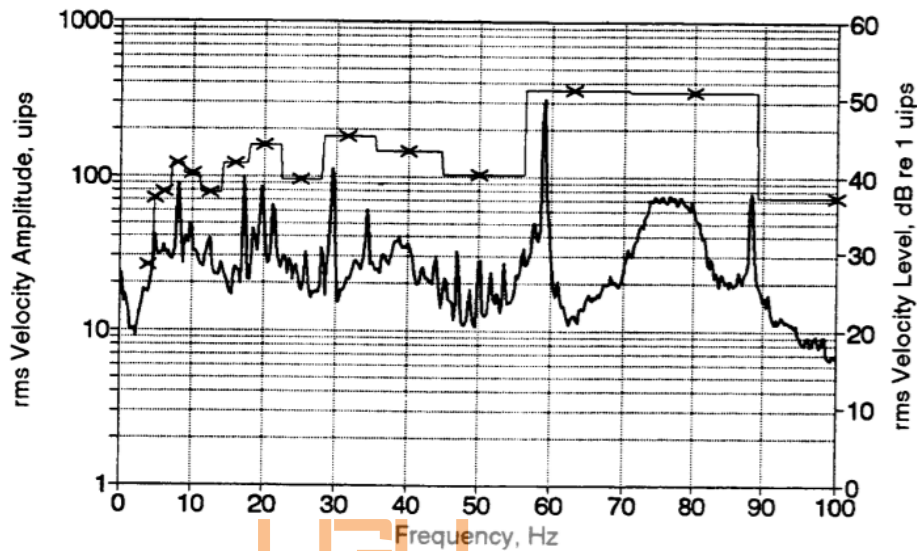


Figure 3-64: Conversion from normal frequency spectrum (bold line) to 1/3 Octave band (thin line, X marker) helps to improve visibility of the chart (Amick & Bui, 1991)

### 3.2.5 Final setup for the thesis's measurements

As studied in section 3.2, the parameters for the experiment have been set up, and they are concluded as follows:

- Using a scaled model of the generator ring and stator arm.
- Using the transfer function in the frequency domain and the logarithmic scale to evaluate the damping effect.
- The process of converting from the time domain to the frequency domain is FFT.
- The shaker will deliver an impulse, effectively a knock on the test specimen.
- The white hammer is used alongside the impulse signal of the generator
- The line at the top of the stator arm is chosen for evaluation
- The laser scanner is set at 2.65m from the stator arm
- Signal averaging is done over 9 points with the complex type
- A low-pass filter of 2 kHz is used

- A bandwidth of 20 kHz and 12800 FFT lines
- The Rectangular window function is used

### 3.3 Measurement procedure

After applying the setup for the parameters (the overall setup of hardware is shown in Figure 3-5 and the parameters concluded in section 3.2.5 above), the experiments can be carried out. The main goal is to compare the damping effect using different filling volumes, and different packages at the same volume. The granulated rubber is used as the particle damping in this thesis.

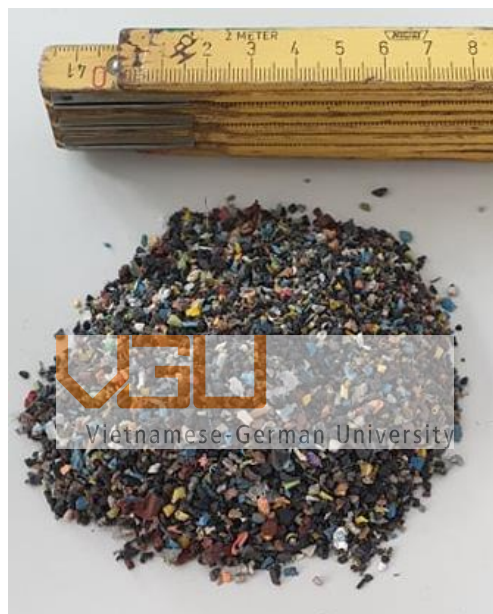


*Figure 3-65: OvGU Rubber*

The damping effectiveness will be evaluated via two different settings. In the first test, the stator arm would be filled with various volumes of materials to evaluate the damping effect. For the second test, materials would be filled into balloons (come in two different sizes), the effectiveness of particle damping in two scenarios will be compared against the pure particle damping of the same mass.

In both cases, the reproducibility will also be checked. This is done by first doing the measurement on a blank specimen as the reference, then removing the stator arm, fixing it again with the same tightening torque, and then carrying out the measurement on it again. If this value matches the reference result at the beginning of each test, then it can be said that the result is reproduced and the experiment is trustworthy.

## 4 Result

### 4.1 Reproducibility

This section would check the reproducibility of the experiments. As can be seen from the graph below, the measurement result of the first set of experiments is reproducible, which means that the measurement data of the experiment is trustworthy. The second set also reports the same result.

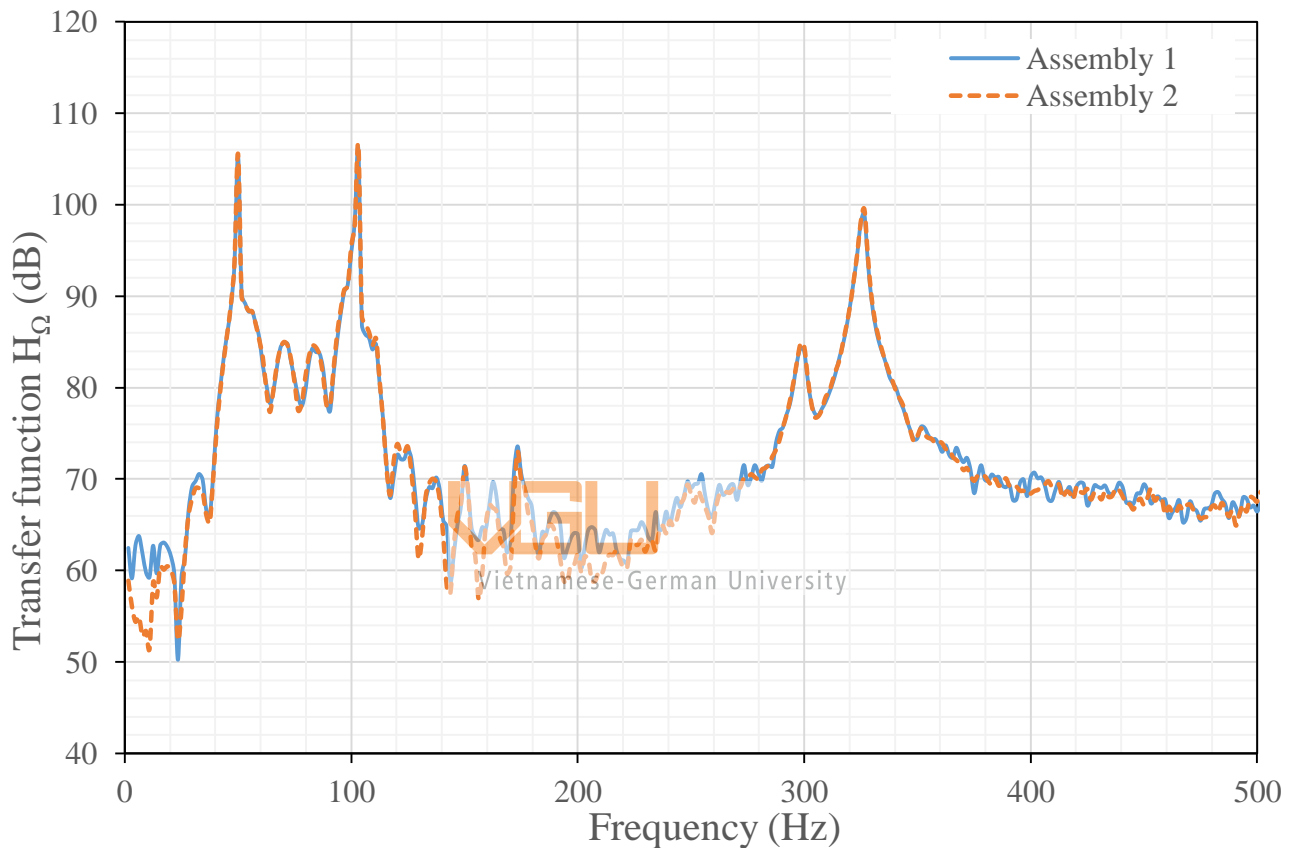


Figure 4-1: Reproducibility of the first set of experiments

### 4.2 Different filling volumes

In the first test, various volumes of granulated materials would be used to fill in the stator arm. A total of six amounts would be used (60, 100, 200, 300, 400, and 500 mL) with the hypothesis is that the damping effect would increase with the rise of filling volume.



Figure 4-2: Filling the stator arm with 400 mL rubber

The effectiveness of particle damping can be seen in Figure 4-3 and Figure 4-4. Here, an octave band graph is used to illustrate the damping effect more clearly. Due to the scaling of the graph and the width of the peaks, the reduction is not clearly illustrated. Furthermore, using the 1/3 octave would simplify the graph, making it much easier to understanding even for non-specialists.

The result of the experiments proves that particle damping can function as expected: there is a clear reduction in vibration. The more granulated material is used, the more damped the structure is. The hypothesis put forth has been proven correct.

Table 4-1: Reduction at peak different frequencies with various rubber volumes

Frequency (Hz) Filling volume	Vietnamese-German University				
	50	100	170	300	330
60 mL	0.601 dB	3.366 dB	3.261 dB	-0.009 dB	0.067 dB
100 mL	2.543 dB	3.471 dB	4.948 dB	0.031 dB	-0.382 dB
200 mL	6.893 dB	5.472 dB	2.850 dB	0.156 dB	0.615 dB
300 mL	6.649 dB	8.423 dB	4.730 dB	0.560 dB	1.281 dB
400 mL	8.708 dB	11.201 dB	5.808 dB	1.149 dB	2.262 dB
500 mL	8.718 dB	14.634 dB	6.778 dB	1.701 dB	2.764 dB



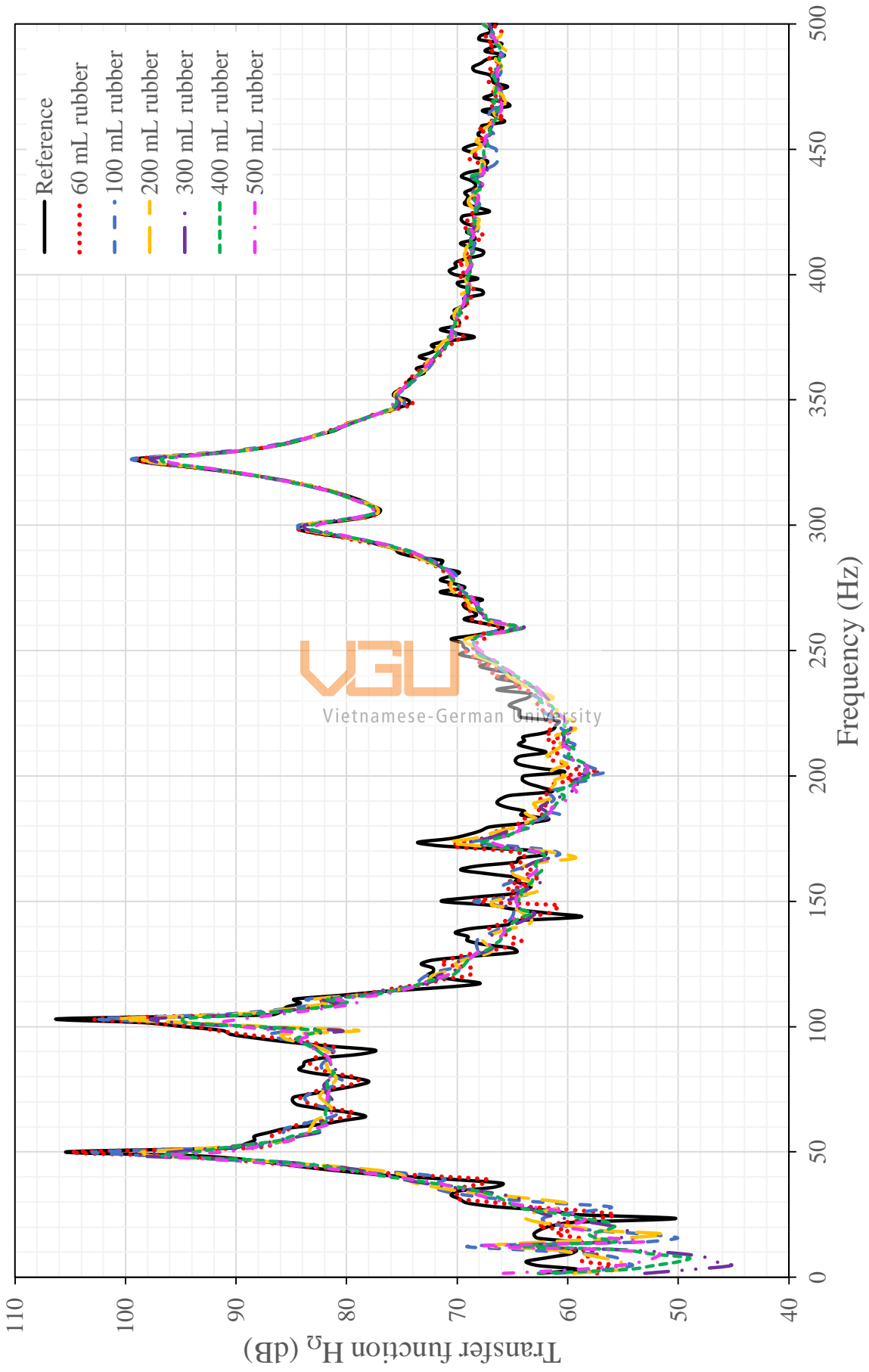


Figure 4-3: Transfer functions of different filling volumes of granulate materials

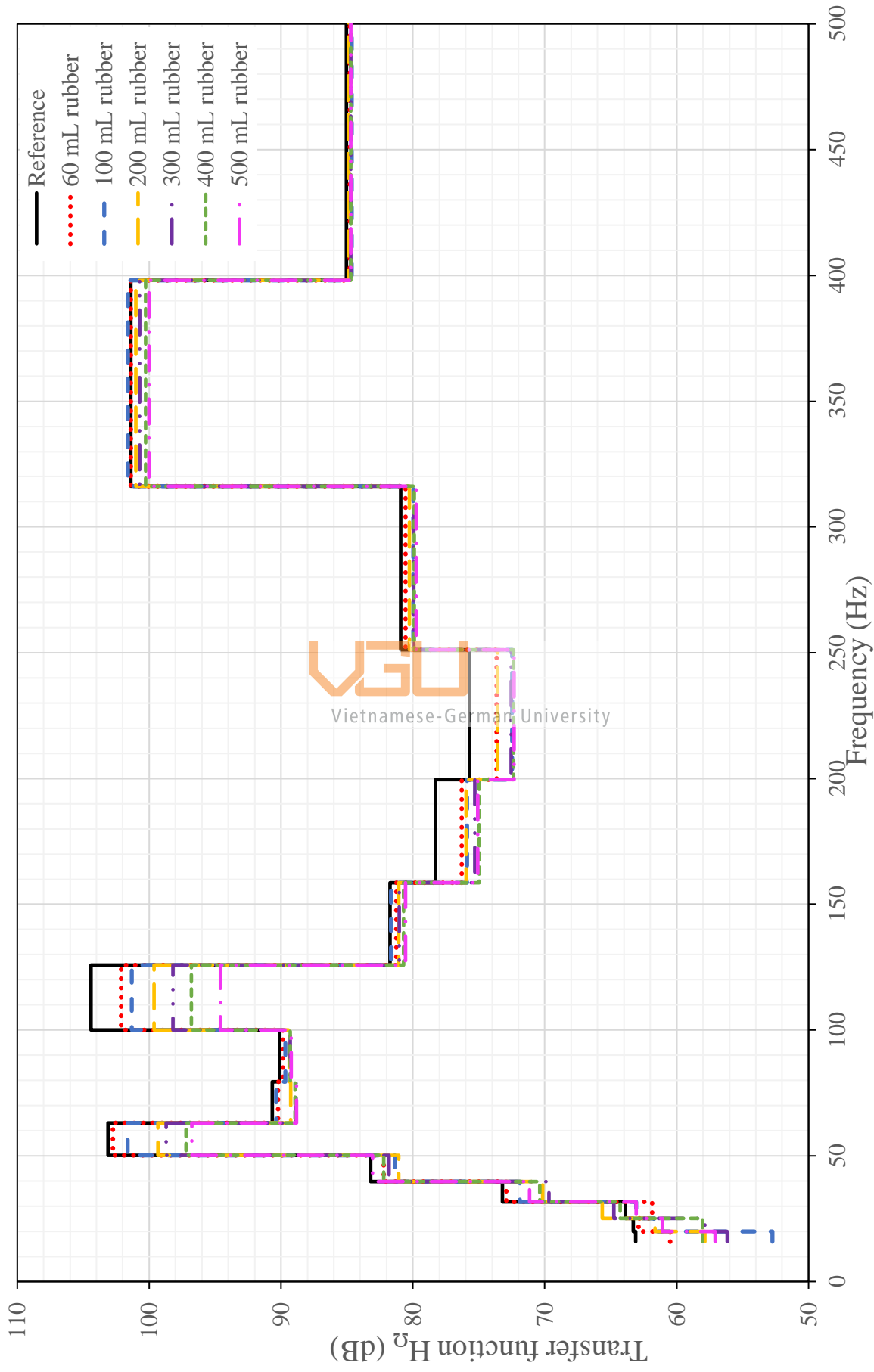


Figure 4-4: Transfer functions in 1/3 octave band of different filling volumes of granulate materials

The damping effect is most evident in the lower frequency (50 and 100 Hz). Meanwhile, for the higher frequencies (most notably 300 and 330 Hz), the damping effect is not that clear. This effect can be attributed to securing the stator arm into the generator ring (see section 3.2.2.1). A torque of 7 Nm might be too high, where it limits the vibration of the stator arm. With a limited vibration, there would be little for the damping effect to act on, which leads to a more modest effectiveness of particle damping.

In addition, certain vibration reductions are in the negative range (see Table 4-1), this means that the vibration is increased, not decreased. While sounds counter-intuitive, it should also be noted that the increased value here is very low (always under 0.5 dB, or 6% difference), and thus can be classified as “no effectiveness in vibration reduction”, with the variance seen here as “noise”.

### 4.3 Usage of packages

As mentioned above, the second set of experiments will investigate the effectiveness of particle damping if the granulated material is packed into containers. For this reason, air balloons are used as packages for this set of experiments. The hypothesis is that, by having containers, there should be more collisions, increasing the effectiveness of the damping.

There are two balloon sizes available for this set of experiments, and they are subsequently dubbed “big packages” and “small packages”. The damping abilities are then compared with pure particle damping (with the same mass of granulated materials). In this specific experiment, the mass of the material is 130g.



Figure 4-5: Big balloons being packed into the stator arm



Figure 4-6: Small balloons being packed into the stator arm

Individually speaking, each small balloon is packed tightly, while the big balloon is not filled up fully. However, within the context of filling up the stator arm, both types of balloons are packed as tightly as possible as seen in the two figures above. Personal observation and feeling report that it is easier to do so using the big balloons. These features may play a part in the effectiveness of particle damping in this scenario.

The damping effect observed in this experiment is similar to the result observed in the first experiment, where the vibration is greatly damped in the low-frequency section (for the first 2 peaks at 50 and 100 Hz) while the later peaks (at 300 and 330 Hz) see no major reduction. The vibration reduction effect can be summarized as below:

Table 4-2: Reduction at peak different frequencies with different types of balloons

Frequency (Hz) \ Type	50	100	170	300	330
Small balloons	4.231 dB	6.913 dB	3.878 dB	0.670 dB	1.779 dB
Big balloons	2.253 dB	9.550 dB	3.239 dB	0.988 dB	2.401 dB
Particle damping	7.816 dB	5.460 dB	3.037 dB	0.969 dB	0.554 dB

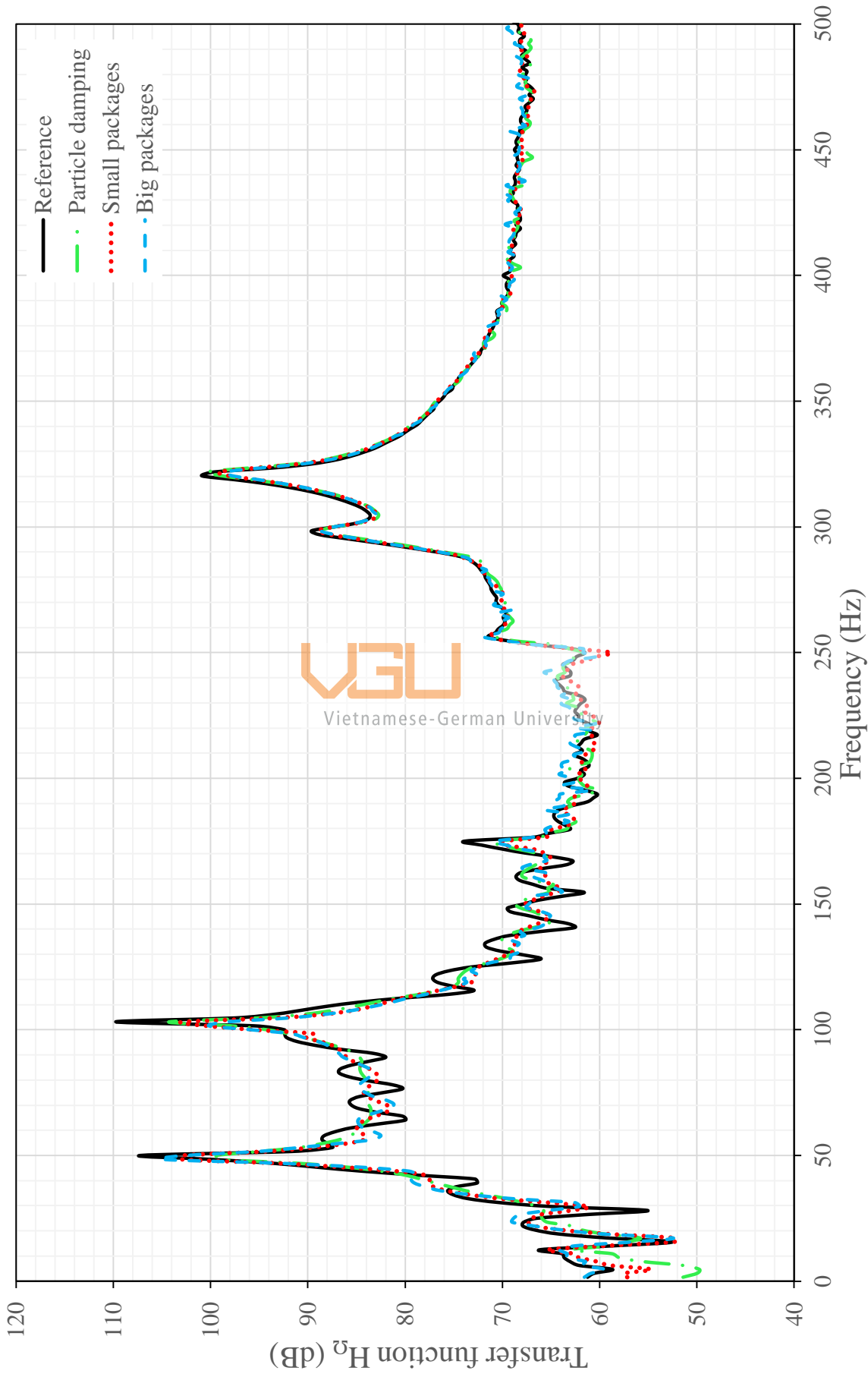


Figure 4-7: Transfer functions of granulated material in different packages

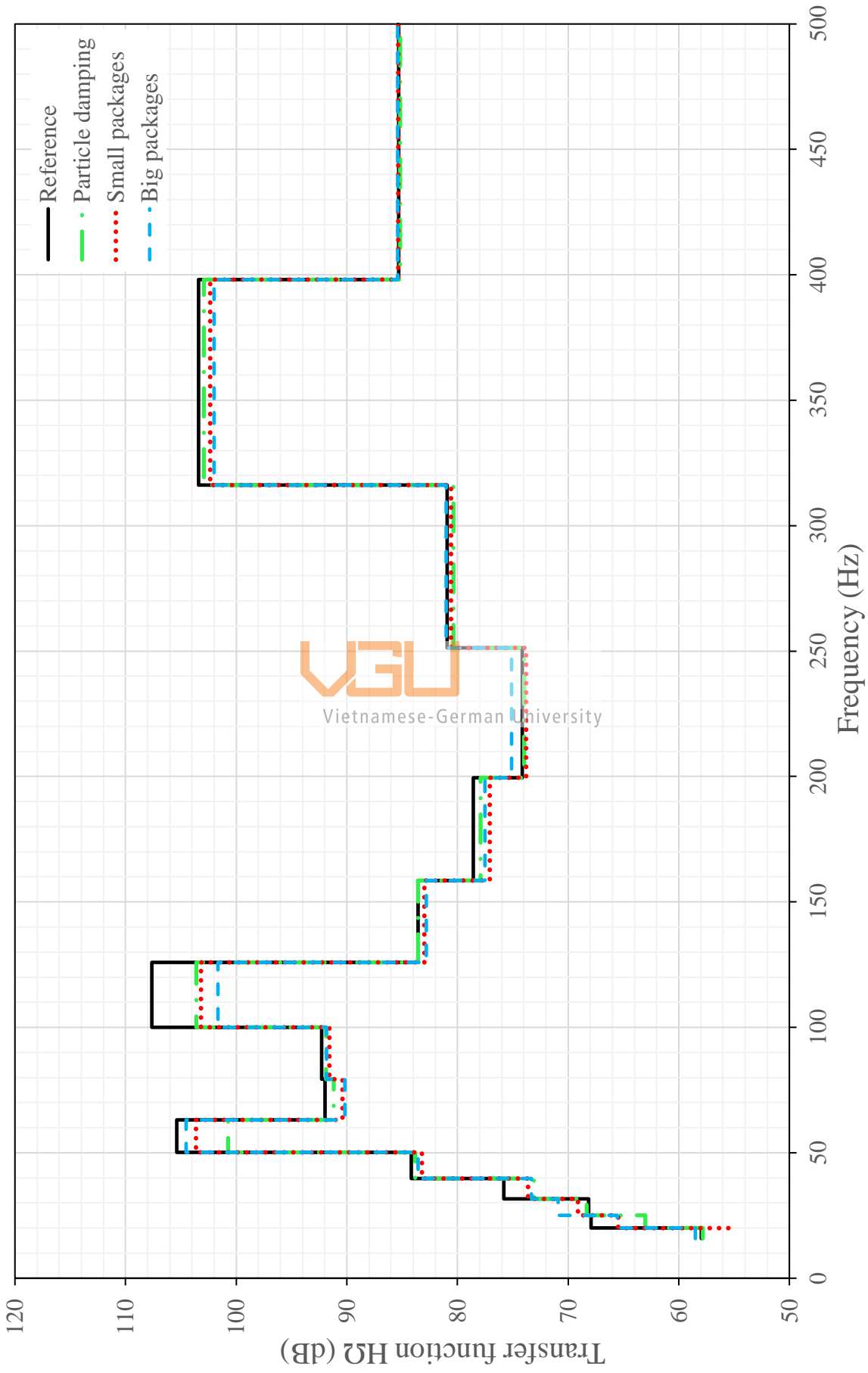


Figure 4-8: Transfer functions in 1/3 octave bands of granulated material in different packages

## 5 Conclusion and discussion

As seen from the charts and tables of this chapter 4, particle damping is proven via experiments that it can reduce vibration, with the specific application on a scaled model section of a wind turbine generator. The most vibration reduction can be achieved in the lower frequency range (up to 200 Hz), though this might be due to the experimental setup in this thesis, and not due to the limit of particle damping. In addition, with more granulate material, the damping effect would increase.

Furthermore, increasing the number of collisions in particle damping (by packing the granulated materials into smaller packages, such as balloons) would slightly increase the damping effect. However, this slight increase (when taken average) is very small and can be neglected. Furthermore, using bigger balloons would yield a better result compared to using small balloons. This can be attributed to how the balloons are prepared in this thesis.

It has been proven experimentally that particle damping can reduce the vibration of mechanical components within the wind turbine. However, the excitation signal in this thesis is an impulse, which is only a singular event and has a high magnitude. Furthermore, the test specimen here is only a section and a scaled model. This means that this thesis is more similar to provide a general concept than an in-depth study. A scaled model of a full generator or pseudo-random excitation signals should be applied in the next set of experiments.

In full-scale application, it would not be wise and safe to simply fill up the cavity inside components, this would add a significant mass within the nacelle of the wind turbine, which is already at a considerable elevation to the ground. This would lift the center of gravity up, increasing the risks during operation. Furthermore, to fill up the interior with granulated material, sufficiently large holes must be made on the structure, which might compromise the integrity of the generator.

A solution for that might also be extracted from this thesis, which involves the usage of packages. Using them would increase the number of collisions and the amount of friction of the particles, which would then improve the damping effect of the system. Furthermore, this would also lead to the option of externally attached modules of PD, requiring less modification and more user-friendly compared to directly filling the interior with granulated materials.

## 6 References

- Amick, H., & Bui, S. K. (1991). Review of several methods for processing vibration data. *Vibration Control in Microelectronics, Optics, and Metrology*. San Jose.  
doi:<https://doi.org/10.1117/12.56844>
- BP PLC. (2020). *Statistical Review of World Energy*. Retrieved November 5, 2020, from BP Official website: <https://www.bp.com/content/dam/bp/business-sites/en/global/corporate/pdfs/energy-economics/statistical-review/bp-stats-review-2020-full-report.pdf>
- Brandt, A. (2011). *Noise and Vibration analysis*. John Wiley & Sons, Ltd.
- Callister, W. D., & Rethwisch, D. G. (2014). *Materials Science and Engineering: An Introduction*. Wiley.
- Chen, J., & Georgakis, C. T. (2013, October 14). Tuned rolling-ball dampers for vibration control in wind turbines. *Journal of Sound and Vibration*, 332(21), 5271-5282.  
doi:<https://doi.org/10.1016/j.jsv.2013.05.019>
- Cimbala, J. M. (2010, February 22). *ME 345, Fall 2014: Instrumentation, Measurements, and Statistics*. Retrieved January 13, 2021, from Pennsylvania State University Website: [https://www.me.psu.edu/cimbala/me345web\\_Fall\\_2014/Lectures/Fourier\\_Transforms\\_DFTs\\_FFTs.pdf](https://www.me.psu.edu/cimbala/me345web_Fall_2014/Lectures/Fourier_Transforms_DFTs_FFTs.pdf)
- Crystal Instruments. (2016). *Basics of Modal Testing and Analysis*. Retrieved January 24, 2021, from Crystal Instruments Website: <https://www.crystalinstruments.com/basics-of-modal-testing-and-analysis>
- Curto, D., Doan, B. V., Franzitta, V., Montana, F., Nguyen, N. Q., & Sanseverino, E. R. (2020). Wave and Wind Energy Systems Integration in Vietnam: Analysis of Energy Potential and Economic Feasibility. *2020 IEEE International Conference on Environment and Electrical Engineering and 2020 IEEE Industrial and Commercial Power Systems Europe (EEEIC / I&CPS Europe*, (pp. 1-6). Madrid.  
doi:<https://doi.org/10.1109/EEEIC/ICPSEurope49358.2020.9160682>
- eFunda. (2019). *Laser Doppler Effect Theory*. Retrieved November 16, 2020, from eFunda Engineering fundamentals:



[https://www.efunda.com/designstandards/sensors/laser\\_doppler/laser\\_doppler\\_effect\\_theory.cfm](https://www.efunda.com/designstandards/sensors/laser_doppler/laser_doppler_effect_theory.cfm)

Escaler, X., & Mebarki, T. (2018). Full-Scale Wind Turbine Vibration Signature Analysis. *Machines*, 6(4), 63. doi:<https://doi.org/10.3390/machines6040063>

European Commission. (2018, November 28). *The Commission calls for a climate neutral Europe by 2050*. Retrieved from European Union Official website:  
[https://ec.europa.eu/commission/presscorner/detail/en/IP\\_18\\_6543](https://ec.europa.eu/commission/presscorner/detail/en/IP_18_6543)

Fladung, W. A. (1997). Windows Used for Impact Testing. *International modal analysis conference*, (pp. 1662-1666). Orlando.

Forrest, D. (1985). Retrieved 2021, from Keysight Technology Website:  
[https://www.keysight.com/upload/cmc\\_upload/All/6C06DATAACQ\\_IMPACT.pdf](https://www.keysight.com/upload/cmc_upload/All/6C06DATAACQ_IMPACT.pdf)

Friend, R. D., & Kinra, V. K. (2000, May 25). Particle impact damping. *Journal of Sound and Vibration*, 233(1), 93-118. doi:<https://doi.org/10.1006/jsvi.1999.2795>

Gagnon, L., Morandini, M., & Ghiringhelli, G. L. (2019, October 27). A review of particle damping modeling and testing. *Journal of Sound and Vibration*, 459, 114865.  
doi:<https://doi.org/10.1016/j.jsv.2019.11.048>

Hartin, J., & Belanus, K. (1997). Data Sampling Techniques For Fourier Analysis., (pp. 2.127.1 - 2.127.7). Milwaukee, Wisconsin. doi:<https://doi.org/10.18260/1-2--6487>

Heckel, M., Sack, A., Kollmer, J. E., & Pöschel, T. (2012, October 1). Granular dampers for the reduction of vibrations of an oscillatory saw. *Physica A: Statistical Mechanics and its Applications*, 391(19), 4442-4447. doi:<https://doi.org/10.1016/j.physa.2012.04.007>

Herlufsen, H. (1987). *Windows to FFT Analysis (Part 1)*. Retrieved from  
<https://www.bksv.com/media/doc/bv0031.pdf>

Hewlett Packard. (1986). *The Fundamentals of Modal Testing (Application note 243-3)*. Hewlett Packard Company.

Hewlett Packard. (1989). *The Fundamentals of Signal Analysis (Application Note 243)*. Hewlett Packard Company.

- Jianu, O., Rosen, M. A., & Naterer, G. (2012, December). Noise Pollution Prevention in Wind Turbines: Status and Recent Advances. *Sustainability*, 4(12), 1104-1117.  
doi:<https://doi.org/10.3390/su4061104>
- Koch, S., Duvigneau, F., Orszulik, R., Gabbert, U., & Woschke, E. (2017, April 14). Partial filling of a honeycomb structure by granular materials for vibration and noise reduction. *Journal of Sound and Vibration*, 393, 30-40. doi:<https://doi.org/10.1016/j.jsv.2016.11.024>
- Kulkarni, S. R. (2016). *ELE 201: Information Signals - Course Notes*. Retrieved November 17, 2020, from Princeton University Website:  
[https://www.princeton.edu/~cuff/ele201/kulkarni\\_text/frequency.pdf](https://www.princeton.edu/~cuff/ele201/kulkarni_text/frequency.pdf)
- Lu, Z., Wang, Z., Masri, S. F., & Lu, X. (2018, June 18). Particle impact dampers: Past, present, and future. *Structural Control Health Monitoring*, 25(1), e2508.  
doi:<https://doi.org/10.1002/stc.2058>
- McKenna, R., Leye, P. O., & Fichter, W. (2016, January). Key challenges and prospects for large wind turbines. *Renewable and Sustainable Energy Reviews*, 53, 1212-1221.  
doi:<https://doi.org/10.1016/j.rser.2015.09.080>
- Michaud, D. S., Feder, K., Keith, S. E., Voicescu, S. A., Marro, L., Than, J., . . . Berg, F. d. (2016, March 31). Personal and situational variables associated with wind turbine noise annoyance. *The Journal of the Acoustical Society of America*, 139(3), 1455-1466.  
doi:<https://doi.org/10.1121/1.4942390>
- Michon, G., Almajid, A., & Aridon, G. (2013, February 4). Soft hollow particle damping identification in honeycomb structures. *Journal of Sound and Vibration*, 332(3), 536-544.  
doi:<https://doi.org/10.1016/j.jsv.2012.09.024>
- Mollasalehi, E., Wood, D., & Sun, Q. (2017, November). Indicative Fault Diagnosis of Wind Turbine Generator Bearings Using Tower Sound and Vibration. *Energies*, 10(11), 1853.  
doi:<https://doi.org/10.3390/en10111853>
- National Instruments Corp. (2019, March 5). *Fast Fourier Transform (FFT) and window function*. Retrieved November 18, 2020, from National Instruments Corp. Website:  
<https://download.ni.com/evaluation/pxi/Understanding%20FFTs%20and%20Windowing.pdf>
- National Instruments Corp. (2019, March 5). *Using a Digitizer for Time-Domain Measurements*. Retrieved November 20, 2020, from National Instruments Corp. Website:

<https://www.ni.com/de-de/innovations/white-papers/09/using-a-digitizer-for-time-domain-measurements.html>

- Nilsson, A., & Liu, B. (2015). *Vibro-acoustics* (Vol. 1). Springer-Verlag Berlin Heidelberg.
- Papalou, A., Strepelias, E., Roubien, D., Bousias, S., & Triantafilou, T. (2015, October). Seismic protection of monuments using particle dampers in multi-drum columns. *Soil Dynamics and Earthquake Engineering*, 77, 360-368. doi:<https://doi.org/10.1016/j.soildyn.2015.06.004>
- Pinder, J. N. (1992). Mechanical Noise from Wind Turbines. *Wind Engineering*, 6(3), 158-168.
- Polytec GmbH. (2011). *Vibration measurement method*. Retrieved November 16, 2020, from Polytec GmbH Website: <https://www.polytec.com/eu/vibrometry/technology/laser-doppler-vibrometry/>
- Polytec GmbH. (2018, September 24). *Polytec Scanning Vibrometer Theory Manual*. Retrieved from Perkins Electro-Acoustics Research Laboratory: [https://pearl-hifi.com/06\\_Lit\\_Archive/05\\_LDV/Polytec\\_Software\\_Manuals/PSV\\_400\\_Theory.pdf](https://pearl-hifi.com/06_Lit_Archive/05_LDV/Polytec_Software_Manuals/PSV_400_Theory.pdf)
- Prabhu, K. M. (2014). *Window functions and their applications in signal processing*. Taylor & Francis Group.
- Prasad, B. B., Duvigneau, F., Woschke, E., & Juhre, D. (2020). Wind turbine blade and generator test specimen for evaluating a passive vibration reduction concept based on granular materials. *International Conference on Noise and Vibration Engineering (ISMA)*, (pp. 3525-3540). Leuven.
- Saavedra, R., & Samanta, B. B. (2015). Noise and Vibration Issues of Wind Turbines and Their Impact – A Review. *Wind Energy*, 39(6), 693-702. doi:<https://doi.org/10.1260/0309-524X.39.6.693>
- Sandanshiv, S., & Chavan, U. (2019). Vibration suppression effects on rotating wind turbine blade using a particle damping method. *Vibroengineering PROCEDIA*, 29, 43-48. doi:<https://doi.org/10.21595/vp.2019.20944>
- Schmidt, J. H., & Klokker, M. (2014, December 4). Health Effects Related to Wind Turbine Noise Exposure: A Systematic Review. *PLoS One*, 9(12), e114183. doi:<https://doi.org/10.1371/journal.pone.0114183>

- Shafiee, S., & Topal, E. (2009, January). When will fossil fuel reserves be diminished? *Energy Policy*, 37(1), 181-189. doi:<https://doi.org/10.1016/j.enpol.2008.08.016>
- Shin, K., & Hammond, J. (2008). *Fundamentals of Signal Processing for Sound and Vibration engineers*. John Wiley & Sons, Ltd.
- Shreve, D. H. (1995, November). Signal processing for effective vibration analysis. *IRD Mechanalysis*, 1-11.
- SIMCENTER. (2019, August 29). *Data Acquisition: Anti-Aliasing Filters*. Retrieved December 21, 2020, from Siemens Community: <https://community.sw.siemens.com/s/article/data-acquisition-anti-aliasing-filters>
- SIMCENTER. (2019, August 29). *What modal impact hammer tip should I use?* Retrieved January 16, 2021, from Siemens Community: <https://community.sw.siemens.com/s/article/what-modal-impact-hammer-tip-should-i-use>
- SIMCENTER. (2019, August 29). *Window Types: Hanning, Flatop, Uniform, Tukey, and Exponential*. Retrieved December 22, 2020, from Siemens Community: <https://community.sw.siemens.com/s/article/window-types-hanning-flatop-uniform-tukey-and-exponential>
- SIMCENTER. (2020, July 10). *Digital Signal Processing: Sampling Rates, Bandwidth, Spectral Lines, and more....* Retrieved December 21, 2020, from Siemens Community: <https://community.sw.siemens.com/s/article/digital-signal-processing-sampling-rates-bandwidth-spectral-lines-and-more>
- SIMCENTER. (2020, July 10). *What is a Frequency Response Function (FRF)?* Retrieved January 15, 2021, from Siemens Community: <https://community.sw.siemens.com/s/article/what-is-a-frequency-response-function-frf>
- Smith, J. O., & Serra, X. (1987). PARSHL: An Analysis/Synthesis Program for Non-Harmonic Sounds Based on a Sinusoidal Representation. *Proceedings of the International Computer Music Conference*. Tokyo.
- Smith, S. W. (1999). *The Scientist and Engineer's Guide to Digital Signal Processing* (2nd ed.). California Technical Publishing.
- The MathWorks, Inc. (2015). *Practical Introduction to Frequency-Domain Analysis*. Retrieved November 17, 2020, from The MathWorks, Inc. Website:

<https://de.mathworks.com/help/signal/ug/practical-introduction-to-frequency-domain-analysis.html;jsessionid=6662cc3646c62430dea58abfeb1c>

Tuzlukov, V. (2010). *Signal Processing Noise*. CRC Press.

Ülgen, D., Özkan, M. Y., & Ertugrul, O. (2016, July). Measurement of ground borne vibrations for foundation design and vibration isolation of a high-precision instrument. *Measurement*, *93*, 385-396. doi:<https://doi.org/10.1016/j.measurement.2016.07.041>

United Nations. (2015). Adoption of the Paris Agreement. *21st Conference of the Parties*. Paris.

Wagner, S., Bareiß, R., & Guidati, G. (1996). *Noise Mechanisms of Wind turbines*. Springer-Verlag Berlin Heidelberg.

Weisstein, E. W. (2005, April 15). *Nyquist Frequency*. Retrieved December 22, 2020, from MathWorld--A Wolfram Web Resource:  
<https://mathworld.wolfram.com/NyquistFrequency.html>

Weisstein, E. W. (2008, August 17). *Fourier Series*. Retrieved December 16, 2020, from MathWorld - A Wolfram Web Resource: <https://mathworld.wolfram.com/FourierSeries.html>

Wickramarachi, P. (2003). Effects of Windowing on the Spectral Content of a Signal. *Sound and vibration*, *13*(1), 10-13.

Xia, Z., Kai, J., Wang, X., Shao, G., Jiang, W., & Sun, Y. (2016, November 15). Study on semi-active particle damping technology for offshore platform truss structure. *Journal of Vibroengineering*, *18*(7), 4248-4260. doi:<https://doi.org/10.21595/jve.2016.17365>

Xia, Z., Liu, X., & Shan, Y. (2011, June 8). Application of particle damping for vibration attenuation in brake drum. *International Journal of Vehicle Noise and Vibration*, *7*(2), 178-194. doi:<https://doi.org/10.1504/IJVNV.2011.040573>

Xu, Z., Wang, M. Y., & Chen, T. (2004, March 5). A particle damper for vibration and noise reduction. *Journal of Sound and Vibration*, *270*(4-5), 1033-1040. doi:[https://doi.org/10.1016/S0022-460X\(03\)00503-0](https://doi.org/10.1016/S0022-460X(03)00503-0)

Yang, W., Tavner, P. J., Crabtree, C. J., Feng, Y., & Qiu, Y. (2014, May). Wind turbine condition monitoring: technical and commercial challenges. *Wind Energy*, *17*, 673-693. doi:<https://doi.org/10.1002/we.1508>

- Ydersbonda, I. M., & Korsnesb, M. S. (2016, February). What drives investment in wind energy? A comparative study of China and the European Union. *Energy Research & Social Science*, 12, 50-61. doi:<https://doi.org/10.1016/j.erss.2015.11.003>
- Ye, H., Wang, Y., Liu, B., & Jiang, X. (2019, July 20). Experimental Study on the Damping Effect of Multi-Unit Particle Dampers Applied to Bracket Structure. *Applied Sciences*, 9(14), 2912. doi:<https://doi.org/10.3390/app9142912>
- Zhang, P., Li, L., Patil, D., Singla, M., Li, H.-N., Mo, Y. L., & Song, G. (2015, December 11). Parametric study of pounding tuned mass damper for subsea jumpers. *Smart Materials and Structures*, 25(1), 015028. doi:<https://doi.org/10.1088/0964-1726/25/1/015028>



Vietnamese-German University